JOINT SPATIAL-TEMPORAL SPECTRUM SENSING AND COOPERATIVE RELAYING FOR COGNITIVE RADIO NETWORKS

by

Tuan T. Do
A Dissertation
Submitted to the
Graduate Faculty
of
George Mason University
In Partial fulfillment of
The Requirements for the Degree
of
Doctor of Philosophy
Electrical and Computer Engineering

Committee:

Dr. Brian L. Mark, Dissertation Director

Dr. Bernd-Peter Paris, Committee Member

Dr. Jill K. Nelson, Committee Member

Dr. Robert Simon, Committee Member

Dr. Andre Manitius, Department Chair

Dr. Lloyd J. Griffiths, Dean, The Volgenau School of Information Technology and Engineering

Date: 12/15/2010

Spring Semester 2011
George Mason University
Fairfax, VA

Joint spatial-temporal spectrum sensing and cooperative relaying for cognitive radio networks

A dissertation submitted in partial fulfillment of the requirements for the degree of Doctor of Philosophy at George Mason University

By

Tuan T. Do
Master of Science
The George Washington University, Washington, DC, 2005
Bachelor of Science
University of Communications and Transports, Vietnam, 2001

Director: Dr. Brian L. Mark, Professor
Department of Electrical and Computer Engineering

Spring Semester 2011
George Mason University
Fairfax, VA

Dedication

To my mother, Huyen Nguyen and Chi Do.

Acknowledgments

Though only my name appears on the cover of this dissertation, a great many people have contributed to its production. First and foremost, I want to thank Dr. Brian L. Mark, my doctoral advisor, for all his encouragement, guidance and support. The members of my dissertation committee, Dr. Bernd-Peter Paris, Dr. Jill K. Nelson and Dr. Robert Simon, have generously given their time and expertise to better my work. I thank them for their contribution and their good-natured support. I sincerely thank the faculty and staff of The Department of Electrical & Computer Engineering of George Mason University for their guidance and cooperation.

My very special thanks to the one person whom I owe everything I am today, my mother, Pham Thi Lan. Her unwavering confidence in my abilities and in me is what has shaped me to be the person I am today. Thank you for everything. I thank my father for teaching me the first lesson about mathematics and inspiring me to study science and technology. My thanks also go out to my beloved wife for her love, support and encouragement. I would also like to thank my sister and my brother in law for their support and my extended family for aiding and encouraging me throughout this endeavor. Finally, I would like to take the opportunity to thank all my teachers.

Table of Contents

List of Figures

Abstract

JOINT SPATIAL-TEMPORAL SPECTRUM SENSING AND COOPERATIVE RELAYING FOR COGNITIVE RADIO NETWORKS

Tuan T. Do, PhD
George Mason University, Spring, 2011
Dissertation Director: Dr. Brian L. Mark

The number of wireless systems and services has grown tremendously over the last two decades. As a result, the availability of wireless spectrum has become extremely limited. Cognitive radio is a new technique to overcome the issue of spectrum scarcity. In cognitive radio networks, the licensed users of the spectrum are called primary users. Secondary users equipped with cognitive radios can opportunistically transmit via so-called "spectrum holes" which can be categorized as spatial or temporal spectrum holes.

In this dissertation, we propose a joint spatial-temporal spectrum sensing scheme for cognitive radios. We show that our joint spatial-temporal spectrum sensing scheme outperforms pure temporal sensing schemes. In addition, joint spatial-temporal sensing increases the point-to-point transmission capacity of cognitive radio link compared to pure temporal or spatial sensing. We also propose a temporal spectrum sensing scheme that exploits multiuser diversity in wireless networks. In wireless networks with fading, multiuser diversity exists because different users experience peak channel quality at different times. By exploiting multiuser diversity, our spectrum sensing method can outperform the spectrum sensing schemes that do not exploit multiuser diversity. We develop and analyze a joint spatial-temporal sensing scheme that incorporates cooperative relaying to further increase the capacity of a cognitive radio network. We consider both amplify-and-forward

and decode-and-forward cooperative transmission strategies. Finally, we study joint spatial-temporal spectrum sensing in a multichannel cognitive radio scenario and present randomized and maximized signal-to-noise ratio algorithms that improve performance in term of symbol error probability.

Chapter 1: Introduction

During the past two decades, the world has witnessed a tremendous growth of the wireless communication industry with over four billion subscribers worldwide. Wireless communications have moved from first-generation (1G) systems that supported voice communication with limited roaming to third-generation (3G) systems that provide Internet connectivity and multi-media applications. The fourth-generation systems will be designed to interconnect different wireless networks such as wireless personal area networks (WPANs), wireless local area networks (WLANs) and wireless wide-area networks (WWANs).

In wireless communications, all users coexisting in the same frequency band interfere with each other due to the broadcast nature of the wireless channel. As the number of wireless systems and services has grown, the availability of wireless spectrum has become severely limited as shown in the National Telecommunications and Information Administration's (NTIA) frequency allocation chart [1]. A number of other studies, e.g., [2], [3], [4], have also shown that the wireless spectrum is highly under-utilized. This has prompted the FCC to propose opening the licensed band to unlicensed users, which has resulted in renewed interest in the concept of cognitive radios [5].

A cognitive radio (CR) transceiver is able to adapt to the dynamic environment and the network parameters to maximize the utilization of the limited radio sources while providing flexibility in wireless access. A cognitive radio must collect and process information about the licensed users within its spectrum, which requires advanced spectrum sensing and signal processing techniques. Cognitive radio enables *opportunistic spectrum access* which allows unlicensed users to access licensed spectrum as long as they do not cause harmful interference to the licensed users. The IEEE has formed a working group (IEEE 802.22) to develop an air interface for opportunistic spectrum access to the TV spectrum via the cognitive radio

technology [6]. This dissertation is motivated by potential capabilities of cognitive radios which hold tremendous promise for increasing spectral efficiency in wireless systems.

1.1 Dissertation Overview

A cognitive radio can intelligently utilizes any available side information such as activity, channel conditions, codebooks or messages of licensed users. Depending on the type of available network side information and regulatory constraints, there are three main cognitive radio network paradigms: underlay, overlay, and interweave. The underlay paradigm allows cognitive users to operate if the interference caused to licensed or primary users is maintained below a given threshold. In overlay systems, cognitive radios attempt to obtain some bandwidth for their own communication without interfering with communication of primary users. In interweave systems, the cognitive radio opportunistically exploits the so-called *"spectrum holes"* to communicate without causing interference to primary systems.

In this dissertation, we develop a framework for cognitive radio systems based on the interweave network paradigm. In this paradigm, cognitive radios seek transmission opportunities through spectrum holes which can be classified as spatial [7] or temporal [8]. We first develop a spectrum sensing technique called joint spatial-temporal spectrum sensing which detects both spatial and temporal spectrum holes. By exploiting the spatial information of primary user, the performance of temporal sensing is significantly improved relative to pure temporal sensing which does not use knowledge of primary user's spatial information.

We also propose a new spectrum sensing scheme that exploits multiuser diversity in wireless networks. Multiuser diversity is a phenomenon inherent in wireless networks provided by independent, time-varying channels across different users. In traditional cellular networks, multiuser diversity can be exploited by scheduling at any one time only the user with the best channel to transmit to the base station. Diversity gain arises from the fact that in a system with many users, whose channels vary independently, there is likely to be a user whose channel is near its peak capacity at any given time. Our multiuser diversity spectrum sensing scheme exploits the independent channel fading among secondary nodes

to improve the performance of spectrum sensing. Our scheme significantly outperforms other schemes that do not exploit multiuser diversity.

We then propose a cooperative transmission scheme for cognitive radio networks based on spectrum holes determined through joint spatial-temporal sensing. In our scheme, a secondary transmitter communicates with a secondary receiver through relay nodes when the primary transmitter is ON and the maximum interference-free transmit power (MIFTP) is not sufficient for a direct transmission to reach the secondary receiver. When the primary transmitter is OFF, the secondary transmitter can communicate directly with the secondary receiver by transmitting at a higher power. The secondary receiver then combines the signal from the relay node and the direct signal from secondary transmitter to achieve a better signal-to-noise ratio. Our cooperative transmission scheme significantly outperforms the traditional cooperative transmission schemes that employ only spatial or temporal sensing knowledge.

1.2 Summary of chapters

- In Chapter 2, we introduce the basic concepts and terminology of opportunistic spectrum access and cognitive radios. We also discuss the research literature relevant to the contributions of this dissertation. The relevant literature includes papers related to cooperative spectrum sensing, multiuser diversity and cooperative communication.

- In Chapter 2.6, we propose a joint spatial-temporal sensing scheme for opportunistic spectrum sharing in cognitive radio networks. The system model consists of a primary transmitter with unknown location and transmit power, which alternates between ON and OFF states, with respect to a given frequency channel. Spatial spectrum sensing is employed to estimate the maximum interference-free transmit power for a secondary node, during an ON period. Estimates of the primary transmitter's location and transmit power obtained in the course of spatial sensing are used by a fusion center to select a subset of the secondary nodes to make a temporal sensing decision, i.e., a

decision as to whether the primary is ON or OFF. Three distributed temporal sensing algorithms are considered: the counting rule detector, linear quadratic detector and multi-level quantization. By incorporating spatial information, we obtain joint spatial-temporal versions of these two detectors. We derived the Additive While Gaussian Noise (AWGN) capacity for pure temporal, pure spatial and joint spatial-temporal sensing. Our simulation results show that joint spatial-temporal sensing approach significantly outperforms pure temporal sensing, in terms of probability of spectrum hole detection and capacity gain.

- In Chapter 4, we develop a cooperative multiuser diversity spectrum sensing scheme that exploits the multiuser diversity inherent in the secondary network to improve the sensing capability of cognitive radio systems. We use a distributed approach wherein each secondary user only has local knowledge about its observed energy. Our simulation results show that the proposed scheme significantly outperforms sensing schemes that do not exploit multiuser diversity.

- In Chapter 5, we propose cognitive amplify-and-forward cooperative relaying schemes with fixed decoding delay and variable decoding delay that exploit the presence of spectrum holes both in time and in space. In the fixed decoding delay protocol, the secondary receiver always decodes the received signal after fixed number of time frames. In the variable decoding delay protocol, the number of time frames the secondary receiver has to wait before it can decode the signal depends on the state of the primary transmitter. The variable decoding delay scheme, which always has a diversity order of two, has lower symbol error probability than the fixed decoding delay scheme. Our simulation and analytical results show that our proposed schemes, employing joint spatial-temporal sensing, significantly reduce the average symbol error probability compared to schemes based on pure temporal or spatial sensing. We also propose an incremental relaying protocol which further improves the spectral efficiency of our protocols.

- In Chapter 6, we propose a cognitive decode-and-forward cooperative transmission strategy that exploits the presence of spectrum holes both in time and in space. Similar to the amplify-and-forward scheme developed in Chapter 5, we consider two variations of the decode-and-forward scheme: fixed decoding delay and variable decoding delay. Our results show that the proposed decode-and-forward schemes, employing joint spatial-temporal sensing, significantly reduce the average symbol error probability compared to schemes based on pure temporal or pure spatial sensing.

- In Chapter 7, we consider a multichannel cognitive radio network scenario in which a secondary transmitter can switch to different channels for opportunistic communications. Multichannel diversity can be achieved by dynamically switching to different channels during transmission. We show that even a simple randomized channel switching scheme can significantly reduce the average symbol error probability. We also propose a scheduling algorithm based on maximizing the signal-to-noise ratio to further improve the performance of cognitive transmission. We study the performance of our multichannel switching schemes combined with *capacity achieving* turbo codes. Our numerical results show that combination of randomized multichannel switching with turbo codes significantly improves the performance of the system.

Chapter 2: Background

In this chapter, we discuss some basic aspects of opportunistic spectrum access (OSA) using cognitive radios (CRs). We provide a brief survey of the research literature with a focus on spectrum sensing techniques for cognitive radios and cooperative relaying.

2.1 Fundamentals of Cognitive radio

Software-defined radio and cognitive radio were first introduced by Mitola [5] and [9]. A software-defined radio or "software radio" is a multiband radio that supports multiple air interfaces and protocols and is reconfigurable through software. A cognitive radio built on a software radio platform is a wireless communication system that intelligently utilizes any available side information about the activity, channel conditions, codebooks or messages of other nodes with which it shares the spectrum [10]. Cognitive radios enable *dynamic spectrum access* (DSA), also called opportunistic spectrum access (OSA), (see [11] and references therein).

Based on the type of network side information along with the regulatory constraints, there are three types of cognitive radio system: underlay, overlay, and interweave [10]

2.1.1 Underlay Paradigm

The underlay paradigm allows communication by the cognitive radio assuming that it has knowledge of the interference caused by its transmitter to the receiver of all non-cognitive users. In this paradigm, concurrent non-cognitive and and cognitive transmission may occur only if the interference caused by the cognitive users to the noncognitive receivers is below some threshold. To meet the interference constraint, multiple antennas can be used to guide the cognitive signals away from the noncognitive receivers. Other techniques use

spread spectrum or ultra-wide-band to spread the cognitive signal below the noise floor; the signal is then de-spread at the cognitive receiver.

2.1.2 Overlay Paradigm

The overlay paradigm is based on the assumption that the cognitive transmitter has knowledge of the noncognitive user's codebooks and its transmitted messages as well. The codebook could be obtained if the noncognitive users follow a publicized standard or if they broadcast their codebooks periodically. The latter condition can be obtained by decoding the message at the cognitive receiver. With the knowledge of noncognitive user's message and/or codebook, the cognitive transmitter can use different techniques such as dirty paper coding (DPC) to mitigate or cancel the interference seen at the cognitive and noncognitive receivers.

The capacity of a cognitive channel in which the cognitive transmitter learns only a part of the noncognitive user's message is analyzed in [12]. The capacity of overlay cognitive channels with the assumption that all codebooks and channel gains are known to the two encoders is analyzed in [13, 14]. Knowledge of the noncognitive user's messages allows the cognitive transmitter to apply several encoding techniques that will improve both its own transmission rates and the noncognitive user's rate. In [15], encoding can achieve a nonzero rate for a noncogntive user such that the cognitive users's transmission causes no interference to the noncognitive receiver.

2.1.3 Interweave Paradigm

The interweave paradigm is based on the idea of opportunistic communication over temporal space-time frequency voids or *spectrum holes*. This technique requires knowledge of activity information of noncognitive users in the spectrum such as when they are active or idle. By monitoring the spectral activities of noncognitive users, cognitive radios can intelligently detect spectrum holes and opportunistically communicate over spectrum holes with minimal interference to the noncognitive users.

2.2 Spectrum holes

The term "spectrum hole" refers to those bands of radio spectrum that are under-utilized (in part or in full) at a particular instant of time and at a specific geographic location [16]. In terms of occupancy, spectrum holes may be categorized as: *white spaces* (frequency bands which are free of RF interferers except for ambient noise made up of natural and man-made sources) or *grey spaces* (frequency bands which are partially occupied by low-powered interferers). In other words, a spectrum hole is a region of space-time-frequency in which a particular secondary use is possible.

A spectrum hole can be characterized as spatial or temporal. A *spatial* spectrum hole can be specified in terms of the maximum transmission power that a secondary user can employ without causing harmful interference to primary users that are receiving transmissions from another primary user that is transmitting on the given channel [17, 18]. Spectrum reuse in this context is similar to frequency reuse among cochannel cells in a cellular network. A *temporal* spectrum hole is a period of time for which the primary transmitter is idle. During such idle periods, a secondary user may opportunistically transmit on the given channel without causing harmful interference.

In temporal spectrum holes, secondary transmissions are allowed during the idle times of the primary users. The exploitation of temporal spectrum opportunities has been studied in [8, 16, 19–24] and references therein. The success of this kind of scheme depends crucially on the accurate prediction of the silent periods of the primary user [19–21]. Temporal spectrum holes are studied in terms of probability of missed detection, probability of false alarm and sensing time together with receiver operating characteristics to evaluate a scheme's performance, reliability and complexity. These approaches are vulnerable to deviations from the assumed model of the primary's transmissions, due to real-world uncertainties. In the absence of noise uncertainty, detection at low SNR directly translates to longer observation times at the detector. In scenarios with noise uncertainty, detection may not be possible, even with infinite sensing time [25].

In [22], by modeling the primary user's spectrum occupancy as a Markov chain, a decision-theoretic framework for optimal PHY-MAC joint design of OSA based on the theory of partially observable Markov decision processes (POMDPs) is presented. The design objective is to maximize the secondary user's throughput under the constraint that the probability of collision perceived by any primary user is below a predetermined threshold.

Besides temporal and spatial aspects, the primary's signal waveform can be viewed as another dimension of a spectrum hole [26]. For example, a direct sequence spread spectrum (DSSS) signal with a spreading code of four chips can accommodate four different users using conventional signal processing techniques. If at any given time and space only one such signal is identified in the primary network, then a spectrum hole consisting of the other three signals exists, which can be used by the secondary network. In [26], the time and frequency domain behaviors of existing signals are characterized by signal detection followed by feature extraction, clustering, signal classification, machine learning and prediction. Then some decision metrics or policies are used to transmit new signals such that those signals do not interfere with the existing ones.

2.3 Spectrum Sensing

Spectrum sensing is defined as the task of finding spectrum holes by sensing the radio spectrum of noncognitive users [27], [28]. Thus, spectrum sensing is a critical component of the interweave network paradigm. There are three main spectrum sensing techniques: matched filter, energy detector, and cyclostationary feature detection. In the context of spectrum sensing, the cognitive and noncognitive users are normally referred to as secondary and primary users, respectively.

2.3.1 Matched Filter

The matched filter [29] is the optimum means for signal detection since it maximizes the received signal to noise ratio. However, the matched filter requires a priori knowledge of the primary signal at both the PHY and MAC layers to demodulate the primary user's signal.

In addition, the secondary user has to perform timing and synchronization or even channel equalization with respect to the primary user. The main advantage of the matched filter is that it requires less time to achieve high processing gain, since only $\mathcal{O}(1/\text{SNR})$ samples are required to meet a given detection probability constraint [30]. However, a significant drawback of the matched filter is that a dedicated spectrum sensing detector is needed for every primary user class.

2.3.2 Energy Detector

Simple, noncoherent detection can be achieved through an energy detector. The implementation of an energy detector is similar to a spectrum analyzer involving averaging frequency bins of a Fast Fourier Transform (FFT) with processing gain proportional to the size of the FFT. Due to noncoherent detection, $\mathcal{O}(1/\text{SNR}^2)$ samples are required to meet the detection probability constraint [30]. The main drawback of an energy detector is that the threshold used for primary user detection is highly susceptible to unknown or changing noise levels. The energy detector does not work for spread spectrum signals.

2.3.3 Cyclostationary feature detection

Modulated signals are generally in the form of sine wave carriers, pulse trains, repeating spreading, hopping sequences or cyclic prefixes, which results in periodicity. These modulated signals have cyclostationary characteristics since their mean and autocorrelation functions exhibit periodicity. Such periodicity is generally incorporated in the signal format so that a receiver can exploit it for parameter estimation, e.g., for carrier phase or pulse timing. This periodicity can be used for detection of random signals with a particular modulation type in a background of noise and other modulated signals.

2.3.4 Sequential Detection

In spectrum sensing, detection delay is an important performance metric. If a primary user stops transmission, then a secondary user should detect this event quickly, in order to be

able to start its own transmission quickly. A small detection delay will allow secondary users to take short transmission opportunities. On the other hand, if the primary user starts transmission, the cognitive user should detect this event as quickly as possible, in order to vacate the band for the primary user

Sequential detection schemes exploit the fact that the number of samples required to achieve a given reliability level may well be dependent on the actual realization of the observed samples. For example, in a simple binary hypothesis testing context, Walds sequential probability ratio test (SPRT) compares the likelihood ratio with two thresholds, and the decision is made as soon as the test statistic exceeds either one of the thresholds. It is known that SPRT minimizes the average sample number (ASN) among all tests with the same false alarm and misdetection probabilities. In [31], sequential sensing is proposed for orthogonal frequency division multiplexing (OFDM) cognitive radios. In other research [32], Lai et al. develops a sequential sensing strategy based on a quickest detection framework.

2.3.5 Cooperative spectrum sensing

The received signal strength at the input of spectrum sensing detector may be severely degraded due to multipath fading and shadowing. Added to these issues of low SNR is the hidden-terminal problem [8]. Secondary users may be shadowed away from the primary user's transmitter but there may be primary receivers close to the secondary users that are not shadowed from the primary transmitter. Hence, if a secondary user transmits, it may cause interference to the primary receivers. One approach to overcome the low SNR problem is to average over longer durations of time while performing the detection. This scheme results in an increased effective SNR and hence in improved performance but at the expense of increased delay.

An alternative approach is for secondary users to cooperate with each other to detect the primary signal. Better performance at low SNR can be achieved since user cooperation increases diversity by providing multiple measurements of the signal. Additionally, having users cooperating over a wide area also provides a possible solution to the hidden-terminal

problem, since this problem would arise only if all the secondary users were shadowed away from the primary. Cooperative sensing has been studied extensively in [8], [23], [33], [34] and [24].

2.3.6 Multichannel Cognitive Radio Networks

In multichannel cognitive radio networks, the licensed wireless spectrum consists of a set of N non-overlapping channels. Secondary users can access all the available channels by switching to their frequencies. Multichannel cognitive radio networks have been studied in [35–38]. In [36, 37], the optimal problem of multichannel cognitive medium access control with opportunistic transmissions is considered. A dynamic programming approach is proposed to search for an optimal sensing order among the channels.

In [35], a *channel-aware switching* algorithm is developed to decide *where* and *when* to switch among the candidate channels. Also in [35], a candidate channel selection algorithm is developed to maximize the spectrum accessibility and then derived the channel-switching decision rule to determine the best channel to switch to is derived. The proposed scheme outperforms the forced-switching due mainly to its ability to analyze the channel characteristics and exploit the dynamic nature of the wireless environment. In [38], sequential sensing algorithms for OFDM-based wideband multichannel cognitive radio systems are developed. The tradeoff between the sensing time and the chance of identifying more unoccupied subchannels is captured in the effective rate achieved by the CR system. Optimal stopping problems are formulated, which maximize the effective rate given the past and current observations.

2.4 Basic components of OSA

Basic components of an OSA model are [11]:

- spectrum opportunity identification,
- spectrum opportunity exploitation,

- regulatory policy

The opportunity identification module is responsible for accurate identifying and intelligently tracking idle frequency bands that are dynamic in both time and space. The main task of spectrum identification is spectrum sensing which detects the spectrum holes in both time and space. Chapter 2.6 and 4 of this thesis focus on developing spectrum identification schemes.

Once spectrum opportunities are detected, secondary users need to determine how to exploit them. The spectrum opportunity exploitation module takes input from the opportunity identification modules and decides whether transmission should take place. Issues with this module include what modulation and transmission power to use and how to share opportunities among secondary users to achieve a network layer objective. We develop a spectrum opportunity exploitation scheme in Chapter 5 wherein a cooperative communication strategy is developed using spatial-temporal spectrum holes.

Policy is also an important piece of OSA. It creates rules of cooperation and joint usage between primary and secondary users. Policy compliance can be executed using specific parameters available in a node, e.g., power spectral estimates, traffic type, priorities, location, delay constraints and other observable of the environment. The range of policies may vary from non-aggressive ("do no harm" policy, e.g., maintain complete orthogonality at all times) to aggressive (e.g., operate without restrictions in times of national emergency). Some major challenges include software implementation of policy, device testing and verification for policy compliance, and resolution of multiple conflicting policies. To determine policy compliance, it may be highly desirable to consider a *policy reasoner* (PR) that is capable of interacting with the sensor/radio and respond to requests by providing constraints (e.g., transmit power limit, transmission duration, etc.) [39].

2.5 Multiuser Diversity

A fundamental characteristic of the wireless channel is the fading of the channel strength due to the multipath effect. An important means to combat channel fading is the use of diversity. Diversity improves performance by creating several independent signal paths between the transmitter and the receiver. Diversity can be obtained over time (interleaving), frequency (combining multiple paths in spread-spectrum or frequency- hopping systems) and space (multiple antennas). These diversity modes pertain to a point-to-point link. Recent results in [40] point to another form of diversity which is inherent in wireless networks with multiple users. Multiuser diversity exists in wireless networks since in a multiuser fading channel, different users experience peaks in their channel quality at different times.

We consider a multiple access model where a group of users communicates with a central base station or access point, i.e., the uplink channel of cellular networks. In this model, multiuser diversity can be exploited based on centralized and distributed approaches. In centralized approaches, multiuser diversity can be exploited by scheduling users so that they transmit when their channel conditions are favorable which results in a total throughput that increases with the number of users. In order to do this, the base station needs to know all the users' channel state information (CSI). This could be gained by having each user transmits a pilot signal to the base station; each user's channel gain would then be estimated and the base station would signal the user with the best channel to transmit. The main drawback of the centralized approach is that it creates too much overhead when the number of users is large.

To overcome the overhead issue, a distributed approach is introduced in [41]. In this approach, each user has knowledge of its own fading channel level, but no knowledge of the fading levels of the other users in the cell. This distributed CSI can be obtained by measuring the pilot signals periodically broadcast from the base station. Reciprocity is required between the downlink and uplink channels, i.e., in a time-division duplex (TDD) system, the channel variation is due to multipath fading and not to other cell interference.

The overhead for this approach does not increase as the number of users increases. However, each user must decide when to transmit without global knowledge of channel gains. In [41], a simple slotted ALOHA protocol is proposed to exploit the multiuser diversity. To implement a real multiuser diversity system, one has to consider two issues: fairness and delay. When the user's fading statistics are the same, the multiuser diversity strategy maximizes not only total capacity of the system but also the throughput of the individual users. However, channel statistics are usually not symmetrical; users close to the base station will have better SNR. Moreover, the multiuser diversity strategy only aims at maximizing the long-term average throughputs and ignores latency requirements.

2.6 Cooperative communications

In wireless networks, multipath fading can be mitigated through the use of diversity transmission of redundant signals over independent channel realizations in conjunction with suitable receiver combining to average the channel effects. Space or multiple-antenna diversity techniques are particularly attractive as they can be readily combined with other forms of diversity, e.g., time and frequency diversity, and still offer dramatic performance gains when other forms of diversity are unavailable. However, the application of multiple antenna technology to mobile networks often faces the practical implementation problem of packing many antennas in a small-sized mobile terminal. To achieve multiple antennas gain, one must guarantee antenna element separation several times the wavelength, a requirement difficult to meet with small sized terminal. In an effort to overcome these limitations, cooperative diversity or cooperative communication was introduced in [42], [43] and [44].

The basic idea of cooperative communication is that the source terminal cooperates with the relay terminals to form a virtual or distributed multi-antenna system to communicate with the destination. The performance of a cooperative communication system depends on the combining mechanism at the relay and at destination nodes. Cooperative protocols studied in the literature include:

- The non-regenerative amplify and forward (AF) strategy which achieve available diversity with maximal ratio combining. The outage behavior and performance of this protocol can be found at [43] and [45]. This strategy is less practical since it requires storage of analog waveforms at relay nodes.

- The regenerative decode and forward (DF) strategy is simple and practical but cannot achieve full diversity unless sophisticated combining is employed at destination to account for the reliability of the source $\rightarrow$ relay $\rightarrow$ destination path. The outage probability of this strategy is analyzed in [43]. In [46], a smart decode-and-forward strategy is proposed to achieve diversity.

- The selective decode-and-forward (SDF) strategy which relies on a cyclic redundancy code (CRC) to detect errors at the relay and selectively forwards to the destination only bits without errors. This strategy achieves available diversity at the expense of decoding delay and spectral efficiency loss due to the use of CRC codes.

- The space-time coded diversity strategy [42], wherein the source and relay uses space-time codes to communicate with the destination, also achieves available diversity.

- The incremental relaying strategy [43] exploits limited feedback, i.e., a single bit feedback from the secondary transmitter to indicate the success or failure of the transmission. This protocol increases the spectral efficiency of cooperative relaying protocols since cooperative relaying protocols are spectral inefficiency because the relay repeats transmission all the time.

Coded cooperative transmission is proposed in [47] wherein each user's codewords are sent via independent fading paths. The basic idea behind coded cooperation is that each user tries to transmit incremental redundancy for other users. Whenever that is not possible, the users automatically revert back to a noncooperative mode. Recently, high performance cooperative transmission strategies based on multiuser detection and network coding were proposed in [48].

Chapter 3: Joint Spatial-Temporal Sensing for Cognitive Radio Networks

3.1 Introduction

In this chapter[1], we discuss the joint spatial-temporal sensing strategy. To recapture the so-called "spectrum holes," various schemes for allowing unlicensed or secondary users to opportunistically access unused spectrum have been proposed. Opportunistic or dynamic spectrum access is achieved by cognitive radios that are capable of sensing the radio environment for spectrum holes and dynamically tuning to different frequency channels to access them. Such radios are often called *frequency-agile* or *spectrum-agile*.

On a given frequency channel, a spectrum hole can be characterized as spatial or temporal. A *spatial* spectrum hole can be specified in terms of the maximum transmission power that a secondary user can employ without causing harmful interference to primary users that are receiving transmissions from another primary user that is transmitting on the given channel. Spectrum reuse in this context is similar to frequency reuse among cochannel cells in a cellular network. A *temporal* spectrum hole is a period of time for which the primary transmitter is idle. During such idle periods, a secondary user may opportunistically transmit on the given channel without causing harmful interference.

Spatial spectrum sensing is investigated [17, 18], wherein the maximum interference-free transmit power (MIFTP) of a given secondary user is estimated based on signal strengths received by a group of secondary nodes. To calculate the MIFTP for a secondary node, estimates of both the location and transmit power of the primary transmitter are estimated collaboratively by a group of secondary nodes. Using these estimates, each secondary node determines its approximate MIFTP, which bounds the size of its spatial spectrum hole. In

[1]The contents of this chapter appeared in [49, 50].

[17, 18], the primary transmitters are assumed to transmit at constant powers. However, this assumption does not allow secondary users to take advantage of temporal spectrum holes. In practice, the primary transmitter may alternate between being active (ON) and idle (OFF).

The problem of detecting when the primary is ON or OFF is called *temporal* spectrum sensing. Cooperative temporal sensing has been studied in [8, 23, 24]. The decision on the ON/OFF status of the primary transmitter can be made either at individual secondary nodes or collaboratively by a group of secondary nodes. Cooperation among secondary nodes for temporal sensing can overcome problems posed by low signal-to-noise ratio (SNR), shadowing, and hidden terminals [8]. A practical solution for cooperative temporal sensing is proposed in [8], whereby individual secondary nodes make decisions about the ON/OFF status of the primary transmitter independently. A fusion center or centralized controller collects the individual hard decisions made by all secondary nodes and then makes a final decision on whether the primary is idle or active. The fusion center is assumed to know the geographic locations of all cooperating secondary nodes and hence can estimate the correlations between their observations. However, the fusion center does not generally have knowledge of the primary's location or transmit power. A suboptimal temporal detector is proposed in [51] based on a linear quadratic (LQ) detector that uses partial statistical knowledge to improve detection performance. As discussed in [8], the LQ detector outperforms a simpler detector based on a counting rule in the regime of moderate to high correlation among the secondary nodes.

In this chapter, we propose a joint spatial-temporal sensing scheme for wireless networks with opportunistic spectrum sharing. We consider the case of a single primary transmitter that alternates between ON and OFF states. During the ON state, secondary nodes perform collaborative spatial spectrum sensing. When the primary transmitter is in the ON state, the secondary nodes employ spatial spectrum sensing to estimate the MIFTP (cf. [17]). Estimation of the MIFTP involves localization of the primary transmitter and estimation of its transmit power. When the primary transmitter is in the OFF state, a given secondary

user can transmit at maximum power. Here, spatial spectrum sensing relies on temporal spectrum sensing in order to determine the ON/OFF state of the primary transmitter. In a pure spatial sensing scheme, the primary transmitter is assumed to be ON at all times. Thus, when the primary is actually OFF for some portion of time, pure spatial sensing will tend to underestimate the transmit power of the primary. Temporal sensing information can be used to trigger spatial sensing activity only during the ON periods of the primary transmitter. This will result in a more accurate estimate of the primary transmitter parameters and hence improve the accuracy of spatial sensing.

Conversely, localization information for the primary transmitter obtained from spatial spectrum sensing are used to improve the performance of temporal sensing. Approximate knowledge of the primary transmitter's location are used to intelligently select a subset of the observations from secondary nodes for temporal sensing. Temporal sensing performance can be improved in this way because the observation set can be selected from the secondary nodes so as to minimize the correlations among the observations. Our simulation results show that the proposed spatial-temporal sensing scheme outperforms pure temporal sensing based on either a counting rule or LQ detector.

We also investigate a multi-level quantization detection strategy for temporal sensing based on the counting rule in which each secondary node sends an m-bit decision to the fusion center. Thus, the observations received from the secondary nodes are quantized to 2^m levels. Previous works on temporal spectrum sensing (cf. [8, 23, 24]) assume that each secondary node sends only a one-bit decision to the fusion center where the final decision is made on whether the primary is ON or OFF. This approach can be useful when there is very limited communication bandwidth between secondary nodes and fusion center, but it leads to significantly poorer performance compared to a centralized approach. A centralized fusion center computes the joint likelihood of all soft observations to obtain the final detection decision. However, the centralized approach is difficult to implement in practice because it requires a relatively large communication bandwidth between the secondary users and the fusion center. Therefore, the proposed multi-level feedback scheme represents a compromise

between the distributed one-bit feedback scheme and the centralized detector.

The remainder of the chapter is organized as follows. Section 3.2 describes the system model for spatial spectrum and temporal spectrum sensing. Section 3.3 develops that joint spatial-temporal sensing scheme and compares its achievable capacity relative to pure spatial and pure temporal sensing schemes. Section 3.4 investigates the performance of temporal sensing based on the counting rule with multi-level feedback. Section 3.5 presents simulation results. Finally, the chapter is concluded in Section 3.6.

3.2 System Model

We consider a discrete-time system model with a single primary transmitter and M secondary users equipped with frequency-agile cognitive radios. The primary transmitter can be in one of two states: an ON state in which it transmits with constant power s_p, and an OFF state in which it does not transmit.

3.2.1 Spatial Spectrum Sensing

All transmissions are assumed to be omnidirectional and the signal propagation follows a lognormal shadowing model. We assume the following path loss model (cf. [52]):

$$L = 10n \log_{10}(d/d_0) + L_0 \text{ [dB]}, \tag{3.1}$$

where d is the distance between transmitting and receiving antennas in meters, L is the path loss in dB, L_0 is the attenuation at a reference distance d_0, $L_0 = 20 \log_{10}(\frac{4\pi}{\lambda})$ and λ is the wavelength in meters. Accounting for the effect of shadowing and noise, the received power at node v due to node p can be represented as a lognormal random variable:

$$R_v = s_p - 10n \log_{10}(d_{p,v}/d_0) + W \text{ [dBm]}, \tag{3.2}$$

where n is the path loss factor, s_p (dBm) is the transmit power of node p at d_0, and $d_{i,j}$ denotes the distance between node i and node j in meters. Here, we approximate the sum of the shadowing and noise powers as a lognormally distributed random variable $W \sim \mathcal{N}(0, \sigma_W^2)$, where σ_W^2 is the shadowing noise variance. We define the path loss function $g(d) \triangleq 10n \log_{10}(d/d_0)$. Then the path loss from node i to node j is given by

$$L_{i,j} \triangleq g(d_{i,j}, n) + W \text{ [dBm]}.$$

We shall make use of some concepts related to spatial spectrum sensing from [17]. The *maximum interference-free transmit power (MIFTP)* of a secondary node is defined as the maximum transmit power on a given channel such that the probability of interference to any potential victim node (i.e., a primary receiver) is less than a prescribed threshold. The *outage probability* of a victim node v with respect to the transmitter p, is the probability that the received power R_v from node p falls below a predetermined detection threshold $r_{\min}$: $P_{\text{out}}(p, v) \triangleq P(R_v < R_{\min})$. The *coverage distance* is the maximum distance between node p and any potential victim node v such that P_{out} does not exceed a predefined threshold $\epsilon_{\text{cov}} > 0$: $d_{\text{cov}}(p) \triangleq \max\{d_{p,v} : P_{\text{out}}(p, v) \leq \epsilon_{\text{cov}}\}$. The *coverage area* of the transmitter p is the disk centered at node p with radius $d_{\text{cov}}(p)$.

The received power at node v from node a is given by $I_v = s_a - g(d_{a,v}) + W$, where s_a is the transmit power of a. The *interference probability* in the spatial domain with respect to a given victim node v is the probability that I_v exceeds a predefined interference tolerance threshold $i_{\max}$: $P_s(a, v) \triangleq P(I_v \geq i_{\max})$. For a single fixed primary transmitter p and FAR node a, the MIFTP is the maximum transmit power of the FAR node such that the interference probability with respect to any potential victim node within the coverage distance from node p does not exceed a threshold $\epsilon_{\text{int}} > 0$:

$$s_a^* \triangleq \max\{s_a : P_s(a, v) \leq \epsilon_{\text{int}}, \forall v : d_{p,v} \leq d_{\text{cov}}(p)\}.$$

The worst-case interference probability is given by

$$P_s(a) \triangleq \max_v P_s(a,v) = Q\left(\frac{i_{\max} - s_a + g(d_a^*)}{\sigma_W}\right). \tag{3.3}$$

where $d_a^* \triangleq d_{p,a} - d_{\text{cov}}(p)$. An approximation for the MIFTP based on received signal strength measurements is developed for the case of a single primary transmitter in [17] and the case of multiple cochannel primary transmitters in [53], respectively.

To mitigate the effect of shadowing and low SNR, cooperation among the secondary nodes is necessary to perform both spatial and temporal spectrum sensing. We assume that all secondary nodes have the same detection distance, i.e., they are equipped with detectors having the same receiver sensitivity. The set of secondary nodes that performs temporal sensing may be different from the set of nodes that performs spatial sensing. Let $\mathcal{S}$ and $\mathcal{T}$ denote the sets of nodes that are involved in spatial sensing and temporal sensing, respectively. The nodes in $\mathcal{S}$ are assumed to be located within a circle centered at primary transmitter location (x_p, y_p) with radius equal to the detection distance $d_{\text{det}}(a)$.

3.2.2 Temporal Sensing Model

We adopt a model of temporal spectrum sensing similar to the one described in [8]. Each node in $\mathcal{T}$ makes an independent decision about the ON/OFF state of the primary transmitter. The fusion center randomly selects a subset $\tilde{\mathcal{T}} \subset \mathcal{T}$ of nodes and requests the ON/OFF decisions from the set of nodes in $\tilde{\mathcal{T}}$. The main task of the fusion center is to decide whether the primary transmitter is in the ON or OFF state. We assume that all secondary nodes use identical energy detectors. Since the nodes in $\mathcal{T}$ are expected to be located relatively close to each other, the distributions of received power at these nodes are assumed to be identical and correlated.

Temporal spectrum sensing can be formulated as a binary hypothesis testing problem in which the fusion center determines whether or not the current mean received power is higher than the received power when the primary transmitter is in the OFF state [8]. We

define two hypotheses: H_0 is the hypothesis that the primary is ON and located close to the secondary nodes, i.e., no spectrum hole exists, and H_1 is the hypothesis that the primary is OFF or far away, i.e., a spectrum hole exists. Thus, under H_1, a secondary node could reuse the frequency channel without causing interference to the primary system. Node $i \in \mathcal{T}$ performs temporal sensing by computing an observation Y_i, obtained by subtracting an estimate of the sum of the noise and interference power from the received power.

Let $\mathbf{Y} = (Y_i : i \in \tilde{\mathcal{T}})$ denote the vector of observations at a given observation epoch. The hypothesis testing problem can then be formulated as follows:

$$H_0 : \mathbf{Y} \sim \mathcal{N}(\alpha \mathbf{1}, \mathbf{\Sigma}), \tag{3.4}$$

$$H_1 : \mathbf{Y} \sim \mathcal{N}(\mathbf{0}, \sigma_0^2 \mathbf{I}), \tag{3.5}$$

with $\alpha \geq \mu$, where $\mu \triangleq E[10 \log_{10}(1+\text{SNR})]$ [dB], and SNR is the signal-to-noise ratio at the secondary nodes at the largest distance from the primary user or, equivalently, the smallest mean received signal-to-noise ratio when the primary is ON. In (3.4) and (3.5), $\mathcal{N}(\mathbf{v}, \mathbf{\Sigma})$ denotes the multivariate Gaussian distribution with mean vector $\mathbf{v}$ and covariance matrix $\mathbf{\Sigma}$ and σ_0^2 is the variance of the noise power under H_1. The symbols $\mathbf{0}$ and $\mathbf{1}$ denote vectors of all zeros and ones, respectively, and $\mathbf{I}$ is the identity matrix of appropriate dimension. The (i, j) element of the covariance matrix $\mathbf{\Sigma}$ is given by $\Sigma_{ij} = \sigma_1^2 \rho^{d_{ij}/D_c}$ where d_{ij} is the distance between nodes i and j in meters, σ_1^2 is the variance of the noise power under H_0, and ρ is the correlation coefficient between secondary nodes separated by a reference correlation distance D_c in meters. The parameter α represents the mean power observed under H_0.

The probability of temporal interference with the primary transmitter is equivalent to the false alarm probability $p_f = P_0(\delta = H_1)$, where δ is the decision rule used by the fusion center and $P_0(\cdot)$ is the probability measure under H_0. In general, the temporal interference probability $P_0(\delta = H_1)$ does not necessarily equal the spatial sensing interference probability

$P_s(a)$ given in (3.3). The temporal sensing system is designed such that the probability of temporal interference is less than or equal to a pre-specified value κ:

$$p_f = P_0(\delta = H_1) \leq \kappa. \tag{3.6}$$

The constraint (3.6) must be satisfied for all values of $\alpha \geq \mu$ in (3.5). Since the prior information about the distribution of the mean power α is unknown, the composite binary hypothesis testing problem given by (3.4) and (3.5) is designed under a robust and universally most powerful detection framework [54]. In other words, the system is designed such that (3.6) is satisfied for the least favorable value of α, i.e., $\alpha = \mu$ [8]. This results in a simple Neyman-Pearson hypothesis testing problem:

$$H_0 : \mathbf{Y} \sim \mathcal{N}(\mu\mathbf{1}, \mathbf{\Sigma}),$$

$$H_1 : \mathbf{Y} \sim \mathcal{N}(\mathbf{0}, \sigma_0^2\mathbf{I}).$$

The final decision δ is made at the fusion center, which has access to only binary-value decisions made individually by the secondary nodes based on the observation vector $\mathbf{Y}$. We denote by U_i the individual decision made by the ith temporal sensing secondary node, based on the observation Y_i. Correspondingly, $\mathbf{U} = (U_i : i \in \tilde{\mathcal{T}})$ denotes the vector of 0-1 hard decisions made by the secondary nodes in $\tilde{\mathcal{T}}$.

Let

$$L(Y_i) \triangleq \frac{p_1(Y_i)}{p_0(Y_i)},$$

denote the likelihood ratio of the observation at node $i \in \tilde{\mathcal{T}}$, where $p_0(\cdot)$ and $p_1(\cdot)$ denote, respectively, the posterior distributions under hypotheses H_0 and H_1, respectively. Then the optimal decision at node i can be represented as $U_i = I_{\{\ln L(Y_i) > \tau\}}$, where I_A denotes

the indicator function of the set A. A secondary node decides H_1 if $U_i = 1$ and otherwise decides H_0. The threshold τ is chosen to ensure that (3.6) is satisfied. The fusion center makes a final decision based on the decision bit vector $\mathbf{U}$.

Under the so-called *counting rule*, the final decision is made by comparing the sum $\sum_{i \in \tilde{\mathcal{T}}} U_i$ to a decision threshold. If the sum $\sum_{i \in \tilde{\mathcal{T}}} U_i$ is greater than the threshold, the fusion center decides H_1 and otherwise decides H_0. The value of this threshold is obtained through simulation [8]. When the observations across all of the nodes are independent and identically distributed under both hypotheses, the counting rule detector is optimal, since the joint likelihood ratio of the bits is a function only type of the number of ones in the received bit vector $\mathbf{U}$. The counting rule detector is also efficient when the correlations between the individual observations Y_i are relatively small.

When the observations at the secondary nodes are correlated, the Linear Quadratic (LQ) detector yields a significant performance gain over the counting rule detector, while still using only partial statistical knowledge about the correlated decision variables [8]. The LQ detector is based on the *generalized signal-to-noise ratio* or deflection criterion, and makes use of fourth-order statistics under H_1 and second order statistics under H_0. We consider a fusion rule based on a class of LQ detectors that compare a linear quadratic function of decision vector to a threshold. The optimal LQ detector is derived in [51] for an arbitrary noise probability distribution with finite fourth order moments. When the observations at the secondary nodes are correlated, the LQ detector provides a simple fusion rule that yields significant performance gain over the Counting Rule while still using only partial statistical knowledge about the correlated decision variables [8].

3.3 Joint Spatial-Temporal Spectrum Sensing

The basic idea of joint spatial-temporal sensing as follows. A group of secondary nodes cooperatively localizes the primary transmitter, e.g., using signal strength observations [17]. Concurrently, a (possibly different) set of secondary nodes performs temporal spectrum

sensing using knowledge of the estimated location and transmit power of the primary transmitter from the spatial sensing process. By performing both spatial and temporal sensing, a group of secondary nodes acquires sufficient knowledge to exploit the presence of both spatial and temporal spectrum holes. In the remainder of this section, we discuss a model for joint spatial-temporal sensing, a heuristic for intelligently node selection for temporal sensing, and capacity expressions for the temporal sensing, spatial sensing, and joint spatial-temporal sensing schemes.

3.3.1 Model

When the primary transmitter is ON, transmitter i transmits with power equal to its estimated maximum interference-free transmit power MIFTP_i. Otherwise, when it is OFF, a given secondary user can transmit with power up to a maximum level P_m. We assume that the secondary users can coordinate among themselves by means of a suitable medium access control (MAC) protocol. Secondary receivers are affected by both large-scale and small-scale fading. The small-scale fading is modeled as Rayleigh block fading where the fading coefficient H_{ii} is constant over N_u time slots, with N_u being the number of transmitter-receiver pairs involved in communications. The shadow fading is modeled by a lognormally distributed random variable [55].

When a temporal spectrum hole occurs, i.e., when the primary transmitter is OFF, a given secondary node can transmit with power up to a maximum level P_m. On the other hand, when the primary transmitter is ON, the secondary node can still transmit, but in this case, its transmit power will be limited to its MIFTP with respect to the primary transmitter. The MIFTP estimated by the secondary node depends on the locations of the secondary node and the primary transmitter, as well as the power of the primary transmitter. The spatial information associated with the primary transmitter must be estimated during the ON state of the primary transmitter. At the same time, the spatial information concerning the primary transmitter can be used to improve the performance of temporal sensing. The availability of more accurate spatial information can improve the

accuracy of temporal sensing, which in turn can improve the accuracy of the estimated spatial information. The simulation results presented in Section 3.5 demonstrate that a significant performance gain can be achieved by joint spatial-temporal sensing relative to pure spatial sensing and pure temporal sensing.

3.3.2 Node Selection for Temporal Sensing

In joint spatial-temporal sensing, the secondary nodes collaboratively perform both spatial and temporal sensing. The primary transmitter parameters estimated via spatial sensing are used to improve the accuracy of temporal sensing. Using the estimated location of the primary transmitter, the fusion center for detecting temporal spectrum holes can intelligently choose a subset of the observation data from the secondary nodes so as to optimize detection performance. We propose two criteria for node selection: (1) minimum distance from the primary transmitter; (2) minimum correlation values between pairs of signal strength observations.

Let $\mathcal{T}$ denote the set of secondary nodes involved in temporal sensing. Then the fusion center fuses the individual decisions from the "best" subset $\tilde{\mathcal{T}}$ of $\tilde{T}$ nodes from the $T = |\mathcal{T}|$ nodes in the set $\mathcal{T}$ based on one of the two criteria. We assume that the fusion center has knowledge of the approximate locations of the nodes in $\mathcal{T}$. In practice, the nodes in $\mathcal{T}$ could send location updates to the fusion center at regular intervals. We remark that the time-scale for location updates would be much larger than that of decision-making for temporal spectrum holes. With knowledge of the locations of the nodes in $\mathcal{T}$, the fusion center can achieve the first criterion straightforwardly: Simply let $\tilde{\mathcal{T}}$ be a subset consisting of the $\tilde{T}$ secondary nodes in $\mathcal{T}$ that are closest to the primary transmitter p.

The second criterion is generally more difficult to achieve. Algorithm 1 is a heuristic that attempts to choose a subset of nodes such that pairs of observations from these nodes have small correlations (cf. [49]). The heuristic initializes $\tilde{\mathcal{T}}$ to be the entire set $\mathcal{T}$ and then successively removes nodes from $\tilde{\mathcal{T}}$ until $|\tilde{\mathcal{T}}| = \tilde{T}$. At each step, the node chosen for

removal from $\tilde{\mathcal{T}}$ is chosen by first finding the pair (a, b) of nodes in $\tilde{\mathcal{T}}$ that are closest to each other. Then a or b is removed from $\tilde{\mathcal{T}}$ according as a or b is farther from the primary transmitter p, respectively. The heuristic of Algorithm 1 is applied in the simulation results discussed in Section 3.5.2.

Algorithm 1 Node selection heuristic for Criterion 2.

```
Input: 𝒯, T̃, d_{i,j}, (i,j) ∈ 𝒯 ∪ {p}; Output: T̃
T̃ ← 𝒯
while |T̃| > T̃ do
    (a,b) ← arg min_{(i,j)∈T̃} d_{i,j}
    if d_{a,p} < d_{b,p} then
        T̃ ← T̃ − {b}
    else
        T̃ ← T̃ − {a}
    end if
end while
```

3.3.3 Achievable capacity

Next, we consider the achievable capacity of the proposed joint spatial-temporal sensing scheme relative to that of pure temporal sensing and pure spatial sensing. We adopt the narrowband spatial capacity model in [56] with the addition of shadow fading. Assume that N_u pairs of secondary transmitters and receivers are placed within a circular region centered at the primary transmitter with radius equal to R. The location of receiver i is assumed to be uniformly distributed over a circular strip bounded by two concentric circles centered at transmitter i, of radius $d_{\min}$ and radius $d_{\max}$, respectively. Under this assumption, the distance D_{ii} has the following pdf (cf. [56]):

$$f_{D_{ii}}(d) = \frac{2d}{d_{\max}^2 - d_{\min}^2}, \quad d \in [d_{\min}, d_{\max}],$$

$i = 1, \ldots, N_u$. In [56], the number of transmitter-receiver pairs, N_u, is assumed to be a Poisson random variable, but for the purposes of this discussion we will assume that N_u is constant. We further assume a time division multiple access (TDMA) model wherein each

frame contains N_u time slots that are scheduled for user transmissions.

Under pure spatial sensing, transmitter i can transmit to receiver i with power level MIFTP_i. Hence, the achievable capacity for the ith transmitter-receiver pair is given by

$$C_{\text{S},i} = B \cdot E\left[\log_2\left(1 + \frac{\text{MIFTP}_i (D_{ii}/d_0)^{-n} W}{N_0 B} |H_{ii}|^2\right)\right], \tag{3.7}$$

where the expectation $E[\cdot]$ is taken with respect to the transmitter-receiver distance D_{ii}, the shadowing noise W and fading coefficients H_{ii}. As in [56], we assume that the channel gain between transmitter i and receiver j is normalized, i.e., $E\{|H_{ij}^2|\} = 1$. Therefore, the average capacity under pure spatial sensing is given by $\overline{C}_{\text{S}} = \frac{1}{N_u}\sum_{i=1}^{N_u} C_{\text{S},i}$.

Let p_{on} and p_{off} denote the probability that the primary transmitter is ON and the probability that it is OFF, respectively. Let $p_d = P_1(\delta = H_1)$ denote the probability of correct detection of a temporal spectrum hole, i.e., the probability that the fusion center correctly decides that the primary transmitter is OFF given that it is in fact in the OFF state. If the primary transmitter is OFF and the fusion center makes a correct detection decision, then secondary node i can transmit with power up to a maximum level P_m. Hence, the achievable capacity under pure temporal sensing for the ith transmitter-receiver pair is given by

$$C_{\text{T},i} = p_{\text{off}} p_d \cdot B \cdot E\left[\log_2\left(1 + \frac{P_m (D_{ii}/d_0)^{-n} W}{N_0 B} |H_{ii}|^2\right)\right]. \tag{3.8}$$

Hence, the average capacity of pure temporal sensing scheme can be expressed as $\overline{C}_{\text{T}} = \frac{1}{N_u}\sum_{i=1}^{N_u} C_{\text{T},i}$.

In joint spatial-temporal sensing, a given secondary node i achieves the temporal sensing capacity $C_{\text{T},i}$ plus additional capacity due to spatial sensing when the primary transmitter is in the ON state. By combining (3.7) and (3.8), we can obtain the achievable capacity of

joint spatial-temporal sensing as follows:

$$C_{\mathrm{ST},i} = C_{\mathrm{T},i} + [p_{\mathrm{off}}(1 - p_d) + p_{\mathrm{on}}(1 - \kappa)]C_{\mathrm{S},i}, \tag{3.9}$$

where κ is the probability of temporal interference with the primary transmitter (cf. (3.6)). Here, we note that there is no spatial capacity gain when the secondary node collides temporally with the primary transmitter, i.e., when the secondary node decides that a temporal hole is present even though the primary transmitter is actually in the ON state. The average capacity under joint spatial-temporal sensing is then given by $\overline{C}_{\mathrm{ST}} = \frac{1}{N_u}\sum_{i=1}^{N_u} C_{\mathrm{ST},i}$.

3.3.4 Overhead

The overhead of joint spatial-temporal sensing compared to pure temporal sensing consists of the additional computation carried out by the fusion center to select the subset of temporal sensing nodes. After the subset of temporal sensing nodes is determined by the fusion center, this set will remain unchanged until the fusion center selects a new subset. In general, the fusion center selects a new subset of temporal sensing nodes when the location of the primary transmitter changes. We assume that the time scale over which the primary transmitter changes its location is much larger than the time scale of its ON/OFF durations. Under this assumption, the extra overhead of joint spatial-temporal sensing compared to temporal sensing is not significant in practice. Compared to pure spatial sensing, the overhead of joint spatial-temporal sensing consists of the overhead of the temporal sensing process. The optimal design of the temporal sensing duration and the associated throughput of a cognitive radio has been studied in [57].

3.4 Temporal sensing with multi-bit feedback

In the counting rule and LQ detectors, all the temporal sensing nodes send only a one-bit decision to the fusion center which fuses all the local hard decisions to arrive at a final decision. We propose an m-bit feedback approach for counting rule detector, whereby each

node divides its observation region into 2^m quantization levels and sends an m-bit decision to fusion center.

3.4.1 Centralized Detector

In centralized detection, a subset $\tilde{\mathcal{T}}$ of secondary nodes sends a set of soft observations Y_i, $i = 1, 2, ..., |\tilde{\mathcal{T}}|$ to the fusion center, where a joint likelihood ratio test on the entire vector $\mathbf{Y}$ is performed. The posterior pdfs are given by

$$f_{\mathbf{Y}}(\mathbf{y}|H_0) = \frac{1}{(2\pi)^{n/2}\det(\Sigma^{1/2})} \exp\left(-\frac{1}{2}(\mathbf{y}-\alpha)^*\Sigma^{-1}(\mathbf{y}-\alpha)\right), \tag{3.10}$$

$$f_{\mathbf{Y}}(\mathbf{y}|H_1) = \frac{1}{(2\pi)^{n/2}} \exp\left(\sum_{i=1}^{|\tilde{\mathcal{T}}|} \frac{-y_i^2}{2\sigma_0^2}\right). \tag{3.11}$$

Combining (3.10) and (3.11) we obtain the joint log likelihood of the received vector at the fusion center as follows:

$$\ln \frac{f_{\mathbf{Y}}(\mathbf{y}|H_1)}{f_{\mathbf{Y}}(\mathbf{y}|H_0)} = \ln(\det \Sigma^{1/2}) - \sum_{i=1}^{|\tilde{\mathcal{T}}|} \frac{y_i^2}{2\sigma_0^2} + \frac{1}{2}(\mathbf{y}-\alpha)^*\Sigma^{-1}(\mathbf{y}-\alpha). \tag{3.12}$$

where $\mathbf{x}^*$ represents the complex conjugate transpose of vector $\mathbf{x}$. The fusion center compares the received log likelihood ratio with a threshold. The threshold is determined such that the false alarm probability is below a predetermined constant κ.

3.4.2 Multi-level quantization

At node i, the log-likelihood ratio $\ln L(Y_i)$ of the observation Y_i is computed. The decision rule at each node is specified as follows:

$$U_i = \begin{cases} 0, & \text{if } \ln L(Y_i) \leq t_l, \\ \theta_i, & \text{if } t_l < \ln L(Y_i) < t_u, \\ 1, & \text{if } \ln L(Y_i) \geq t_u, \end{cases} \tag{3.13}$$

where $0 < \theta_i < 1$ and the region (t_l, t_u) is called the region of no confidence. If the log-likelihood ratio of node i falls into this region, it transmits a soft decision θ_i to the fusion center. The other two complementary regions to (t_l, t_u) are called confidence regions. For a given node i the value of θ_i is quantized using a scalar quantizer $\mathcal{Q}_i$, which maps the input variable θ_i belonging to the interval $[0, 1]$ into the output variable θ_{ij}, $j = 1, 2, \ldots, q$ where $\theta_{i1} = 0$ if $\ln L(Y_i) \leq t_l$ and $\theta_{iq} = 1$ if $\ln L(Y_i) \geq t_u$. The number of quantization levels, q, is constrained by the communication rate of the channel, R_i, $i \in \tilde{\mathcal{T}}$. If m_i is the number of assigned bits, the communication rate satisfies $0 \leq 2^{m_i} \leq R_i$, $i \in \tilde{\mathcal{T}}$.

We consider a uniform quantizer [58] that divides the closed interval $[0, 1]$ into q quantization levels, where 0 and 1 are two of the levels. Hence, the open interval $(0, 1)$ is divided into $q - 2$ quantization levels with uniform step size $\psi = 1/(q - 2)$. If the value of the log-likelihood function falls within the jth quantization interval ($j = 2, 3, \ldots, q - 1$) the quantized value is taken to be the middle of that interval. The transfer characteristic function of the quantizer can be specified as

$$\theta_i = \begin{cases} \theta_{i1} = 0, & \text{if } \ln L(Y_i) \leq t_1, \\ \theta_{ij}, & \text{if } t_{j-1} < \ln L(Y_i) < t_j, \quad j = 2, \ldots, q-1, \\ \theta_{iq} = 1, & \text{if } \ln L(Y_i) \geq t_{q-1}, \end{cases} \tag{3.14}$$

where

$$\theta_{ij} \triangleq \Big(\frac{2j-1}{2}\Big)\psi, \quad i = 1, 2, \ldots \tilde{T}, \quad j = 2, 3, \ldots, q, \tag{3.15}$$

$t_1 = t_l$ and $t_{q-1} = t_u$. At the fusion center, the decision is made by comparing the sum of all received observations to a threshold τ:

$$\delta = \begin{cases} H_0, & \text{if } \sum_{i=1}^{\tilde{T}} \theta_i < \tau, \\ H_1, & \text{if } \sum_{i=1}^{\tilde{T}} \theta_i > \tau. \end{cases} \tag{3.16}$$

Since the detection metric is discrete-valued, *randomization* may be required to achieve equality in the interference probability constraint [54]. *Randomization* for the counting rule detector can be implemented by finding two thresholds

$$\tau_1 = \max\{\nu : P_0(\delta = H_1 | \tau = \nu) < \kappa\}, \tag{3.17}$$

$$\tau_2 = \min\{\nu : P_0(\delta = H_1 | \tau = \nu) > \kappa\}, \tag{3.18}$$

where κ is a threshold that limits the probability of interference for temporal sensing (cf. (3.6)). Let P_{t1} and P_{t2} denote the interference probabilities obtained when using thresholds τ_1 and τ_2, respectively. The thresholds τ_1 and τ_2 are chosen with probabilities $1-p$ and p, respectively, where

$$p = \frac{\kappa - P_{\text{t1}}}{P_{\text{t2}} - P_{\text{t1}}}. \tag{3.19}$$

The average interference probability is then given by

$$\kappa = pP_{\text{t2}} + (1-p)P_{\text{t1}}. \tag{3.20}$$

When the observations are independent or the correlations between observations are small, the counting rule in (3.16) is optimum or near-optimum[58]. However, when the correlations

among the observations are high, the counting rule detector (3.16) performs poorly.

3.5 Numerical results

In this section, we compare the performance gain of the joint spatial-temporal sensing scheme with a pure temporal and spatial sensing schemes via simulation in various scenarios. In all scenarios, we assume that the transmit power, s_p, of the primary transmitter is unknown. Under joint spatial-temporal sensing, the secondary nodes collaboratively estimate both s_p and the location of the primary transmitter. The following parameter settings are used in our simulation experiments:

- $r_{\min} = -30$ dBm, $i_{\max} = -80$ dBm, $\epsilon_{\text{int}} = 0.01$ and $\epsilon_{\text{cov}} = 0.05$;
- $\sigma_W = 4$ dB , $s_p = 80$ dBm, path loss factor $n = 3$, $\sigma_0 = 1$ dB;
- $\sigma_1 = 2.1$ dB, $\mu = 3.4$ dB .

In the simulation experiments for achievable capacity, additional parameter settings are given as follows:

- $d_0 = 1$ m, $r_{\min} = 10$ m, $r_{\max} = 100$ m, $N_u = 50$;
- $P_m = 90$ dBm, $p_{\text{off}} = p_{\text{on}} = 0.5$ and $B = 1$ Hz.

The primary transmitter is located at $L_p = (5, 5)$ km. All secondary nodes are located in a disk of radius $R = 100$ km. The MIFTP values of the secondary nodes range from zero to 60 dBm. The reference distance for temporal sensing nodes may be different from the reference distance in the disk centered at L_p with radius R because the temporal sensing nodes are located very far from the primary transmitter, i.e., where the received SNR = 0 dB. As shown in Fig. 3.1, the locations of $|\mathcal{S}| = 20$ secondary nodes for spatial spectrum sensing are generated randomly with uniform distribution inside the circle centered at L_p with radius equal to $d_{\text{det}}(a)$. All temporal sensing nodes are placed inside a square with the smallest possible mean received SNR = 0 dB. For the simulation results shown in Figs. 2-12,

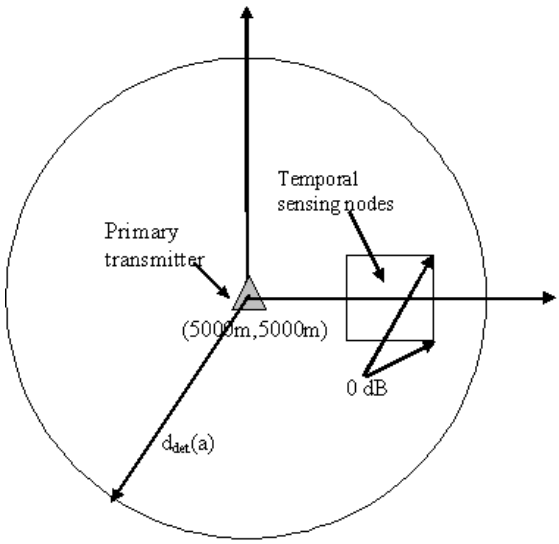

Figure 3.1: Generation of secondary node locations.

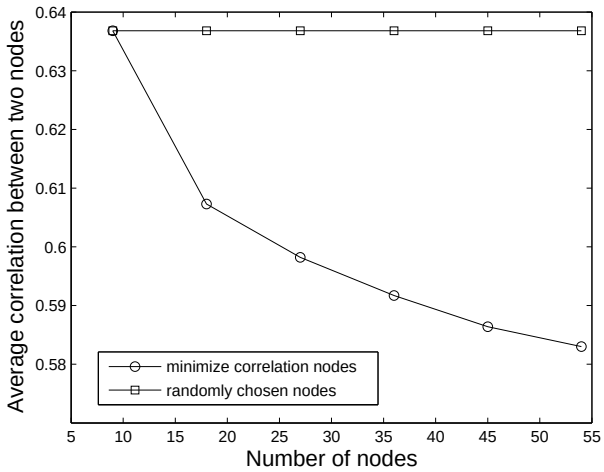

Figure 3.2: Average correlation between the signal strength observations of two nodes over a subset of nodes selected by Algorithm 1 to minimize pairwise correlations.

95% confidence intervals were computed, but they are omitted from the figures to maintain visual clarity of the plots.

3.5.1 High correlation scenario

In the first scenario, we assume the suburban environment correlation model in [59] with $d_0 = 1$ m, correlation coefficient $\rho = 0.6$, and correlation distance $D_c = 250$ m. We place 18 temporal sensing nodes inside the square area indicated in Fig. 3.1 with edge length equal to $D_c/2 = 125$ m. Out of the 18 nodes, nine are placed in fixed locations along the edges of the square, with even spacing. In particular, assume that the bottom left corner of the square has coordinates $(0, 0)$ and the length of an edge is 2. Then the coordinates of the nine fixed locations are: $(0, 0)$, $(0, 1)$, $(0, 2)$, $(1, 0)$, $(2, 0)$, $(1, 1)$, $(1, 2)$, $(2, 1)$, and $(2, 2)$. This placement of the nine nodes is the same as that used in [8]. The remaining 9 nodes are placed inside the square randomly according to a uniform distribution, i.e., the x and y coordinates for each of these nodes are drawn randomly from a uniform distribution on $[0, 2]$. Because the nodes inside the square have different SNRs and the correlation ρ is relatively large, the fusion center chooses the decisions from the nine nodes closest to the primary transmitter based on its estimated location.

Fig. 3.3 compares the detection performance of several temporal spectrum sensing schemes in this scenario. In both figures, the horizontal axis shows the probability of interference, $P_0(\delta = H_1)$. In Fig. 3.3, the performance of a single sensor is shown as the solid line. The performance of pure temporal sensing under the counting rule and the LQ detectors are shown with circles and diamonds, respectively. The LQ detector is seen to clearly outperform the counting rule, which confirms the results in [8]. Performance curves for joint spatial-temporal sensing using the counting rule and LQ detectors are shown with triangles and squares, respectively. The spatial-temporal sensing scheme is carried out using criterion 1 (see Section 3.3). We see that the spatial-temporal LQ detector has the best performance over all values of $P_0(\delta = H_1)$. We also observe that the spatial-temporal counting rule detector performs worse than the temporal LQ detectors when $P_0(\delta = H_1)$ is small and

better when $P_0(\delta = H_1)$ is larger; the crossover point is approximately 0.005. Fig. 3.3 clearly shows the benefit of incorporating spatial information into temporal spectrum sensing.

Fig. 3.4 compares the average capacity of joint spatial-temporal sensing vs. pure temporal and pure spatial sensing. Clearly, the capacity achieved by the joint spatial-temporal scheme is significantly higher then that of the other schemes. In this figure, two performance curves associated with pure spatial sensing are shown. The curve labelled "spatial sensing" corresponds to the performance of a pure spatial sensing scheme when the primary transmitter is ON at all times. In this case, the secondary cannot benefit from the time intervals during which the primary transmitter may be OFF. The curve labelled "spatial sensing 2" shows the performance of a pure spatial sensing scheme operating in the presence of a primary transmitter that follows an ON-OFF pattern, but no additional temporal sensing information is employed. In this case, the MIFTP calculated by the secondary node varies over time due to the ON-OFF pattern of the primary transmitter, but the MIFTP cannot be determined accurately because signal strength measurements are taken by the secondary node regardless of whether the primary transmitter is ON or OFF. As a result, the MIFTP computed by a pure spatial sensing scheme at a given time may underestimate or overestimate the permissible transmit power. The latter case may result in harmful interference to primary users, while the former case may result in inefficient spectrum use. We observe from Fig. 3.4 that the capacity performance of "spatial sensing 2" is significantly poorer than that of the joint temporal-spatial schemes, though slightly better than that of "spatial sensing."

Note that the LQ-based detectors perform better than the counting rule based detectors, which one would expect, due to the relatively high correlation in this scenario.

3.5.2 Moderate correlation scenario

In the second simulation scenario, we set $d_0 = 100$ m, $\rho = 0.3$, correlation distance $D_c = 300$ m. All nodes in $\mathcal{T}$ have almost the same received SNR. In this scenario, we have $|\mathcal{T}| = 18$ total nodes for temporal sensing, which are located randomly in the square shown

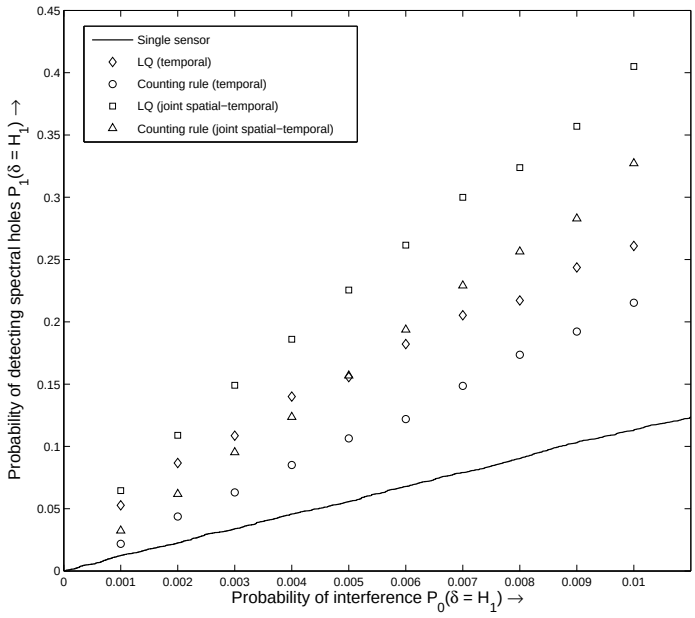

Figure 3.3: Spatial-temporal sensing vs. temporal sensing with $\rho = 0.6$.

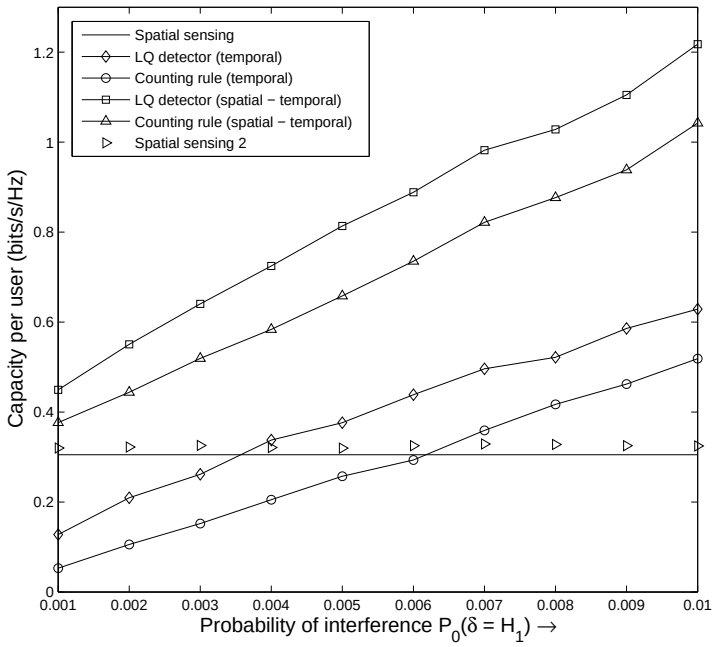

Figure 3.4: Achievable capacity gain of joint spatial-temporal sensing, spatial sensing, and temporal sensing with $\rho = 0.6$.

in Fig. 3.1 according to a uniform distribution. A subset, $\tilde{\mathcal{T}}$ of $\tilde{T} = 9$ nodes is chosen from the original set $\mathcal{T}$ according to one of the two criteria discussed in Section 3.3. Fig. 3.5 compares the performance of the following four joint spatial-temporal detectors: (1) LQ detector under criterion 1; (2) Counting rule detector under criterion 1; (3) LQ detector under criterion 2; (4) Counting rule detector under criterion 2.

In this scenario, the heuristic given as Algorithm 1 in Section 3.3 is used to implement criterion 2 approximately. Fig. 3.2 shows that the heuristic succeeds in reducing the average correlation between two nodes. As expected, the reduction in average correlation improves as the total number of secondary nodes increases. From Fig. 3.5, we observe that when the correlation is small and the received SNRs are similar, better performance is achieved with criterion 2, i.e., the nodes are selected using Algorithm 1. Under criterion 2, the counting rule detector outperforms the LQ detector because criterion 2 achieves low correlation among the observations, and when the correlation is small the counting rule detector outperforms the LQ detector according to [8]. However, under criterion 1, the LQ detector still outperforms the counting rule detector because the correlation remains relatively high. In Fig. 3.6, capacity gains of the proposed scheme under both criteria are compared with that of a pure spatial sensing scheme. It can be seen that the use of criterion 2 achieves the largest capacity gain over spatial sensing.

In Fig. 3.7, we compare the performance of Algorithm 1 relative to an optimal selection of nodes. The optimal node set is found through simulation by searching over all possible node combinations. There are $\binom{|\mathcal{T}|}{|\tilde{\mathcal{T}}|}$ possible combinations, where $\mathcal{T}$ is the set of all nodes in the square area and $\tilde{\mathcal{T}}$ is the selected subset. In our simulations, we set $|\mathcal{T}| = 9$ and $|\tilde{\mathcal{T}}| = 5$. It can be seen that the performance of achieved by Algorithm 1 is quite close to that of an optimum node selection strategy. We remark that finding the optimum node subset is impractical when the number of combinations $\binom{|\mathcal{T}|}{|\tilde{\mathcal{T}}|}$ is large.

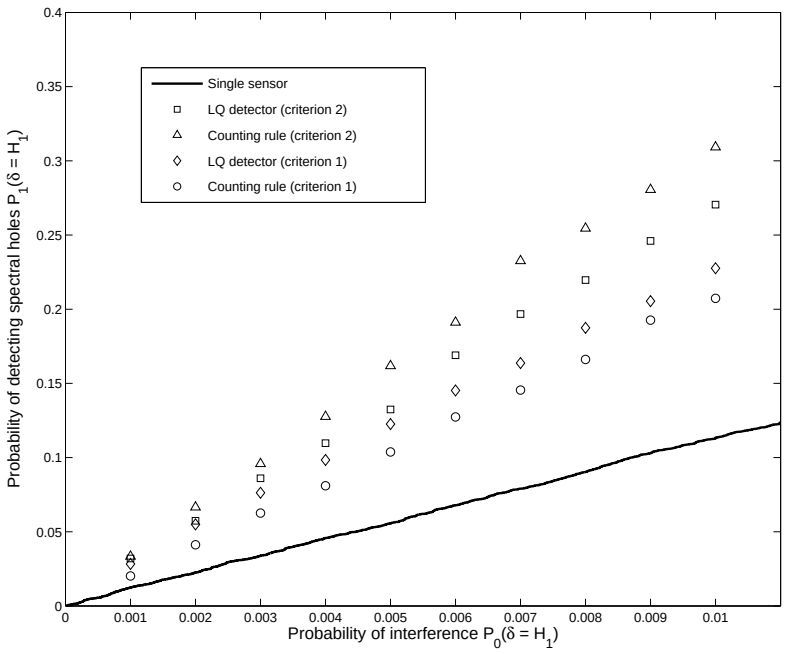

Figure 3.5: Joint spatial-temporal sensing with different node selection criteria and $\rho = 0.3$.

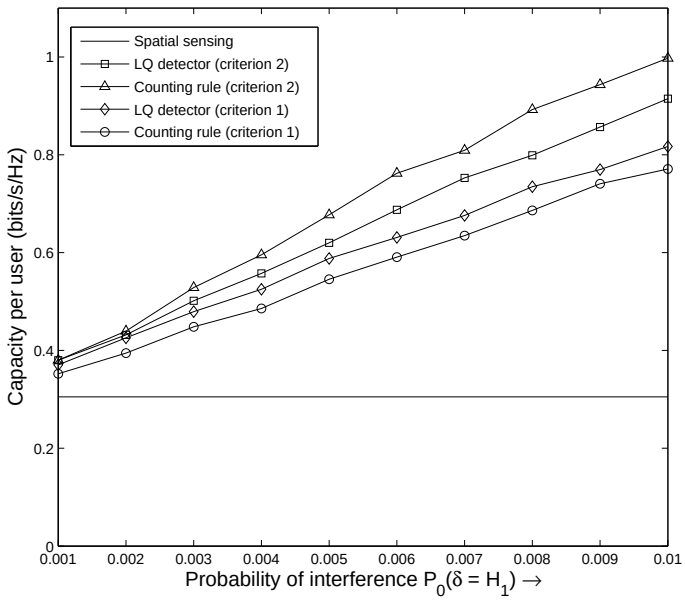

Figure 3.6: Achievable capacity gain of joint spatial-temporal sensing with $\rho = 0.3$

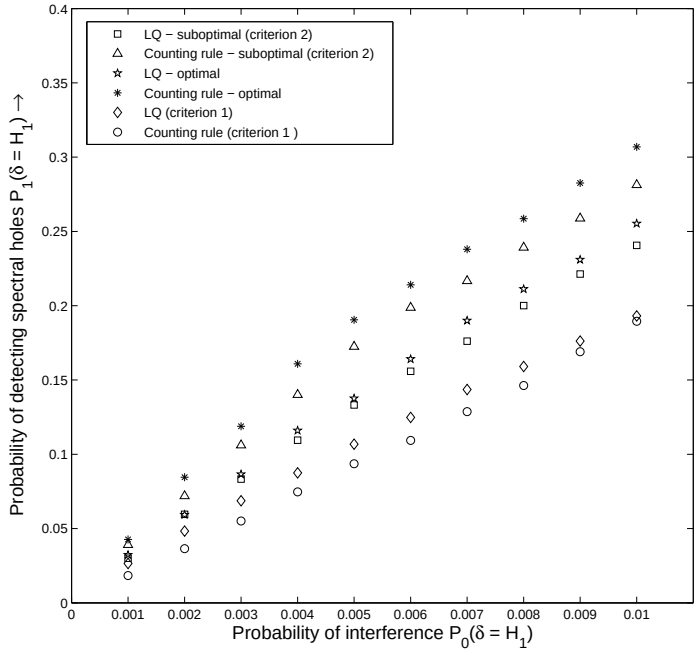

Figure 3.7: Performance of optimum node selection vs. node selection based on Algorithm 1 with correlation parameter $\rho = 0.3$.

3.5.3 Multi-bit feedback scheme

In Fig. 3.8, we compare the performance of multi-bit counting rule temporal sensing in terms of detection probability and capacity vs. single-bit temporal sensing in a low correlation scenario with $\rho = 0.2$. In this scenario, 9 nodes are uniformly distributed over the coverage area. In a region where the correlation is low, the multi-bit scheme significantly outperforms the counting rule detector. However, when the correlation parameter is high, the multi-bit scheme does not perform well, as shown in Fig. 3.9. This is because the detection rule at the fusion center is based on the counting rule, which performs well only when the correlation is small. The results of Fig. 3.9 also confirm that in a region with high correlation, the performance of the LQ detector is higher than that of counting rule based detection schemes. In Fig. 3.10, we compare the performance of the pure temporal LQ detector, the pure temporal counting rule detector, and pure temporal and joint spatial-temporal sensing with multi-level quantization ($m = 2$). The correlation parameters are set as follows: $\rho = 0.3$,

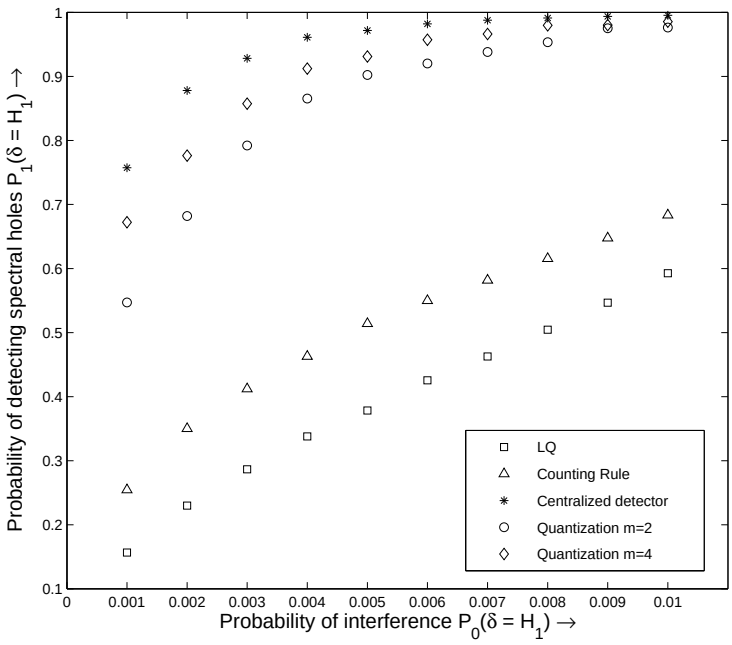

Figure 3.8: Performance of multi-level quantization vs. other hard decision detection rules, $\rho = 0.2$.

$d_0 = 100$ m, $D_c = 300$ m. A total of $|\mathcal{T}| = 18$ nodes perform temporal sensing and are located randomly in the square shown in Fig. 3.1 according to a uniform distribution. A subset, $\tilde{\mathcal{T}}$, of 9 nodes is chosen from the original set $\mathcal{T}$ using Algorithm 1, which seeks to minimize the correlation between nodes. In Fig. 3.11, we compare the capacity of the joint spatial-temporal sensing scheme with 2-bit feedback vs. pure temporal and spatial sensing. We see that the capacity achieved by joint spatial-temporal sensing is significant higher than that of the pure temporal and spatial sensing schemes. Fig. 3.12, shows the performance of the LQ detector, counting rule detector, and multi-bit counting rule detector with $m = 2$ and $m = 4$ as a function of the correlation parameter ρ and the interference probability constraint $P_0(\delta = H_1) = 0.003$. Again, the LQ detector has the best performance when ρ is large while the counting rule detector and multi-level counting rule detector perform well when ρ is small. When the correlation is high, increasing the number of bits m for multi-level feedback system does not improve the system performance appreciably. Note that the performance curves for the counting rule based detectors decrease monotonically as functions of the correlation parameter ρ. On the other hand the performance curves for

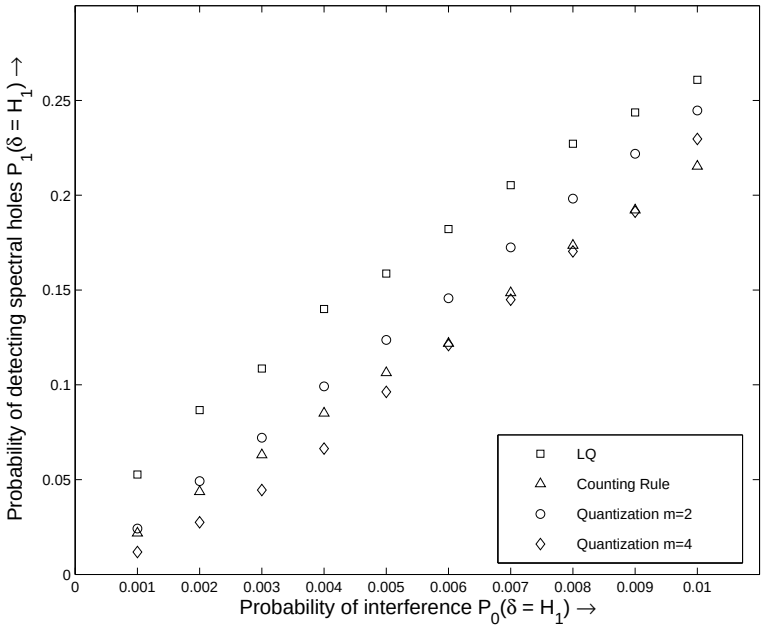

Figure 3.9: Performance of multi-level quantization vs. other hard decision detection rules, $\rho = 0.6$.

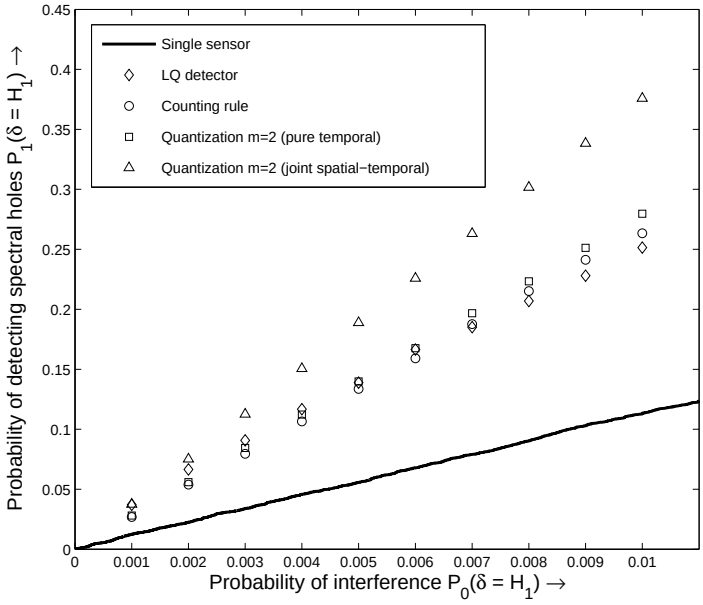

Figure 3.10: Performance of multi-bit feedback detector vs. LQ and counting rule detectors, $\rho = 0.3$.

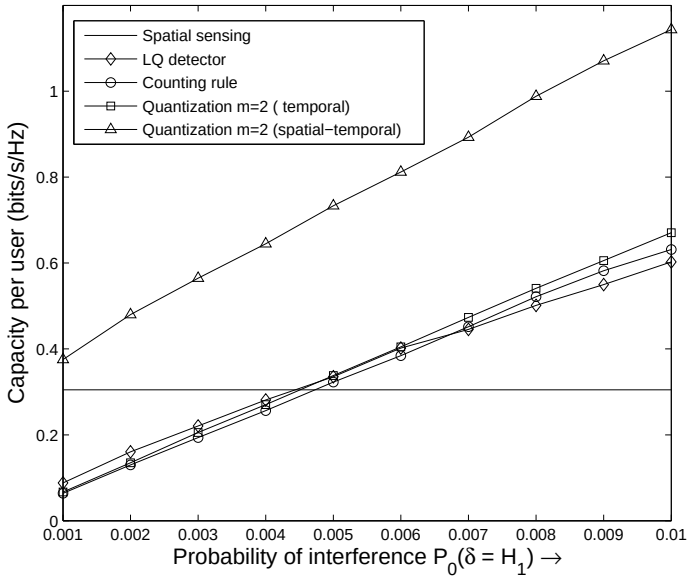

Figure 3.11: Capacity gain of joint spatial-temporal sensing with 2-bit feedback.

the LQ detector and the centralized detector are non-monotonic: they first decrease and then increase as functions of ρ. This can be explained in terms of two different features that can be exploited in the hypothesis testing problem given by (3.4) and (3.5). When the correlation parameter ρ is small, the two hypotheses are distinguishable mainly by the mean values of the observations. In this case, the counting rule based detectors are expected to perform well. On the other hand, when ρ is larger, the two hypotheses are more distinguishable in terms of second-order statistics, which the counting rule fails to capture. On the other hand, the LQ and centralized detectors exploit both features; hence, as we observe in the results, the performance curves first decrease and then increase as ρ increases.

3.6 Conclusion

We proposed a joint spatial-temporal sensing scheme for opportunistic spectrum sharing in cognitive radio networks. The system model consists of a primary transmitter with unknown location and transmit power, which alternates between ON and OFF states, with respect to

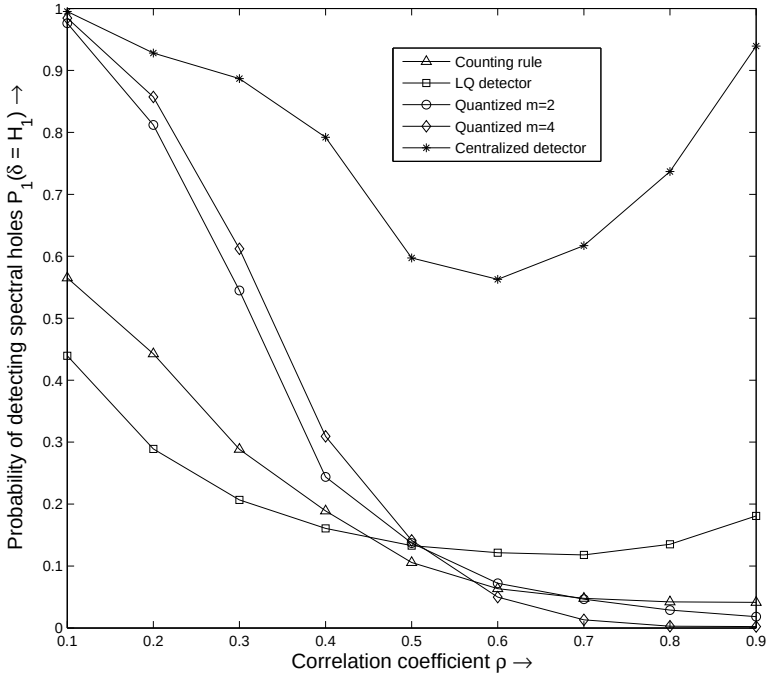

Figure 3.12: Comparison of performance of LQ, Counting Rule and multi-bit feedback detectors as functions of correlation parameter ρ with $P_0(\delta = H_1) = 0.003$.

a given frequency channel. Spatial spectrum sensing is employed to estimate the maximum interference-free transmit power for a secondary node during an ON period. Estimates of the primary transmitter's location and transmit power obtained in the course of spatial sensing are used by a fusion center to select a subset of the secondary nodes to make a temporal sensing decision, i.e., a decision as to whether the primary is ON or OFF. Three distributed temporal sensing algorithms were considered: the counting rule detector, linear quadratic detector and counting rule with multi-bit feedback. By incorporating spatial information, we obtained joint spatial-temporal versions of these detectors. We derived the achievable capacity for pure temporal sensing, pure spatial sensing, and joint spatial-temporal sensing.

Our simulation results show that joint spatial-temporal sensing significantly outperform pure temporal sensing in terms of probability of spectrum hole detection and capacity gain. In this chapter, we assumed only a single primary transmitter on a given frequency channel.

Chapter 4: Spectrum Sensing with Multiuser Diversity

4.1 Introduction

In this chapter[1], we focus on the cooperative spectrum sensing with multiuser diversity. In general, spectrum sensing can be performed either at individual secondary node or by a group of cooperative secondary nodes. Cooperative sensing has been studied in a number of papers[8,23,24]. Cooperation between secondary nodes can mitigate the effects of low signal to noise ratio (SNR), shadowing, and hidden terminals [8]. In cooperative sensing, secondary users at different locations sense the channel independently and send their observation to a fusion center. They can communicate either the soft information about the channel or a one-bit hard decision to the fusion center [61]. The optimum soft combination is derived in [61] wherein the optimal weight coefficients are identical to *maximal ratio combining* (MRC).

In a wireless network with fading, different users experience different channel fading conditions during the same observation period. Multiuser diversity can be exploited by scheduling users to transmit when their channel conditions are favorable [40]. Multiuser diversity systems can be centralized or distributed. In centralized systems, a central processor maintains channel state information for all users and always schedules the user with the best channel for transmission. In distributed multiuser diversity systems, each user has knowledge of its own channel state, but has knowledge of the fading levels of other users. In [41], Qin and Berry proposed a distributed approach for exploiting multiuser diversity based on a protocol called channel-aware slotted ALOHA wherein each user decides, based on the channel state, in which slot to transmit and how much power to use.

[1]The contents of this chapter appeared in [60].

The design of a multiuser diversity system should consider two important issues: fairness and delay [62]. In the ideal situation when users fading statistics are the same, the multiuser diversity maximizes not only the total capacity of the system but also the throughput of individual users. However, in reality, users that are closer to the base station have a better average SNR. Some users are stationary, while others are moving. A pure multiuser diversity strategy maximizes long-term average throughput, without regard to delay requirement.

In this chapter, we propose a distributed approach to spectrum sensing that exploits multiuser diversity among secondary users to improve sensing capability in cognitive radio networks. We adopt a cooperative sensing framework is to overcome low SNR and shadowing. Unlike traditional multiuser diversity schemes for wireless networks, fairness and delay issues can be ignored in spectrum sensing scenario because the only performance metric of interest is the detection probability. We consider two cases: when secondary users are equipped with single antenna and multiple antennas. We also propose a MAC protocol bases on carrier sense multiple access (CSMA) protocol to facilitate the transmission of observation from secondary users to fusion center. The opportunistic MAC protocols which exploit multiuser diversity have been investigated in literature. In [63], Zhao and Tong investigated the opportunistic CSMA for energy-efficient information retrieval in sensor networks. The key idea in [63] is to exploit the channel state information (CSI) in the backoff strategy of carrier sensing in which the backoff time is a decreasing function of CSI. This scheme ensures that only sensor with the best channel transmit. In [64], authors incorporate multiuser diversity into p-persistent CSMA. In [64], each user will send a packet if the CSI is above threshold which is determined such that the probability of accessing the medium is p. The proposed opportunistic p-persistent CSMA has a significant capacity increasing compare to traditional p-persitent CSMA. Also in [65], Hwang and Cioffi investigated the opportunitic CSMA/CA to achieve multi-user diversity in wireless LAN. In this chapter, our MAC protocol uses different backoff window to exploit the multiuser diversity inherent in secondary networks. We name our MAC protocol as cognitive CSMA MAC protocol

which controls the communication between secondary users and fusion center. Our numerical results show that the proposed spectrum sensing scheme significantly outperforms schemes that do not exploit multiuser diversity. Furthermore, we show by simulation the benefit of using multiple antennas for spectrum sensing.

The remainder of the chapter is organized as follows. Section 4.2 describes the system model. Section 4.3 proposes the distributed scheme for exploiting multiuser diversity to improve the sensing capability. Section 4.4 proposes a practical MAC protocol for coordination of transmission between secondary users and fusion center. Section 4.5 presents simulation results. Finally, the chapter is concluded in Section 4.6.

4.2 System Model

We consider a discrete-time system model with a single primary transmitter and S secondary users equipped with frequency-agile cognitive radios. Each user make a local decisions about the presence of the primary user and communicate a one-bit hard decision to the fusion center, which makes the final decision. Alternatively, the system can operate in a distributed manner wherein secondary users exchange their local decisions with each user. Without loss of generality, we shall assume a fusion center in this chapter.

Due to communication constraints between secondary users and the fusion center, not all the secondary users are able to communicate their decisions to fusion center. We assume that N out of S secondary users are able to communicate with the fusion center. Because of multiuser diversity, each of the S secondary users has different fading channel parameters during a given observation time period.

We adopt a spectrum sensing model similar to that in [61]. Each secondary user uses M samples for energy detection. We define two hypotheses: H_1 is the hypothesis that the primary is ON and located close to the secondary nodes and H_0 is the hypothesis that the primary is OFF or far away. In other words, H_0 is the hypothesis that the spectrum hole exists and the frequency channel is available for reuse by secondary users. The observed

energy value at the jth user is given by

$$Y_j = \begin{cases} \sum_{i=1}^{M} n_{ji}^2, & \text{under } H_0, \\ \sum_{i=1}^{M} (s_{ji} + n_{ji})^2, & \text{under } H_1, \end{cases} \tag{4.1}$$

where n_{ji} is the white noise signal in the ith sample of the jth user and s_{ji} denotes the received primary signal at each secondary user, $1 \leq j \leq N$, $1 \leq i \leq M$. The noise samples n_{ji} are assumed to be independently and identically distributed (i.i.d.) Gaussian random variables with zero mean and unit variance.

The instantaneous SNR of the jth secondary user is defined as

$$\gamma_j \triangleq \frac{1}{M} \sum_{i=1}^{M} s_{ji}^2.$$

Following [61], we assume that the total energy of the transmitted primary signal is constant within each observation block. Thus, the γ_j's represent the power of the instantaneous channel gain and can be modeled by a Rayleigh or Nakagami distribution [66] and are i.i.d. over different secondary users j and observation block. Within a given observation block, multiuser diversity exists because of the differences in γ_j across users.

If the primary user is absent or in the OFF state, Y_j can be modeled as a central chi-square random variable with M degree of freedom. Otherwise, if the primary user is in the ON state, Y_j follows a non-central chi-square distribution with M degree of freedom and a non-centrality parameter $\lambda_j = M\gamma_j$ [61]:

$$H_0: \; Y_j = \chi_M^2,$$

$$H_1: \; Y_j = \chi_M^2(\lambda_j).$$

For large M, Y_j can be approximated by a Gaussian distribution [61]:

$$H_0: \; Y_j \sim \mathcal{N}(M, 2M),$$

$$H_1: \; Y_j \sim \mathcal{N}(M(1+\gamma_j), 2M(1+\gamma_j)). \tag{4.2}$$

In [61], a Gaussian approximation of the received energy distribution is used to derived the optimal soft combination weights. The weighted summation at fusion center is given by

$$Y = \sum_{j=1}^{N} \omega_j Y_j. \tag{4.3}$$

The distribution of Y can be approximated by a Gaussian distribution as follows: Under H_0,

$$H_0: \; Y \sim \mathcal{N}\left(M\sum_{j=1}^{N}\omega_j, 2M\sum_{j=1}^{N}\omega_j^2\right)$$

$$H_1: \; Y \sim \mathcal{N}\left(M\sum_{j=1}^{N}(1+\mu_j), 2M\sum_{j=1}^{N}\omega_j^2(1+\mu_j)\right). \tag{4.4}$$

The fusion center chooses hypothesis H_1 if $Y > \tau_f$ and H_0 otherwise, where τ_f is the decision threshold at the fusion center. The performance metrics of interest are the false probability and the detection probability:

$$P_F \triangleq \Pr\{Y > \tau_f | H_0\}, \quad P_D \triangleq \Pr\{Y > \tau_f | H_1\}.$$

For a given false alarm probability, the objective is to maximize the probability of (correct) detection. The performance of different sensing schemes can be evaluated by comparing P_D at a predetermined P_F value.

4.3 Multiuser Diversity Spectrum Sensing

In this section, we develop a multiuser diversity spectrum sensing scheme for cognitive radio networks. There are S total number of secondary nodes equipped with identical energy detector. The energy distribution between secondary nodes are i.i.d. with some distribution i.e., Rayleigh or Nakagami fading distribution. We consider the case of secondary users equipped with a single antenna and with multiple antennas.

4.3.1 Soft combination

Let τ_l and τ_u be predefined lower and upper thresholds, respectively, where $\tau_l < \tau_u$. In the proposed scheme, a node j ($j = 1, \ldots, S$) with received energy level satisfying

$$Y_j > \tau_u \quad \text{or} \quad Y_j < \tau_l \tag{4.5}$$

sends its observation to the fusion center. As stated earlier, we assume that communication capacity of the channel between the secondary nodes and the fusion center is limited such that only N out of S nodes can communicate with the fusion center. If the number of nodes with received energy level satisfying (4.5) is $\tilde{N} < N$, then $N - \tilde{N}$ nodes are randomly chosen to communicate theirs observations to the fusion center. This guarantees that the total number of observation sent to fusion center is always equal to N. There is a dedicated control channel for enabling the communication between secondary users and fusion center. We also assume that there exists a *perfect* MAC protocol that coordinates transmissions between secondary nodes and fusion center. A practical MAC protocol based on CSMA is proposed in section 4.4.

To understand the benefit of exploiting multiuser diversity, we consider a simple soft information equal gain combining (EGC) strategy at the fusion center:

$$Y = \sum_{j=1}^{N} Y_j.$$

The distribution of Y can be approximated by a Gaussian distribution as given in (4.4) with $\omega_j = 1, j = 1, 2 \ldots, N$ for EGC. For $S \gg N$, the thresholds τ_l and τ_u can be chosen such that

$$\Pr(Y_j < \tau_l | H_1) \approx 0, \quad \Pr(Y_j > \tau_u | H_0) \approx 0, \quad j = 1, 2, \ldots S.$$

Suppose that $\tilde{N} > 0$ nodes satisfy (4.5) and denote their received energy levels by

$$\tilde{Y}_j, \quad j = 1, \ldots \tilde{N}.$$

Under hypothesis H_1, the following inequality holds with probability one:

$$\sum_{j=1}^{\tilde{N}} \tilde{Y}_j \geq \sum_{j=1}^{\tilde{N}} Y_j,$$

where $\{Y_j\}_{j=1}^{N}$ denotes a set of observations that does not exploit multiuser diversity; i.e., a set of N out of S nodes is randomly selected to send their observations to fusion center. Hence,

$$\tilde{Y} = \sum_{j=1}^{\tilde{N}} \tilde{Y}_j + \sum_{j=\tilde{N}+1}^{N} Y_j \geq Y = \sum_{j=1}^{N} Y_j, \tag{4.6}$$

where the inequality is understood to hold almost surely. Thus,

$$P_{\text{mud}} \triangleq \Pr\{\tilde{Y} > \tau_f\} \geq \Pr\{Y > \tau_f\} \triangleq P_c \tag{4.7}$$

where P_{mud} and P_c denote the detection probability of the multiuser diversity spectrum sensing scheme and a conventional scheme, respectively. Therefore, multiuser diversity spectrum sensing results in a superior detection probability compared to conventional spectrum sensing. A similar approach can be applied for hypothesis H_0. In this case, the false alarm probability of the multiuser diversity spectrum sensing scheme can be shown to

be smaller than that of conventional scheme. Simulation results presented in Section 4.5 validate the benefit of exploiting multiuser diversity for spectrum sensing.

The optimal soft combination is derived in [61], where the optimal weight coefficient is

$$\omega_j = \frac{\gamma_j}{\sqrt{\sum_{k=1}^{N} \gamma_k^2}}, \tag{4.8}$$

γ_j is the instantaneous SNR, and the soft combination rule is given by (4.3). Since ω_j derived in (4.8) is similar to *maximal ratio combining* (MRC), we refer to this approach as the MRC scheme. In this case, the fusion center compares the obtained soft combination metric Y in (4.3) with a predetermined threshold τ_f and decides on hypothesis H_1 if $Y > \tau_f$ and H_0 otherwise. The value of τ_f is determined by simulation [61] such that the probability of interference is smaller than or equal to a threshold on the probability of false alarm, P_F.

4.3.2 Hard combination

The soft combination scheme may be impractical due to the overhead in sending the observation data to the fusion center. As an alternative, a hard combination scheme could be adopted at fusion center. In this scheme, each node compares its observation Y_j with a given threshold τ_n. If Y_j satisfies (4.5), the node will send a hard decision $U_i = 1$ to the fusion center if $Y_j > \tau_n$ and $U_i = 0$ otherwise:

$$U_i \triangleq I_{\{Y_i > \tau_n\}},$$

where I_A denotes the indicator function on the event A. At the fusion center two fusion rules that could be applied are:

1. 1 out of N (OR) rule [67]: The primary signal will be declared present if any one of the cooperative users decides locally that the primary signal exists.

2. Counting rule: The final decision is made by comparing the sum $\sum_{i=1}^{N} U_i$ to a decision

threshold. The value of this threshold is obtained through simulation [8].

The threshold at each node τ_n for the OR rule is also determined by simulation such that the constraint on the probability of false alarm is satisfied at the fusion center. However, the 1 out N rule tends to have a high probability of false alarm [67]. Moreover, this rule may not be used in case communication is not available between the secondary nodes and the fusion center. The counting rule ensures that the constraint on the probability of false alarm is met both at individual nodes and at the fusion center. However, *randomization* between two fusion thresholds may be required at the fusion center in order for the counting rule to achieve the false alarm probability constraint [8].

4.3.3 Multiple antenna case

We now extend the preceding discussion for the case when each secondary user has N_t antennas. As before, we assume that the primary transmitter has a single antenna as before. An energy detector is used at each antenna of the secondary user. We assume that the distance between the antennas is sufficiently far that the fadings for the attennas may be considered i.i.d. Assume that M samples are collected at each detector. The observed energy from the kth antenna at a node j is given by

$$Z_{j,k} = \begin{cases} \sum_{i=1}^{M} n_{ji}^2, & \text{under } H_0, \\ \sum_{i=1}^{M} (s_{ji} + n_{ji})^2, & \text{under } H_1, \end{cases} \tag{4.9}$$

For a multiple receive antenna system, *equal gain combination* (EGC) is used [61]:

$$Y_j = \sum_{k=1}^{N_t} Z_{j,k}, \quad j = 1, \ldots, S, \tag{4.10}$$

where Y_j is the combined total received energy at the output of secondary user j. We then compare Y_j with two thresholds $\tilde{\tau}_u$ and $\tilde{\tau}_l$. If Y_j satisfies

$$Y_j > \tilde{\tau}_u \quad \text{or} \quad Y_j < \tilde{\tau}_l \tag{4.11}$$

then node j will communicate its observation to the fusion center.

Similar to the single antenna scenario, if the number of nodes with energy level satisfying (4.11) is smaller than N, say $\tilde{N}$, then $N - \tilde{N}$ nodes are randomly chosen to communicate their observations to the fusion center. This guarantees that the number of observations sent to fusion center is always equal to N. As before, we assume that there exists a MAC protocol that coordinates transmissions between the secondary nodes and fusion center. In the multiple antenna case, we assume that the each user sends only a one-bit hard decision to the fusion center for hard combination. If the observation Y_j satisfies $Y_j > \tilde{\tau}_n$, then node sends the value 1 to the fusion center and 0 otherwise. The 1 out of N or the counting rules can be used at fusion center as the detection rule. The threshold $\tilde{\tau}_f$ at the fusion center and the thresholds $\tilde{\tau}_n$ and $\tilde{\tau}_n$ are determined by simulation to meet the false alarm probability requirement.

4.4 Cognitive CSMA MAC protocol

In this section, we develop a cognitive CSMA MAC protocol for secondary users transmit their observation to fusion center. The proposed cognitive MAC is used for the communication between secondary user and fusion center during spectrum sensing period. Clearly, a different MAC protocol may be used for communication between secondary users during spectrum hole period. We assume there exists a control channel for secondary users to exchange information with fusion center. Also, the physical layer between fusion center and user is assumed to be perfect, i.e., the fusion center receive what the users send without error. Our proposed opportunistic MAC protocol based on CSMA 802.11 standard protocol [68]. In our scenario, the MAC protocol is used to communicate secondary users to fusion

center. Therefore, there is no hidden terminal issue and Request to Send/Clear to Send (RTS/CTS) packets can be ignored.

The time scale is divided in to time slots and user is allowed to transmit only at the beginning of each time slot. If a secondary user want to communicate its observation to fusion center, it monitors the channel activity. If the channel is idle for a specified time period i.e., distributed interframe space (DIFS) in 802.11 standard, the secondary user transmits. Otherwise, if the channel is busy, the user continue to monitor the channel until it is idle for a DIFS. If the channel is sensed idle for DIFS, user generate a random backoff interval before transmitting (802.11 collision avoidance feature). We accept the exponential backoff scheme in 802.11 standard with modification to exploit multiuser diversity. Each user i will generate random backoff time which is randomly chosen in the range $(0, w_i - 1)$. The value w_i is called contention window of user i. At first transmission attempt or after a successful transmission, $w_i = CW_1$ if the observation Y_i satisfies condition in (4.5) otherwise $w_i = CW_2$. After each failed transmission, i.e., when there is more than one user transmit at the beginning of a time slot, w_i is doubled until it reach CW_{max} where $CW_{max} = 2^m CW_1$ if Y_i satisfies condition in (4.5) otherwise $CW_{max} = 2^m CW_2$.

The backoff time counter is decremented as long as the channel is sensed idle, frozen when the channel is busy. When the backoff time counter reaches zero, user transmit its observation to fusion center. We choose $CW_1 \ll CW_2$. Hence, users satisfying condition in (4.5), will likely have a smaller random backoff timer and have channel access with higher probability. The fusion center will make the final decision whenever it receives the observations of N users.

4.5 Numerical Results

In this section, we compare the performance of the proposed multiuser diversity spectrum sensing scheme with a conventional scheme that does not exploit multiuser diversity. The following parameters are used for all simulations

- False alarm probability requirement $\tau_{\text{FA}} = 0.01$;
- Number of samples $M = 6$;
- Number of secondary nodes $N = 4$.
- $CW_1 = 8$, $CW_2 = 64$, $m = 3$

In all simulations, we use the dotted line for the performance with cognitive MAC protocol. In Fig. 4.1, we compare the performance of multiuser diversity spectrum sensing with conventional spectrum sensing when soft optimal combination and the 1 out N rule are used at the fusion center. Here, the total number of users is $S = 12$. We reproduce the results for conventional 1 out of N rule and optimal soft combination considered in [61] and compare with the corresponding results from the multiuser diversity scheme. The thresholds τ_u and τ_l are chosen to satisfy

$$P(Y_i < \tau_l | H_0) = \frac{N}{S} \text{ and } P(Y_i > \tau_u | H_1) = \frac{N}{S}. \tag{4.12}$$

These thresholds can easily be calculated using (4.2). The threshold τ_n is set by simulation to meet the false alarm probability requirement. We can see that the performance in term of detection probability of our scheme is much better than that of conventional scheme especially when the signal-to-noise ratio is relatively small. For $S = 12$ and $N = 4$, the hard combination (OR rule) with multiuser diversity can outperform the optimal soft combination scheme. In Fig. 4.2, we compare the performance of cognitive MAC protocol over different value of $CW2$. The performance of OR rule with cognitive MAC approaches the performance of OR rule with perfect MAC protocol at $CW2 = 64$. However, there is a MAC delay trade-off when increasing the $CW2$. In Fig. 4.3, we compare the performance of the multiuser diversity scheme with conventional optimum soft combination and the OR rule with different values of S at SNR= 0 dB. The thresholds τ_u and τ_l are similar to those used in the simulation of Fig. 4.1 at SNR= 0 dB. When the total number of users S increases, the detection probability of multiuser diversity spectrum sensing increases. When

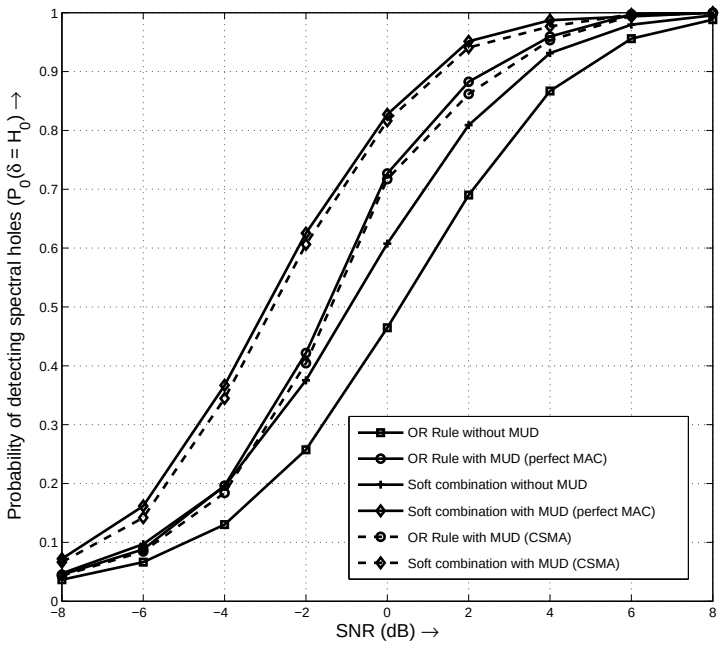

Figure 4.1: Performance of 1 out N rule (OR) rule and soft combination scheme with multiuser and conventional spectrum sensing.

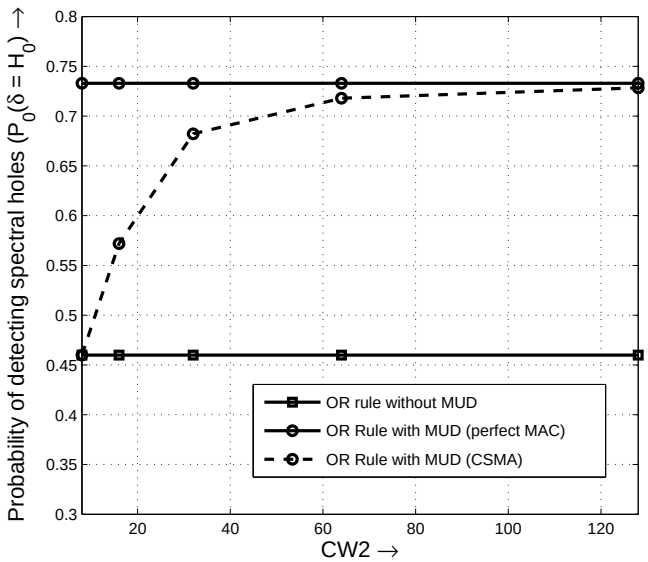

Figure 4.2: Performance of OR Rule with perfect MAC and CSMA MAC vs. the contention window $CW2$.

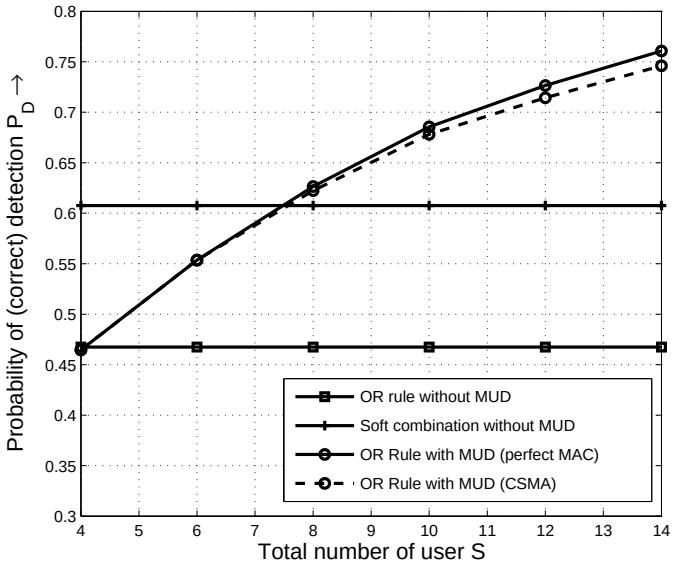

Figure 4.3: Performance of conventional OR rule and soft combination scheme and OR rule with multiuser diversity vs. total number of users S.

$S \geq 8$, the multiuser diversity hard combination based OR rule outperforms the conventional soft optimal combination studied in [61]. In Fig. 4.4, we compare the performance of the conventional and multiuser diversity spectrum sensing schemes with the counting rule at the fusion center. All of the schemes meet the requirement of τ_{FA} at the fusion center, but only the counting rule satisfies the τ_{FA} requirement at both the nodes and the fusion center. The performance of the 1 out N rule (OR) rule is better than that of the conventional counting rule because the OR rule increase the false alarm probability at each node [67]. At low SNR, single user detection can outperform the counting rule because of the effect of fading. At low SNR, nodes which have severe fading can create a wrong decision about the presence of primary detection. When combining at the fusion center, these may lead to wrong decision at the fusion. In Fig. 4.5, we compare the performance gain of secondary users equipped with multiple antennas over those equipped with only a single antenna. Hard combination with 1 out of N rule is used. Each multi-antenna user is equipped with $N_t = 2$ antennas. We consider $S = 12$ nodes and set the thresholds as $\tilde{\tau}_u$=$2\tau_u$ and $\tilde{\tau}_l$=$2\tau_l$, where τ_u and τ_l are obtained from the simulation in Fig. 4.1. Fig. 4.5

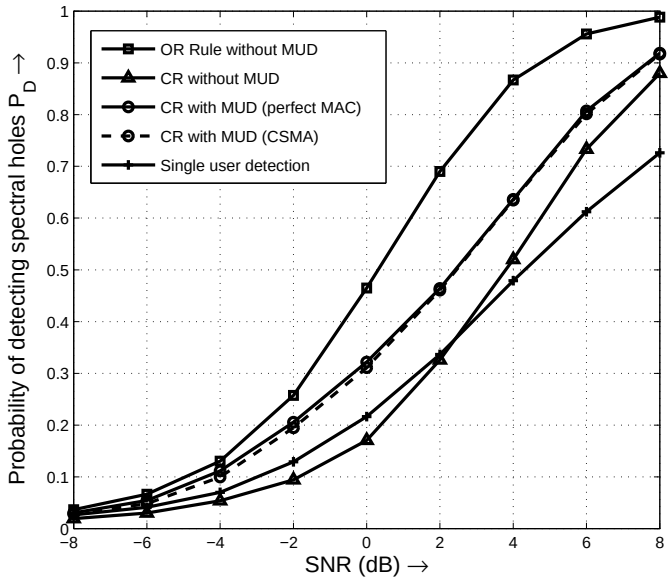

Figure 4.4: Performance of Counting Rule (CR) with multiuser and conventional spectrum sensing.

clearly shows the benefit of multiple antennas over single antennas and also the benefit of multiuser diversity in multi-antennas systems.

4.6 Conclusion

We proposed a cooperative multiuser diversity spectrum sensing scheme that exploits the multiuser diversity inherent in the secondary network to improve the sensing capability of cognitive radio systems. We use a distributed approach in the sense that each secondary user only has local knowledge about its observed energy. We studied two detection rules for the fusion center, counting rule and the OR rule and also considered the case of users equipped with multiple antennas. We also propose a cognitive MAC protocol for secondary users to communicate their observation to fusion center. The simulation results show that our proposed scheme significantly outperforms conventional cooperative sensing schemes that do not take advantage of multiuser diversity. In this chapter, we assumed that the fadings between secondary user antennas were independent. In the ongoing work we are investigating the case of correlated fading between antennas.

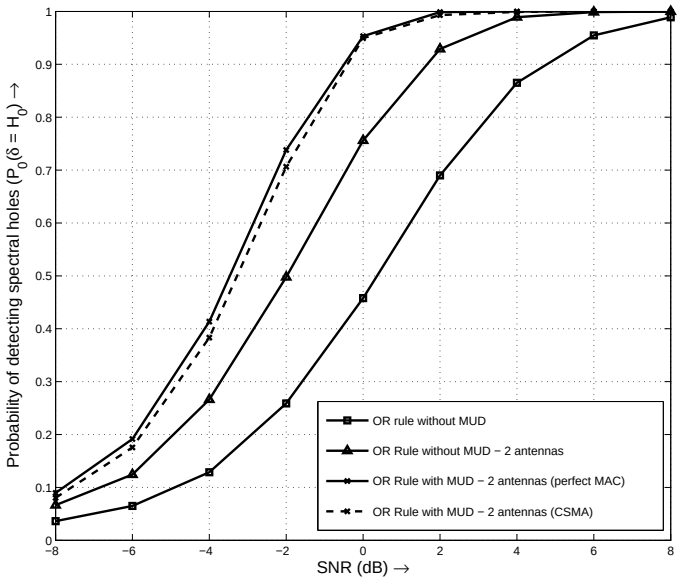

Figure 4.5: Performance of OR rule rule with multiuser and conventional spectrum sensing, 2 antennas used at secondary users.

Chapter 5: Amplify-and-Forward Cooperative Transmission in Cognitive Radio Networks

5.1 Introduction

In this chapter[1], we consider a scenario in which a secondary transmitter can communicate with a secondary receiver via a direct communication link or a relay channel, depending on the state of a primary transmitter. We propose cognitive amplify-and-forward with fixed decoding delay and cognitive amplify-and-forward with variable decoding delay that exploit the presence of spectrum holes both in time. In fixed decoding delay protocol, the secondary receiver always decodes the received signal after fixed number of time frames. However, in variable decoding delay, the number of time frames the secondary receiver has to wait before it can decode the signal depends on the state of the primary transmitter. The variable decoding delay scheme, which always has a diversity order of two, has lower symbol error probability than fixed decoding delay scheme. Our simulation and analytical results show that our proposed schemes, employing joint spatial-temporal sensing, significantly reduces the average symbol error probability compared to schemes based on pure temporal or spatial sensing. We also propose an incremental relaying protocol which improves the spectral efficiency of our protocols.

Spectrum holes exist both in time and in space. A temporal spectrum hole may arise, for example, when a licensed or primary user of the spectrum is idle, i.e., not transmitting. In this case, a temporal spectrum hole is characterized by the duration in which the primary transmitter is in the idle or OFF state. A spatial spectrum hole with respect to a given frequency channel may occur if a given secondary user is sufficiently far from a primary user that is actively transmitting. In this case, the secondary user may transmit up to a certain

[1]The preliminary contents of this chapter appeared in [69].

level, which we called the maximum interference-free transmit power (MIFTP), without causing harmful interference to primary users who are receiving the transmissions.

Spatial spectrum sensing is investigated [17, 18], wherein the maximum MIFTP of a given secondary user is estimated based on signal strengths received by a group of secondary nodes. To calculate the MIFTP for a secondary node, estimates of both the location and transmit power of the primary transmitter are estimated collaboratively by a group of secondary nodes. Using these estimates, each secondary node determines its approximate MIFTP, which bounds the size of its spatial spectrum hole.

The problem of detecting when the primary is ON or OFF is called *temporal* spectrum sensing. The decision on the ON/OFF state of the primary transmitter can be made either at individual secondary nodes or collaboratively by a group of secondary nodes. Cooperative temporal sensing has been studied in [8, 23, 24]. Cooperation among secondary nodes for temporal sensing can overcome problems posed by low signal-to-noise ratio (SNR), shadowing, and hidden terminals [8].

In earlier work [49, 50], a joint spatial-temporal sensing was proposed whereby a secondary node performs spatial sensing to determine its MIFTP when the primary transmitter is ON and uses localization information obtained in the process of spatial sensing to perform the temporal sensing.

In this chapter, we propose a cooperative communication strategy that employs joint spatial-temporal sensing to maximize the transmission capacity of secondary users in a cognitive radio network. In Fig. 5.1(a), the secondary transmitter (ST), labeled as node a can communicate directly with the secondary receiver (SR), labeled as node b, due to the existence of a spatial spectrum hole with respect to the primary transmitter (PT). However, in the scenario depicted in Figs. 5.1(b), ST can communicate directly with SR only when PT is in the OFF state. In these scenarios, when PT is ON, ST transmits to SR via a relay (R), labeled as node r. By enabling the use of both the direct and relay channels, joint spatial-temporal sensing can significantly improve the transmission performance of the secondary system.

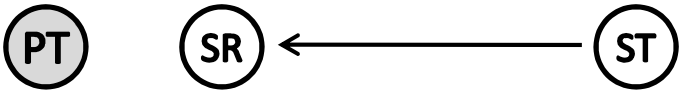

(a) Direct communication.

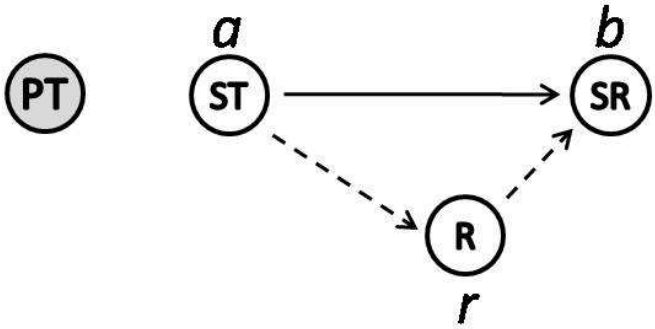

(b) Single relay cooperative communication.

Figure 5.1: Cooperative communication with joint spatial-temporal sensing.

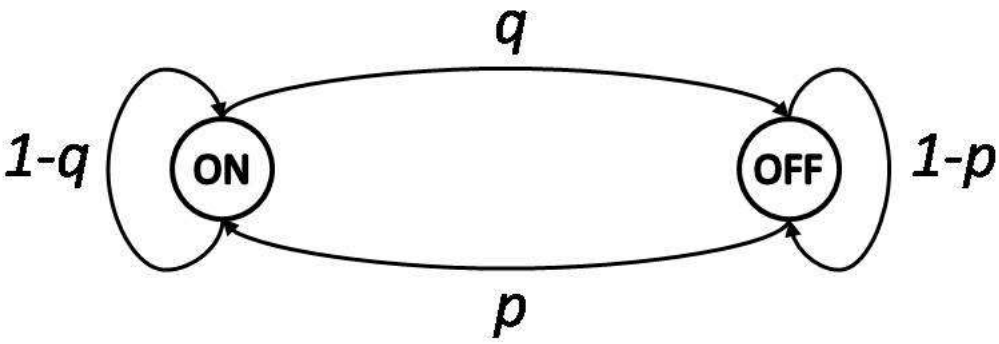

Figure 5.2: Two stage Markov chain model for PT's ON/OFF process

Cooperative relay communications or cooperative diversity has received much attention in recent years (cf. [42, 43, 45, 70]). The basic idea of cooperative communication is that the source terminal cooperates with relay terminals to form a virtual or distributed multi-antenna system to communicate with the destination. The performance of a cooperative communication system depends on the combining mechanism at the relay and the destination nodes. Two well-known cooperative strategies are amplify-and-forward (AF) and decode-and-forward (DF)

- The non-regenerative amplify and forward (AF) strategy which achieves the available diversity using maximal ratio combining. The outage behavior and performance of this protocol are studied in [43] and [45]. This strategy achieves the available diversity of the channel [43].

- The regenerative decode and forward (DF) strategy is simple and practical but cannot achieve full diversity unless sophisticated combining is employed at the destination to account for the reliability of the links between the source and relay and between the relay and the destinatin. The outage probability of this strategy is analyze in [43]. In [46], a smart decode-and-forward strategy is proposed that achieve the available diversity.

In this chapter, we focus on the AF protocol. In [69], an AF strategy is proposed for cognitive radio network scenario wherein the status of primary transmitter is in the ON state for a greater proportion of time than OFF, on average. It is assumed that the secondary receiver has to wait until it receives signals from both the relay and the secondary transmitter to decode the received signals. This may result in excessive delay on the communication link. In this chapter, we propose a practical AF cooperative communication protocol. Our protocol decodes the received signals after a fixed number of time frames. No constraints are placed on the ON/OFF activity of the primary transmitter, i.e., the proportion of time spent in the ON state may be greater or less than that in the OFF state. We focus on the case of a single relay channel.

The remainder of the chapter is organized as follows. Section 5.2 describes the system model. Section 5.3 present cognitive amplify-and-forward with fixed decoding delay. Section 5.4 present cognitive amplify-and-forward with variable decoding delay. Section 5.5 presents simulation results. Finally, the chapter is concluded in Section 5.6.

5.2 System Model

5.2.1 Transmission frames and PT behavior

We assume the basic system configuration shown in Fig. 5.1. For convenience, we label ST as a, SR as b, and R as r. Time on the wireless channel is divided into frames consisting of N_s symbols each. We shall assume perfect symbol-level timing synchronization between the nodes of the secondary system. Imperfect synchronization can be accommodated using approach of [70]. The PT alternates between the ON and OFF states on a per-frame basis according to the on-off Markov model of Fig. 5.2. The ON and OFF durations of the PT are modeled as geometric random variables with parameters q and p, respectively (cf. [71]). The steady-state probability that PT is ON is given by $p_{\text{on}} = q/(p+q)$, while the probability that PT is OFF is $p_{\text{off}} = p/(p+q)$. In [69], we considered the scenario in which on average, PT in the ON state a greater proportion of time than in the OFF state, i.e., $q > p$. In this chapter, this restriction is removed.

5.2.2 Channel modeling

The received signal of a simple wireless channel model with flat (frequency non-selective) fading without shadowing is given by [72]

$$y = \sqrt{P(d,\epsilon)}hs + n, \tag{5.1}$$

where

$$P(d,\epsilon) \triangleq \delta^2 \left(\frac{d_0}{d}\right)^{\alpha} \epsilon$$

denotes the equivalent transmitted power after taking into account the effect of path loss. Here, δ^2 is the free space signal-power attenuation factor between the source and a reference distance d_0, d is the distance between the source and destination, α is the propagation exponent, $h \sim \mathcal{CN}(0,1)$ is a complex Gaussian random variable with zero mean and unit variance, $n \sim \mathcal{CN}(0, N_0)$, and s is the transmitted signal.

When PT is ON, ST and R are limited in the amount of power they can use in order to avoid causing harmful interference to the primary users who receive the transmissions from the PT. The maximum power that can be used by a given secondary node while avoiding harmful interference to primary users is called the *maximum interference-free transmit power* (MIFTP) (cf. [17, 73]). A method for a secondary node to estimate its MIFTP is presented in [17] for the case of a single primary transmitter; the multiple transmitter case is addressed in [53]. Let ϵ_a and ϵ_r denote the MIFTPs of ST and R, respectively, when PT is ON. We also define

$$P_{ar} = P(d_{ar}, \epsilon_a), \;\; P_{rb} = P(d_{rb}, \epsilon_r),$$

as the equivalent transmitted powers when PT is ON from ST to R and from R to SR, respectively. Here, d_{ar} and d_{rb} denote the distances between the node pairs (ST, R) and (R, SR), respectively. When PT is ON, the received signal at R and SR consists of the transmitted signal, the noise at the receiver and the co-channel interference from PT. We treat the co-channel interference as noise. The total noise at the receiver has zero mean and variance $N_0 + N_p$ where N_p is the variance of the co-channel noise. The co-channel noise is assume to be very small compare to the receiver noise, thus, we can approximate the noise component at receiver when PT is ON by $\mathcal{N}(0, N_0 + N_p)$.

For the case when PT is OFF, we define

$$\tilde{P}_{ab} = P(d_{ab}, \epsilon_m), \;\; \tilde{P}_{ar} = P(d_{ar}, \epsilon_m), \;\; \tilde{P}_{rb} = P(d_{rb}, \epsilon_m),$$

as the equivalent transmitted powers from ST to SR, ST to R, and R to SR, respectively. Here, d_{ab} denotes the distance between ST and SR and ϵ_m denotes the maximum transmit

power that secondary nodes can use when PT is OFF. In a cognitive radio network where $\epsilon_a \ll \epsilon_m$, ST may not be able to communicate directly with ST when PT is ON because P_{ar} could be below the required threshold for SR to detect the received signal. In this case, ST can communicate with SR through the relay node R, since $d_{ar} < d_{ab}$.

5.2.3 Spatial Sensing

When only spatial sensing is available, i.e., ST and R have only knowledge of their MIFTPs, the ST has to transmit the signal through the relay R. Consider the relay channel ST $\rightarrow$ R $\rightarrow$ SR. We wish to transmit a frame of N_s symbols using the relay channel over K time frames. The channel resource allocation for link ST $\rightarrow$ R and R $\rightarrow$ SR is K_u and K_v time frames, respectively. When only spatial sensing is available, the transmitted power is limited to MIFTP. Hence, the receiver may operate in a low SNR regime. For this reason, repetition codes [74] are used to transmit signal from ST to R over K_u and from R to SR over K_v time frames to increase the SNR at receiver. We remark that repetition codes have been shown to be nearly optimal in low SNR regime [74]. The received signal at the relay R is the maximal ratio combination (MRC) of the repetition codes from K_u time frames:

$$y_u = \sum_{i=1}^{K_u} g_i^*(g_i\sqrt{P_{ar}}s + n_i) = \tilde{g}\sqrt{P_{ar}}s + \tilde{n} \tag{5.2}$$

where $\tilde{g} = \sum_{i=1}^{K_u} |g_i|^2$, $\tilde{n} = \sum_{i=1}^{K_u} g_i^* n_i$. g_i is the channel gain between ST and R, n_i is the noise at R when PT is ON with zero mean and variance $N_0 + N_p$. The received signal at SR is

$$\begin{aligned} y_v &= \sum_{i=1}^{K_v} h_i^*(\sqrt{P_{rb}}h_i A(\tilde{g}\sqrt{P_{ar}}s + \tilde{n}) + n_i) \\ &= \sqrt{P_{ar}P_{rb}}\tilde{h}A\tilde{g}s + n_v, \end{aligned} \tag{5.3}$$

where $\tilde{h} = \sum_{i=1}^{K_v} |h_i|^2$, $n_v = \sum_{i=1}^{K_v}(|h_i|^2 A\sqrt{P_{rb}}\tilde{n} + h_i^* n_i)$. Here, h_i is the channel gain between R and SR during time frame i and A is the amplification factor, which is chosen to maintain average constant power output at R: $A^2 = 1/(P_{ar}\tilde{g}^2 + N_0\tilde{g})$. The resulting SNR is

$$\gamma_b = |A\tilde{g}\tilde{h}|^2 \frac{P_{ar}P_{rb}}{\sigma_v^2} \tag{5.4}$$

where σ_v is the variance of the noise n_v.

$$\gamma_b = |A\tilde{g}\tilde{h}|^2 \frac{P_{ar}P_{rb}}{\sigma_v^2} = \frac{\gamma_u\gamma_v}{\gamma_u + \gamma_v + 1}, \tag{5.5}$$

with $\gamma_u = \tilde{g}\frac{P_{ar}}{N_0+N_p}$ and $\gamma_v = \tilde{h}\frac{P_{rb}}{N_0+N_p}$.

Proposition 1. *The average SEP of the relay channel is minimized when $K_u = K_v$ if K is even and $K_u = K_v + 1$ or $K_v = K_u + 1$ if K is odd where $K_u + K_v = K$.*

The proof of Proposition 1 can be found in the appendix. Our analysis of proposition 1 is confirmed by the simulation results presented in Section 5.5.

5.3 Cognitive Amplify-and-Forward Protocol with Fixed Decoding Delay (CAF-FD)

We develop a cognitive amplify-and-forward with fixed decoding delay (CAF-FD) cooperative transmission protocol for cognitive radio networks. We assume that both ST and R employ omnidirectional antennas. The secondary receiver (SR) decodes received signals once every three time frames. In general, the SR can decode the signal after any number of time frames. However, as the number of transmission time frames increases the spectral efficiency of the system decreases and decoding delay is increased. Therefore, in this chapter we consider the use of three frames for transmission and compare the performance of

our scheme for for different spectrum sensing strategies. In Section 5.4, we show that by intelligently allocating the number of frame depending on the state of PT, the proposed scheme in Section 5.4 can outperform the CAF-FD in term of both probability of error and spectral efficiency.

Suppose the secondary transmitter (ST) desires to transmit N_s symbols to ST; i.e., it requires one full frame in which PT is OFF. We assume that a time division multiple access (TDMA) protocol is used to coordinate the transmissions of ST and R. During a given time frame, only ST or R is allowed to transmit to SR. Our proposed CAF-FD works as follows:

- In the first two time frames, if PT is OFF, ST transmits to SR. Otherwise, ST transmits to R.
- In the third time frame, R transmits to SR.

In order to achieve this, the secondary nodes perform joint spatial-temporal sensing, as discussed in [49]. In particular, all secondary users estimate their MIFTPs based on signal strength measurements, which they exchange with one another. They also decide whether the PT is ON or OFF, by transmitting their local decisions to a fusion center, which then makes the final decision. Maximal ratio combining (MRC) is used at both R and SR to combine the received signals.

The state of PT over three consecutive time frames can be characterized by a three-bit state sequence $c_1c_2c_3$ where $c_i = 1$ if PT is ON during the ith frame and $c_i = 0$, otherwise. Therefore, there are $2^3 = 8$ possible state sequences. During a frame in which PT is OFF, ST communicates directly with SR using the maximum transmission power ϵ_m. Since an omnidirectional antenna is used at ST, the relay node R receives the signal transmitted by ST.

Let $\boldsymbol{c}$ denote a sequence of frame states and let $|\boldsymbol{c}|$ denote the length of the sequence. For a given state sequence $\boldsymbol{c}$, let $w_{\boldsymbol{c}}$, $u_{\boldsymbol{c}}$ and $v_{\boldsymbol{c}}$ denote the signals received at SR for link (ST, SR), R for link (ST, R) and at SR for link (R, SR), respectively, at the end of the $|\boldsymbol{c}|$-th frame. For example, u_{10} denotes the received signal at R due to source ST after two

time frames, where PT is ON in the first frame and OFF in the second. Let $y_{c_1c_2c_3}$ denote the final MRC-received signal (i.e., the signal obtained after applying MRC) at SR after three time frames. For example y_{000} is the MRC-received signal at SR after a sequence of three time frames in which PT is OFF during all three frames.

Let f_i, g_i and h_i denote the fading channel coefficient during time frame $i, i = 1, 2, 3$ from ST to SR, ST to R and R to SR, respectively. We assume that f_i, g_i and h_i are constant and independently identically distributed from one frame to another. Further, the channel states f_i and h_i are available at SR, i.e., via training sequences, but they are not available at ST and R. Also, the g_i are available at R, but not at ST. Hence, maximum likelihood detection can be used at R and SR. Let s be the transmitted signal at ST. Let n_i be the noise variable during time frame i, $i = 1, 2, 3$. For example, y_{000} denotes the MRC received signal at SR after three OFF time frames sequence. We denote the complex conjugate of x by x^*. The noise component during time frame i is $n_i \sim \mathcal{CN}(0, N_0)$ when PT is OFF and $n_i \sim \mathcal{CN}(0, N_0 + N_p)$ when PT is ON.

In the amplify-and-forward protocol, the received signal at the relay node R is multiplied by an amplification factor $A_{c_1c_2}$ to guarantee that the transmitted power at R is limited to P_{rb} or $\tilde{P}_{rb}$ depending on the state of PT. The subscript c_1c_2 in $A_{c_1c_2}$ denotes the ON/OFF state of the first two time frames. For state sequence 000, in the first two time frames, by using a repetition code [74], i.e., ST transmits the same signal to SR, the received signal at SR from ST is

$$w_{00} = \sqrt{\tilde{P}_{ab}} \sum_{i=1}^{2} |f_i|^2 s + \sum_{i=1}^{2} f_i^* n_i \tag{5.6}$$

and the received signal at relay R is

$$u_{00} = \sqrt{\tilde{P}_{ar}} \sum_{i=1}^{2} |g_i|^2 s + \sum_{i=1}^{2} g_i^* n_i \tag{5.7}$$

In the third time frame, R amplifies the received signal and forwards it to SR. The received

signal at SR from R is $v_{000} = \sqrt{\tilde{P}_{rb}} h_3 A_{00} u_{00} + n_3$ where

$$A_{00} = 1/\sqrt{\tilde{P}_{ar}(|g_1|^2 + |g_2|^2)^2 + (|g_1|^2 + |g_2|^2)N_0}. \tag{5.8}$$

The final received signal at SR with MRC is

$$y_{000} = w_{00} + h_3^* v_{000}. \tag{5.9}$$

For state sequence 001, the received signal at SR from ST after the first two OFF-state time frames is w_{00} in (5.6). By using a repetition code, the received signal at relay R with MRC over first two time frames is u_{00} in (5.7). The relay amplifies and forwards u_{00} to SR during the third time frame when PT is ON. The received signal at SR from R is $v_{001} = h_3 \sqrt{P_{rb}} A_{00} u_{00} + n_3$ where A_{00} is presented in (5.8). The final received signal at SR with MRC is

$$y_{001} = h_3 * v_{001} + w_{00}. \tag{5.10}$$

For state sequence 010, In the first time frame, ST transmits to SR,

$$w_0 = \sqrt{\tilde{P}_{ab}} f_1 s + n_1 \tag{5.11}$$

In the second time frame ST transmit to R. The received signal at R after two time frame is

$$u_{01} = (\sqrt{\tilde{P}_{ar}}|g_1|^2 + \sqrt{P_{ar}}|g_2|^2)s + g_1^* n_1 + g_2^* n_2 \tag{5.12}$$

the R amplifies and forwards u_{01} to SR. We have, $v_{010} = \sqrt{\tilde{P}_{rb}} h_3 A_{01} u_{01} + n_3$ where

$$A_{01} = 1/\sqrt{(\sqrt{\tilde{P}_{ar}}|g_1|^2 + \sqrt{P_{ar}}|g_2|^2)^2 + |g_1|^2 N_0 + |g_2|^2 (N_0 + N_p)}. \tag{5.13}$$

The final received signal at SR is given by,

$$y_{010} = f_1^* w_0 + h_3^* v_{010} \tag{5.14}$$

For state sequence 011, the received signal at SR after first time frame is t_0 in (5.11). The received signal at R after two time frames u_{01} in (5.12). In the third frame, R amplifies and forwards the u_{01} to SR, $v_{011} = \sqrt{P_{rb}} h_3 A_{01} u_{01} + n_3$ where A_{01} is in (5.13). The final MRC received signal of t_0 and v_{011} is

$$y_{011} = f_1^* w_0 + h_3^* v_{011}. \tag{5.15}$$

For state sequence, 100, in the first time frame when PT is ON, ST forwards signal to R. In the second time frame which PT is OFF, ST can transmit signal to SR directly. We have

$$w_{10} = \sqrt{\tilde{P}_{ab}} f_2 s + n_2 \tag{5.16}$$

and the received signal at the relay R

$$u_{10} = (|g_1|^2 \sqrt{P_{ar}} + |g_2|^2 \sqrt{\tilde{P}_{ar}}) s + g_1^* n_1 + g_2^* n_2 \tag{5.17}$$

The relay R amplifies and forwards u_{10} to SR, $v_{100} = \sqrt{\tilde{P}_{rb}} h_3 A_{10} u_{10} + n_3$ where

$$A_{10} = 1/\sqrt{(\sqrt{P_{ar}}|g_1|^2 + \sqrt{\tilde{P}_{ar}}|g_2|^2)^2 + |g_1|^2(N_0 + N_p) + |g_2|^2 N_0} \tag{5.18}$$

The final received signal at SR with MRC is

$$y_{100} = f_2^* w_{10} + h_3^* v_{100}. \tag{5.19}$$

For state sequence 101, the received signal at R after first two time frame is u_{10} in (5.17)

and $v_{101} = \sqrt{P_{rb}} h_3 A_{10} u_{10} + n_3$, where A_{10} is in (5.18). The final MRC received signal combining w_{10} in (5.16) and v_{101} is

$$y_{101} = h_3^* v_{101} + f_2^* w_{10}. \tag{5.20}$$

For state sequence 110, we have

$$u_{11} = (|g_1|^2 + |g_2|^2)\sqrt{P_{ar}} s + g_1^* n_1 + g_2^* n_2 \tag{5.21}$$

and $v_{110} = h_3 \sqrt{\tilde{P}_{rb}} A_{11} u_{11} + n_3$, where

$$A_{11} = 1/\sqrt{(P_{ar}(|g_1|^2 + |g_2|^2)^2 + (|g_1|^2 + |g_2|^2)(N_0 + N_p)}. \tag{5.22}$$

The final received signal at SR is

$$y_{110} = h_3^* v_{110} \tag{5.23}$$

Similarly, for state sequence 111, we have $v_{111} = h_3 \sqrt{P_{rb}} A_{11} u_{11} + n_3$ where A_{11} is in (5.22) and u_{11} is in (5.21) and the final received signal at SR is

$$y_{111} = h_3^* v_{111}. \tag{5.24}$$

Pure spatial sensing: The transmission strategy is similar to state sequence 111 in (5.24) scenario $y_s = y_{111} = h_3^* v_{111}$ where y_s denotes the received signal at SR for spatial sensing only.

Pure temporal sensing: Except for the state sequence 000, transmission strategy is a simple repetition code over time frames in which PT is OFF. We denote $y^t_{c_1 c_2 c_3}$ as the received

signal at SR for state sequence $\mathcal{S}_{c_1c_2c_3}$. We have

$$y^t_{000} = y_{000}$$

$$y^t_{010} = (|f_1|^2 + |f_3|^2)\sqrt{\tilde{P}_{ab}}s + f_1^* n_1 + f_3^* n_3$$

$$y^t_{011} = |f_1|^2\sqrt{\tilde{P}_{ab}}s + f_1^* n_1$$

$$y^t_{100} = (|f_2|^2 + |f_3|^2)\sqrt{\tilde{P}_{ab}}s + f_2^* n_2 + f_3^* n_3$$

$$y^t_{101} = |f_2|^2\sqrt{\tilde{P}_{ab}}s + f_2^* n_2$$

$$y^t_{110} = |f_3|^2\sqrt{\tilde{P}_{ab}}s + f_3^* n_3$$

where y_{000} is in (5.9). There is no transmission for state sequence 111.

The spectral efficiency for joint spatial temporal sensing and spatial sensing are equal. The spectral efficiency of temporal sensing is smaller than that of joint spatial-temporal sensing because there is no transmission during state sequence 111. If the joint spatial-temporal sensing has spectral efficiency of 1 then temporal sensing has an efficiency of $1 - \left(\frac{\mathrm{q}}{\mathrm{p+q}}\right)^3$ where $\frac{\mathrm{q}}{\mathrm{p+q}}$ is the steady-state probability of PT being in the ON state for a given frame.

5.3.1 Performance Analysis

In the literature, the performance of a cooperative transmission strategy is measured based on one of two criteria: the outage probability [42, 43] and the average symbol error parobability (SEP) [45, 75, 76]. In this chapter, we have analyzed the performance of the proposed cognitive cooperative transmission protocol in term of SEP. Derivations of the exact SEP for cooperative communication is quite involved even for one relay and Rayleigh fading [75].

In [45], SEP is derived for general cooperative links and general fading models as long as the probability density function (pdf) $p(t)$ of the SNR of the first hop, second hop and direct link are non zero at $t = 0$. However, this approach cannot use in the present chapter because the pdf of the first hop which is a chi-square distribution is equal to zero at $t = 0$. For state sequences 110 and 111, the SEP at SR is the SEP of the relay channel with the first hop SNR has a chi-square distribution and the second hop SNR has a Rayleigh distribution. In [77], both the outage probability and the SEP for two hop relay channels are derived for Nakagami's fading channels and thus the results can be used in this chapter for calculating the SEP for frame sequences 110 and 111. However, the derivation of SEP is quite complicated because it involves the calculation of the harmonic mean of two gamma distributions.

We propose a simple approach to analyze the SEP lower bound of our propose scheme. The numerical results in Section 5.5 show that the lower bound match closely with the numerical results at high and moderate SNR. For the state sequence 111, the amplification factor A_{11} at high SNR, i.e., $P_{ar} \gg (N_0 + N_p)$, can be approximated by

$$A_{11} = 1/\sqrt{(|g_1|^2 + |g_2|^2)^2 P_{ar} + (|g_1|^2 + |g_2|^2)(N_0 + N_p)} \approx 1/(\sqrt{P_{ar}}(|g_1|^2 + |g_2|^2)). \quad (5.25)$$

The relay multiplies the received signal by A_{11} in (5.25) and forwards to SR

$$u_{11}A_{11} = s + (g_1^* n_1 + g_2^* n_2)/(\sqrt{P_{ar}}(|g_1|^2 + |g_2|^2).$$

At high SNR the noise component of $u_{11}A_{11}$ can be negligible, and the received signal at SR can be approximated by, $z_{111} = \sqrt{P_{rb}} h_3 s + n_3$ where $z_{c_1c_2c_3}$ denotes the lower bound of

the received signal at SR for state sequence $\mathcal{S}_{c_1c_2c_3}$. Similarly,

$$
\begin{aligned}
z_{000} &= \sqrt{\tilde{P}_{ab}}\sum_{i=1}^{2}|f_i|^2 s + \sqrt{\tilde{P}_{rb}}|h_3|^2 s + \sum_{i=1}^{2} f_i^* n_i + h_3^* n_3, \\
z_{001} &= \sqrt{\tilde{P}_{ab}}\sum_{i=1}^{2}|f_i|^2 s + \sqrt{P_{rb}}|h_3|^2 s + \sum_{i=1}^{2} f_i^* n_i + h_3^* n_3, \\
z_{010} &= \sqrt{\tilde{P}_{ab}}|f_1|^2 s + \sqrt{\tilde{P}_{rb}}|h_3|^2 s + f_1^* n_1 + h_3^* n_3, \\
z_{011} &= \sqrt{\tilde{P}_{ab}}|f_1|^2 s + \sqrt{P_{rb}}|h_3|^2 s + f_1^* n_1 + h_3^* n_3, \\
z_{100} &= \sqrt{\tilde{P}_{ab}}|f_2|^2 s + \sqrt{\tilde{P}_{rb}}|h_3|^2 s + f_2^* n_2 + h_3^* n_3, \\
z_{101} &= \sqrt{\tilde{P}_{ab}}|f_2|^2 s + \sqrt{P_{rb}}|f_3|^2 s + f_2^* n_2 + h_3^* n_3, \\
z_{110} &= \sqrt{\tilde{P}_{rb}} h_3 s + n_3.
\end{aligned}
$$

Let $\mathrm{SEP}_{\mathrm{c_1c_2c_3}}$ denote the average lower bound SEP of state sequence $\mathcal{S}_{c_1c_2c_3}$ and $\mathrm{SEP_j}$ denote the average lower bound SEP over all state sequence for joint spatial temporal sensing. We have

$$
\begin{aligned}
\mathrm{SEP_j} = \Big[&\mathrm{p_{off}^3 SEP_{000}} + \mathrm{p_{off}^2 p_{on}}(\mathrm{SEP_{001}} + \mathrm{SEP_{010}} + \mathrm{SEP_{100}}) \\
&+ \mathrm{p_{off} p_{on}^2}(\mathrm{SEP_{011}} + \mathrm{SEP_{101}} + \mathrm{SEP_{110}}) + \mathrm{p_{on}^3 SEP_{111}}\Big]
\end{aligned} \tag{5.26}
$$

We shall assume that M-PSK modulation is used. Using the moment generating function approach in [78, 79], the SEP of M-PSK signals with MRC of L independent fading paths can be expressed as

$$
\frac{1}{\pi}\int_0^{\frac{(M-1)\pi}{M}} \prod_{k=1}^{L} M_{\gamma_k}\left(-\frac{g_{\mathrm{PSK}}}{\sin^2\phi}\right) \mathrm{d}\phi, \tag{5.27}
$$

where $g_{\text{PSK}} = \sin^2(\pi/M)$ and $M_{\gamma_l}(u) = (1 - u\gamma_l)^{-1}$ is the moment generating function of Rayleigh fading with average SNR γ_l. Let $\mathbf{\Gamma} = (\gamma_1, \gamma_2, \ldots, \gamma_L)$ denote a vector of L average SNR values corresponding to L independent fading paths. Then the SEP can be expressed as

$$\psi(\mathbf{\Gamma}) = \frac{1}{\pi} \int_0^{\frac{(M-1)\pi}{M}} \prod_{k=1}^{L} \left(1 + \frac{g_{\text{PSK}}}{\sin^2 \phi} \gamma_k\right)^{-1} \mathrm{d}\phi. \tag{5.28}$$

$$\begin{aligned}
\text{SEP}_{000} &= \psi(\tilde{\gamma}_{ab}, \tilde{\gamma}_{ab}, \tilde{\gamma}_{rb}) && (5.29)\\
\text{SEP}_{001} &= \psi(\tilde{\gamma}_{ab}, \gamma_{rb}) && (5.30)\\
\text{SEP}_{010} &= \psi(\tilde{\gamma}_{ab}, \tilde{\gamma}_{rb}) && (5.31)\\
\text{SEP}_{011} &= \psi(\tilde{\gamma}_{ab}, \gamma_{rb}) && (5.32)\\
\text{SEP}_{100} &= \text{SEP}_{010} && (5.33)\\
\text{SEP}_{101} &= \text{SEP}_{011} && (5.34)\\
\text{SEP}_{110} &= \psi(\tilde{\gamma}_{rb}) && (5.35)\\
\text{SEP}_{111} &= \psi(\gamma_{rb}) && (5.36)\\
& && (5.37)
\end{aligned}$$

where $\tilde{\gamma}_{ab} = E\big[|f_i|^2 \frac{\tilde{P}_{ab}}{N_0}\big] = \frac{\tilde{P}_{ab}}{N_0}$ is the average SNR at SR when the transmitter is ST and $\gamma_{rb} = E\big[|h_i|^2 \frac{P_{rb}}{N_0+N_p}\big] = \frac{P_{rb}}{N_0+N_p}$ and $\tilde{\gamma}_{rb} = E\big[|h_i|^2 \frac{\tilde{P}_{rb}}{N_0}\big] = \frac{\tilde{P}_{rb}}{N_0}$, are the average SNRs at SR when the transmitter is the relay R when PT is ON and OFF, respectively. Substituting the right hand sides of equations (5.29)-(5.35) into (5.26) we obtain the average SEP lower bound.

5.3.2 Performance of pure spatial and temporal sensing

The performance of spatial sensing is given by SEP_{111}. The performance of temporal sensing is given by

$$\mathbf{SEP}^{\mathrm{t}} = \frac{1}{(1-\mathrm{p}_{\mathrm{on}}^{3})}\big[\mathrm{p}_{\mathrm{off}}^{3}\mathrm{SEP}_{000} + \mathrm{p}_{\mathrm{off}}^{2}\mathrm{p}_{\mathrm{on}}(\mathrm{SEP}_{001}^{\mathrm{t}} + \mathrm{SEP}_{010}^{\mathrm{t}} + \mathrm{SEP}_{100}^{\mathrm{t}})$$

$$+ \mathrm{p}_{\mathrm{off}}\mathrm{p}_{\mathrm{on}}^{2}(\mathrm{SEP}_{011}^{\mathrm{t}} + \mathrm{SEP}_{101}^{\mathrm{t}} + \mathrm{SEP}_{110}^{\mathrm{t}})\big]$$

where $\mathrm{SEP}_{001}^{\mathrm{t}} = \mathrm{SEP}_{010}^{\mathrm{t}} = \mathrm{SEP}_{100}^{\mathrm{t}}$, $\mathrm{SEP}_{001}^{\mathrm{t}} = \psi(\tilde{\gamma}_{\mathrm{ab}}, \tilde{\gamma}_{\mathrm{ab}})$

$\mathrm{SEP}_{101}^{\mathrm{t}} = \mathrm{SEP}_{110}^{\mathrm{t}} = \mathrm{SEP}_{011}^{\mathrm{t}}$, $\mathrm{SEP}_{101}^{\mathrm{t}} = \psi(\tilde{\gamma}_{\mathrm{ab}})$

5.4 Cognitive Amplify-and-Forward with Variable Decoding Delay (CAF-VD)

In this section, we propose a modified CAF protocol which guarantees that the final received signals after maximal ratio combining at secondary receiver always have a diversity order of 2. In order to achieve this, the decoding delay will be variable. We call this scheme a Cognitive Amplify-and-Forward with variable delay (CAF-VD)

5.4.1 Diversity analysis

We analyze the diversity order of our general cooperative transmission protocol. *For state sequences* 000 and 001, the final received signals at SR y_{000} and y_{001} is the MRC of three independent signals with independent fading coefficients f_1, f_2 and h_3. Therefore, y_{000} and y_{001} have a diversity order of 3. Similarly, the diversity order state sequence 011 is 2. The received signal y_{011} is the MRC of w_0 and v_{011}. The received signal y_{011} is the combination of two independent signals with channel fading coefficients f_1 and h_3. The signal y_{100} has diversity order of 2 with independent fading coefficients f_2 and h_3. The signal y_{101} has a diversity order of 2 with independent fading f_2 and h_3 coefficients. The signal y_{110} and

y_{111} has a diversity order of only 1. The average symbol error probability (SEP) decreases exponentially with the order of diversity. For example, for M-PSK signal, Rayleigh fading, same average SNR, the average SEP are upper and lower bounded by [78]

$$\frac{S(L)}{(1+\kappa\mathrm{SNR})^{\mathrm{L}}} \leq \mathrm{SEP} \leq \frac{\mathrm{S(L)}}{(\kappa\mathrm{SNR})^{\mathrm{L}}},$$

where $S(L)$ and κ are constant and L is the diversity order.

We propose a CAF-VD protocol in which the MRC received signals at SR always have a diversity order of 2. If PT is OFF in the first time frame, the SR will decode the received signals at the end of the second time frame. The MRC received signal at SR for state sequence 00 is

$$y_{00} = \sqrt{\tilde{P}_{ab}} \sum_{i=1}^{2} |f_i|^2 s + \sum_{i=1}^{2} f_i^* n_i. \tag{5.38}$$

For state sequence 01, the received signal at SR at the end of the first time frame $w_0 = \sqrt{\tilde{P}_{ab}} f_1 s + n_1$ and the received signal at R is $u_0 = \sqrt{\tilde{P}_{ar}} g_1 s + n_1$. In the second time frame, when PT is ON, R amplifies and forwards its received signal u_0 to SR. The received signal at SR from R is $v_{01} = h_2 \sqrt{P_{rb}} A_0 s + n_2$ where $A_0 = 1/\sqrt{\tilde{P}_{rb}|g_1|^2 + N_0}$. Finally, the received signal at SR with MRC is

$$y_{01} = h_2^* v_{01} + f_1^* w_0. \tag{5.39}$$

If PT is ON during the first time frame and OFF during the second time frame, we have two possible state sequence 100 and 101. The transmission strategy and the received signals at SR for these two *frame sequences* is similar to (5.19) and (5.20). When PT is ON for the first and second time frames, the possible state sequences for the CAF-FD is 110 and 111. If SR decodes the received signal after 3 time frames, the received signals have the

diversity orders of 1 (5.23) and (5.24). To make the protocol more efficient, SR decodes the received signal after 4 frames. We have the following possible state sequences: 1100, 1101, 1110 and 1111. In the first and second time frames when PT is ON, ST forward the signals to R using repetition code. The relay R then combines the signals using MRC and forwards the received signals to SR in the third and fourth time frames. SR combines the received signal during the third and fourth time frames. Hence, the final received signal at SR with MRC has a diversity order of 2. For state sequence 1100, the received signal at R is $u_{11} = \sqrt{P_{ar}} \sum_{i=1}^{2} |g_i|^2 s + \sum_{i=1}^{2} g_i^* n_i$. R amplifies u_{11} and forwards it to SR. After combining two signals, the received signals at SR is

$$y_{1100} = (|h_3|^2 + |h_4|^2)\sqrt{\tilde{P}_{rb}} A_{11} u_{11} + h_3^* n_3 + h_4^* n_4, \tag{5.40}$$

where A_{11} is in (5.22). Similarly, the received signals for 1101, 1110 and 1111 can be expressed as:

$$y_{1101} = (|h_3|^2 \sqrt{\tilde{P}_{rb}} + |h_4|^2 \sqrt{P_{rb}}) A_{11} u_{11} + h_3^* n_3 + h_4^* n_4, \tag{5.41}$$

$$y_{1110} = (|h_3|^2 \sqrt{P_{rb}} + |h_4|^2 \sqrt{\tilde{P}_{rb}}) A_{11} u_{11} + h_3^* n_3 + h_4^* n_4, \tag{5.42}$$

$$y_{1111} = (|h_3|^2 + |h_4|^2)\sqrt{P_{rb}} A_{11} u_{11} + h_3^* n_3 + h_4^* n_4. \tag{5.43}$$

5.4.2 Performance Analysis

The CAF-VD has following state sequences 00, 01, 100, 101, 1100, 1101, 1110 and 1111. The SEP lower bound for state sequence 100 and 101 can be obtained from (5.32) and

(5.33). We also have,

$$\mathrm{SEP}_{00} = \psi(\tilde{\gamma}_{ab}, \tilde{\gamma}_{ab}) \tag{5.44}$$

$$\mathrm{SEP}_{01} = \psi(\tilde{\gamma}_{ab}, \gamma_{rb}) \tag{5.45}$$

$$\mathrm{SEP}_{1100} = \psi(\tilde{\gamma}_{rb}, \tilde{\gamma}_{rb}) \tag{5.46}$$

$$\mathrm{SEP}_{1101} = \psi(\tilde{\gamma}_{rb}, \gamma_{rb}) \tag{5.47}$$

$$\mathrm{SEP}_{1110} = \mathrm{SEP}_{1101} \tag{5.48}$$

$$\mathrm{SEP}_{1111} = \psi(\gamma_{rb}, \gamma_{rb}) \tag{5.49}$$

The average SEP lower bound for CAF-VD $\mathrm{SEP_d}$ is

$$\begin{aligned}\mathrm{SEP_d} = {} & \mathrm{p_{off}^2 SEP_{00}} + \mathrm{p_{off} p_{on} SEP_{01}} + \mathrm{p_{off}^2 p_{on} SEP_{100}} \\ & + \mathrm{p_{off} p_{on}^2 SEP_{101}} + \mathrm{p_{off}^2 p_{on}^2 SEP_{1100}} + \mathrm{p_{off} p_{on}^3 SEP_{1101}} \\ & + \mathrm{p_{off} p_{on}^3 SEP_{1110}} + \mathrm{p_{on}^4 SEP_{1111}}\end{aligned} \tag{5.50}$$

5.4.3 Spectral efficiency

We normalize the spectral efficiency of CAF-FD with spatial sensing and joint spatial-temporal sensing to 1 and denote them by $\mathrm{SE_s}$ and $\mathrm{SE_j}$, respectively, $\mathrm{SE_j} = \mathrm{SE_s} = 1$. In both the spatial sensing and joint spatial-temporal sensing schemes, one frame of signal (N_s symbols) is decoded after 3 time frames. In CAF-FD with temporal sensing, there is no transmission for the state sequence 111. Hence, the spectral efficiency of temporal sensing is $\mathrm{SE_t} = 1 - \mathrm{p_{on}^3}$. In the CAF-VD with joint spatial-temporal sensing, for state sequence 00, one signal frame is decoded after two time frame. Thus, the spectral efficiency of state sequence 00 is 3/2. Similarly, the spectral efficiency of state sequence 01, 100, 101, 1100, 1101, 1110 and 1111 are 3/2, 3/3, 3/3, 3/4, 3/4, 3/4 and 3/4, respectively. The spectral

efficiency of CAF-VD is given by

$$\mathrm{SE_v} = 1.5(\mathrm{p_{off}^2} + \mathrm{p_{off}p_{on}}) + \mathrm{p_{on}p_{off}^2} + \mathrm{p_{on}^2p_{off}} + 0.75(\mathrm{p_{on}^2p_{off}^2} + 2\mathrm{p_{on}^3p_{off}} + \mathrm{p_{on}^4})$$

5.4.4 Incremental Relaying Protocol

Both CAF-FD and CAF-VD are inefficient in terms of spectral efficiency because the relay and ST repeat their transmissions at all time. In this section, the incremental relaying protocol, proposed in [43] is investigated for our cognitive scenarios. The incremental protocol that exploit the limited feedback, i.e., a single bit feedback from secondary transmitter to indicate the sucess or failure of the transmission. The incremental relaying (IR) protocol can be viewed as a hybrid automatic-repeat-request (ARQ)scheme wherein the secondary transmitter or the relay retransmits if the secondary receiver provides a negative feedback. Every time the SR receives a signal from ST or R, it decodes the received signal and send a feedback bit to both ST and R indicating the success or failure of the transmission. If the transmission is successful, ST continues to transmit the next frame. Otherwise, ST or R continues to transmit signal according to the operation of protocol. We show by simulation in Section 5.5 that incremental relaying significantly improves the spectral efficiency of the system.

5.5 Numerical Results

In this section, we investigate the performance of our proposed cooperative communication scheme in terms of the average SEP. We assume that BPSK modulation is used and $f_i, g_i, h_j \sim \mathcal{CN}(0,1)$. The frame length is 100 symbols. The co-channel noise is assumed to be very small, i.e., $N_p = 0$. We use $\tilde{P}_{ab} = P_{ar} = P_{rb}$ and $\tilde{P}_{ar} = \tilde{P}_{rb} = \tilde{P}_{ab} + 10$ (dB) and $\mathrm{SNR} = \tilde{\mathrm{P}}_{\mathrm{ab}}/\mathrm{N}_0$.

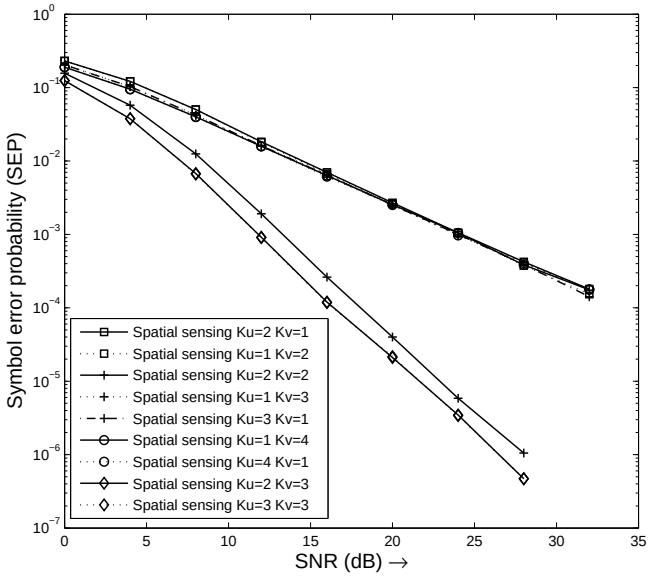

Figure 5.3: Transmission with different resource allocations of K_u and K_v

5.5.1 Spatial Sensing

In Fig. 5.3, we compare the performance of spatial sensing with $K = 3$, $K = 4$ and $K = 5$. When $K = 3$, transmission strategy with $K_u = 2, K_v = 1$ and $K_u = 1, K_v = 2$ show the same performance. When $K = 4$, the transmission strategy with $K_u = K_v = 2$ outperforms the strategy with $K_u = 3, K_v = 1$ and $K_u = 1, K_v = 3$. For $K = 5$, the performance with $K_u = 3, K_v = 2$ and $K_u = 2, K_v = 3$ are optimal. All of our numerical results confirm the results stated in the Proposion 1.

5.5.2 CAF-FD

In Fig 5.4, we show that our analytical lower bound is matched closely with simulation result for relay channel with $K_u = 2, K_v = 1$. As the SNR increases, the simulation and analytical are matched closely. This also confirms our analysis in Section 5.3.1 that the lower bound will close to the true performance as the SNR increases. In Fig. 5.5, we compare the performance of different strategy for the scenario in which the PT is equally in the ON or OFF states, $\mathrm{p_{off}} = \mathrm{p_{on}} = 0.5$. For temporal sensing, both simulation and analytical results

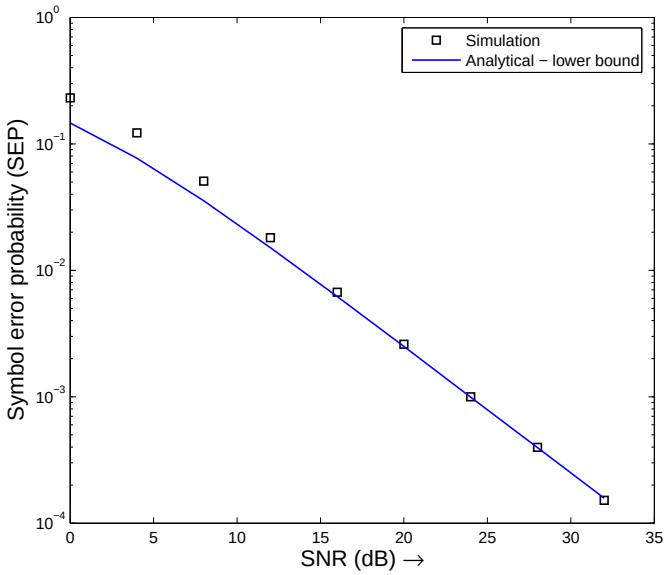

Figure 5.4: Comparision of simulation and analytical results

are matched closely even for small SNR. For spatial sensing, simulation and analytical results are matched closely even for moderate and large SNR. The numerical and analytical results for CAF-FD are plotted using plus sign and a solid line, respectively. At almost any BER of interest, CAF-FD is 10 dB better than spatial sensing and 5 dB better than temporal sensing. Also CAF-FD has a spectral efficiency of $1/(1 - \mathrm{p}_{\mathrm{on}}^3) = 1.1429$ compare to temporal sensing. The CAF-VD is 5 dB and 10 dB better than cognitive amplify-and-forward strategy at BER $= 10^{-3}$ and BER $= 10^{-4}$, respectively. The performance of CAF-VD is much better compare to CAF-FD because it guarantees that the received signal at SR always has a diversity order of 2. The performance of CAF-FD is adversely affected by frame sequence 110 and 111 in which the diversity order at SR is of order 1. However, the decoding delay at SR in CAF-VD is varied with 2, 3 or 4 time frames compare to fixed 3 time frames of CAF-FD. In Fig. 5.6, we study a scenario in which the state of PT is OFF more than ON, i.e., $\mathrm{p}_{\mathrm{off}} = 2\mathrm{p}_{\mathrm{on}} = 0.666667$. The CAF-FD is 15 dB and 7 dB better than spatial sensing and temporal sensing, respectively. The SEP of CAF-FD decreases as the probability of PT is OFF increases because the probability of the state sequences 110 and 111 decreases. These two state sequences which have a diversity order of 1, are the main

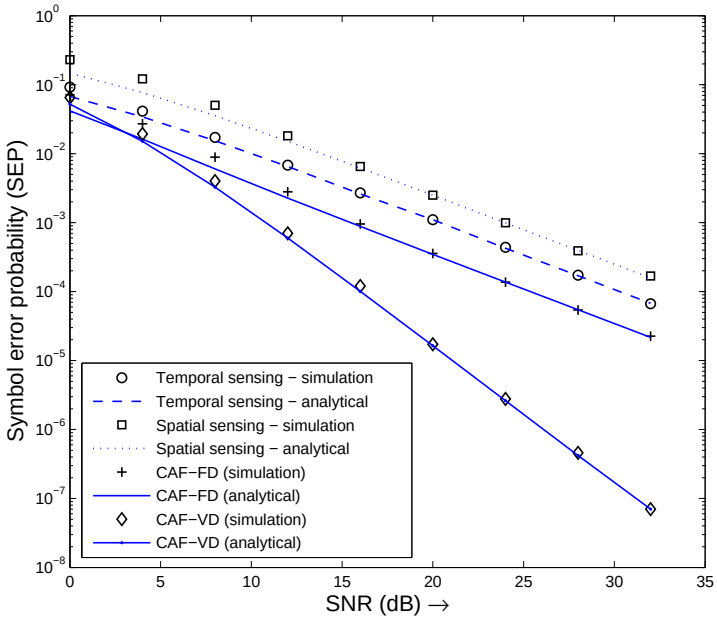

Figure 5.5: Comparision of SEP for all transmission schemes $p_{off} = p_{on} = 0.5$

sources of decoding errors at SR. The CAF-VD is 1 dB, 5 dB and 10 dB better than CAF-FD at BER $= 10^{-3}$, BER $= 10^{-4}$ and BER $= 10^{-5}$, respectively. When the probability that PT is OFF increases, the performance of CAF-FD approaches that of CAF-VD.

In Fig. 5.7, we study the a scenario that the state of PT is ON more than OFF, i.e., $2p_{off} = p_{on} = 0.666667$. The CAF-FD is 6 dB and 3 dB better than spatial sensing and temporal sensing, respectively. The SEP of the CAF-FD increases as p_{on} increases because the probability of state sequence 110 and 111 increases. The CAF-VD is 7 dB and 12 dB better than cognitive amplify-and-forward strategy at BER $= 10^{-3}$ and BER $= 10^{-4}$, respectively. As p_{on} increases, the difference in performance of CAF-FD and CAF-VD increases. Fig. 5.8 shows the performance of different strategies for different value of p_{off}. In Fig. 5.8, two special cases are shown, i.e., $p_{off} = 0$, the CAF-FD become spatial sensing because the PT is always ON. $p_{off} = 1$, CAF-FD become temporal sensing because the PT is always OFF. In Fig. 5.8, SNR = 20 dB. The performance of spatial sensing does not depend on the state of the PT because spatial sensing assumes that PT is always ON and secondary nodes communicate with each other using their maximum interference free transmit power

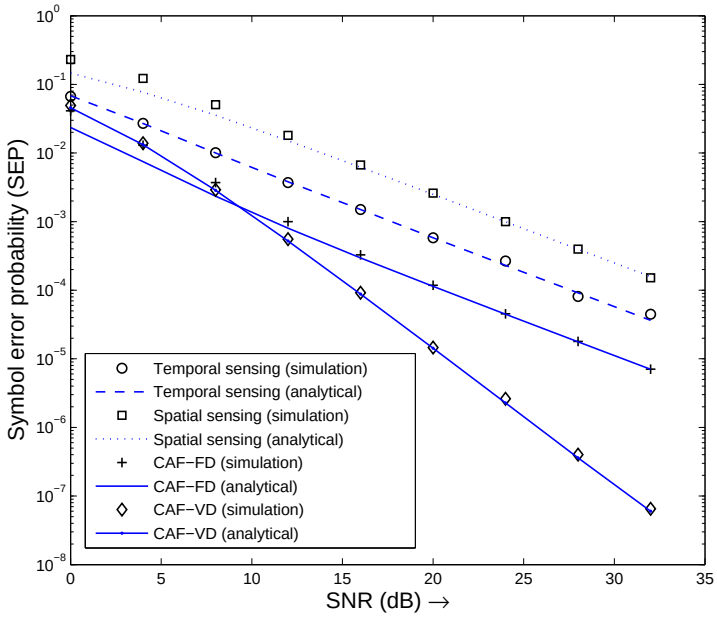

Figure 5.6: Comparision of SEP for all transmission schemes $p_{off} = 2p_{on} = 0.66667$

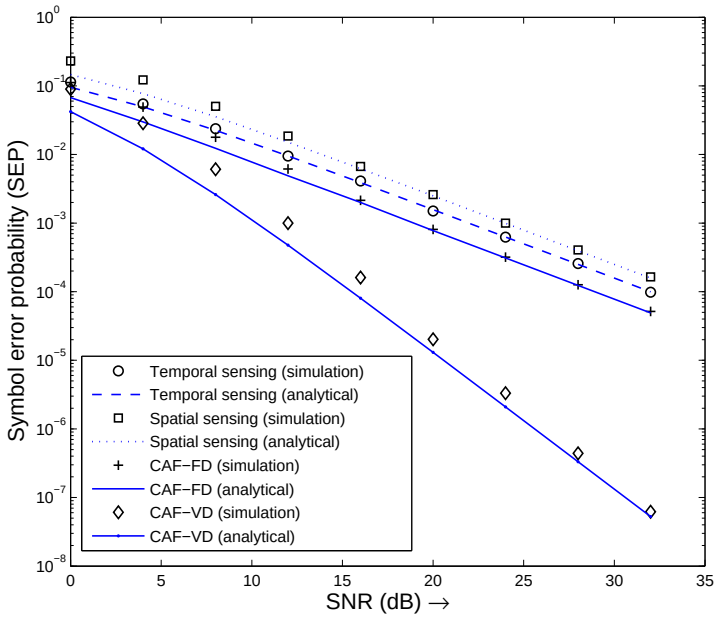

Figure 5.7: Comparision of SEP for all transmission schemes $2p_{off} = p_{on} = 0.6667$

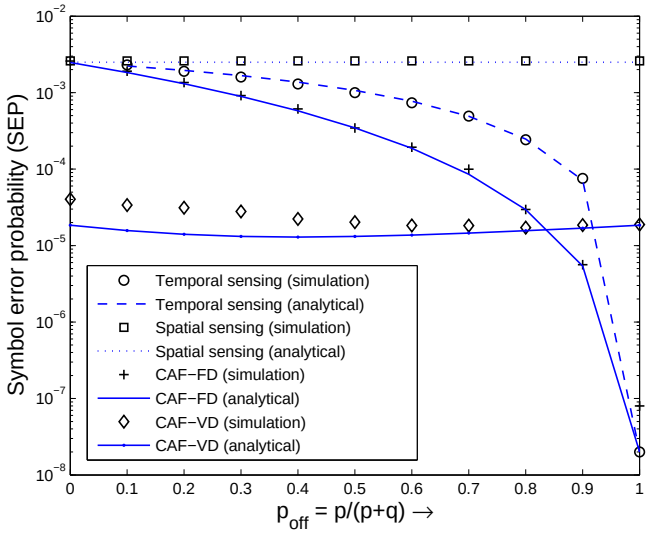

Figure 5.8: Performance of cooperative communication schemes over p_{off}

(MIFTP). The SEP of temporal sensing and CAF-FD decreases when p_{off} increases. For temporal sensing when p_{off} increases, the probability of state sequences 011, 110 and 101, which have a diversity order of 1, are the main sources of decoding error at SR decreases. Hence, the average SEP decreases. For CAF-FD, the probability of state sequences 110, and 111 which have a diversity order of 1 decreases and thus the average SEP decreases. When $p_{off} = 1$, the performances of temporal sensing and CAF-FD are equal. The average SEP of CAF-VD is almost unchanged because the diversity order is always equal to 2 for any frame sequences. For $p_{off} < 0.81$, the CAF-VD always outperforms the CAF-FD. Fig. 5.9 show the spectral efficiency of all various schemes as a function of p_{off}. The spatial sensing and CAF-FD have the same spectral efficiency. We also normalize the spectral efficiency of spatial sensing and CAF-FD 1. The spectral efficiency of temporal sensing and CAF-VD increases as p_{off} increases. The CAF-VD is more spectrally efficient than CAF-FD when $p_{off} > 0.3$. In addition, the CAF-VD outperforms CAF-FD when $p_{off} < 0.81$. Therefore, for $0.3 < p_{off} < 0.81$, CAF-VD has better performance and spectral efficiency than CAF-FD.

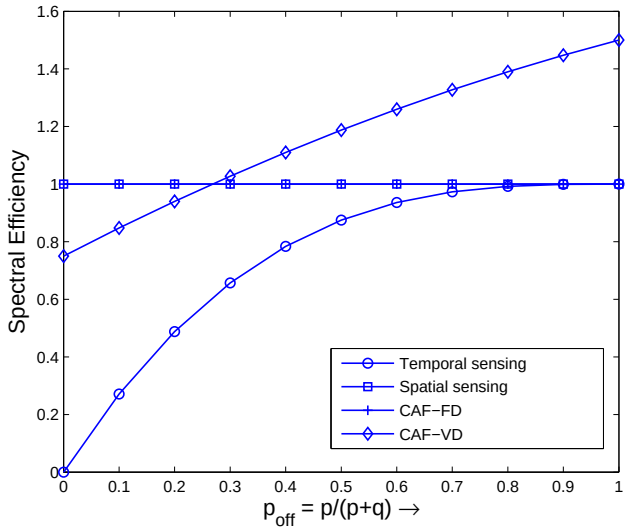

Figure 5.9: Spectral efficiency of different transmission schemes

5.5.3 Incremental Relaying Protocol

In Fig. 5.10, we compare the average SEP of temporal sensing, CAF-FD and CAF-VD with incremental relaying protocol over p_{off}. In term of SEP, both protocols have the same performance. However, in Fig. 5.11, the spectral efficiency of incremental protocol is significantly improved over the protocol without incremental relaying. In Fig. 5.12, the spectral efficiency of the incremental protocol increases when SNR increases.

5.6 Conclusion

We proposed a two cooperative transmission strategies CAF-FD and CAF-VD that exploit spatial and temporal spectrum holes in a cognitive radio network. We used a moment generating function approach to analyze the average symbol error rate of all strategies. Our analytical and simulation results show that our cooperative communication strategies, which exploit both spatial and temporal spectrum holes, significantly reduce the average symbol error probability compared to that of pure spatial and temporal sensing. Of the two cooperative schemes, the CAF-VD results in a lower symbol error probability because the diversity order of the received signal at secondary receiver has the order of two.

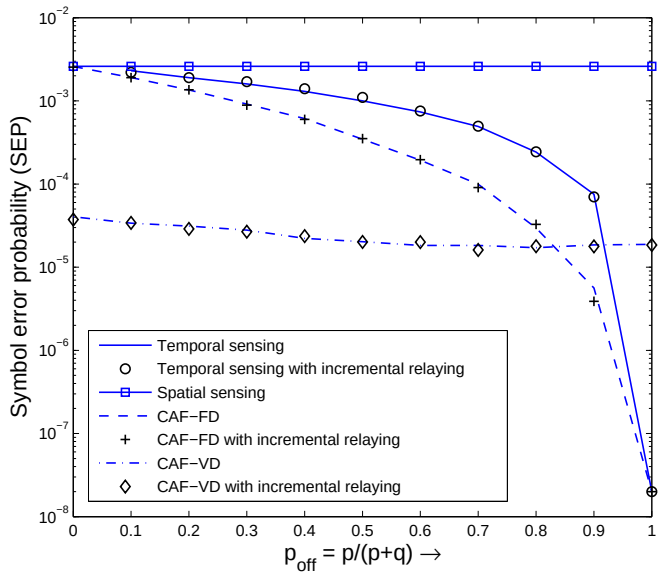

Figure 5.10: Performance of incremental relaying protocol

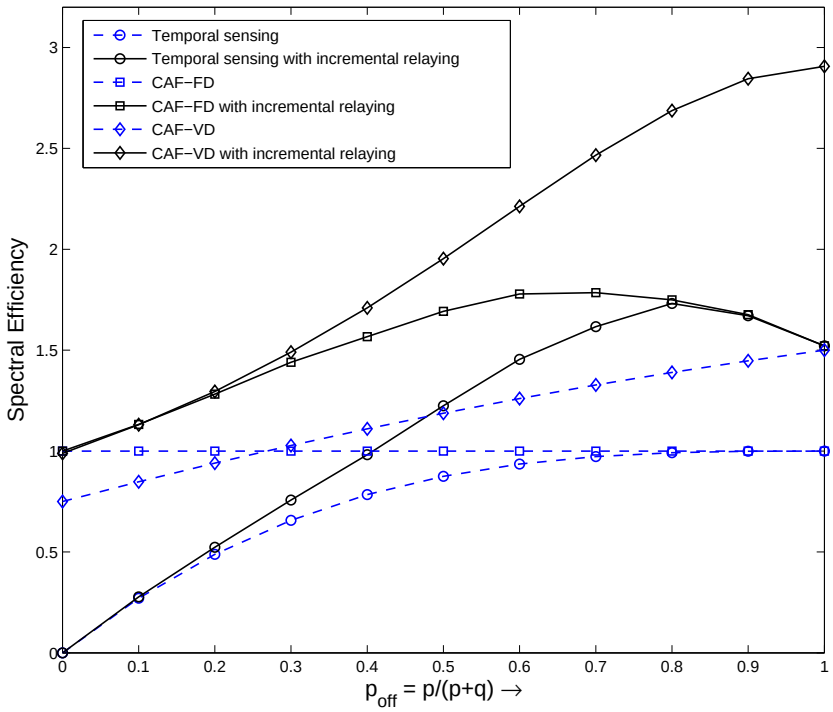

Figure 5.11: Spectral efficiency of incremental relaying protocol

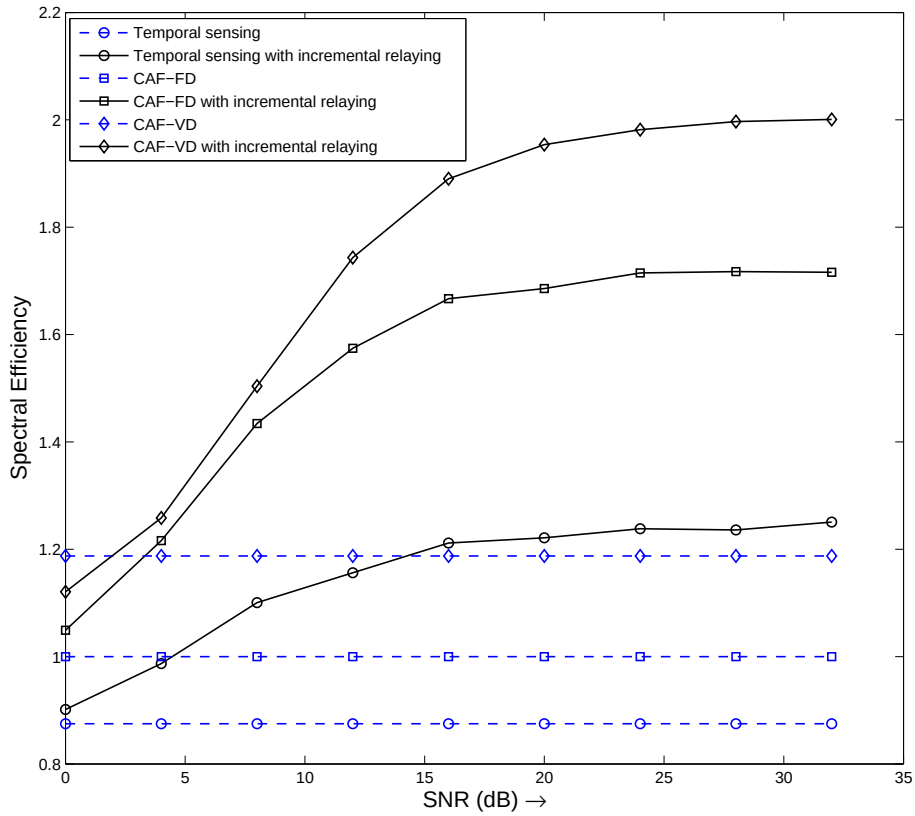

Figure 5.12: Spectral efficiency of incremental relaying protocol over SNR

Chapter 6: Decode-and-Forward Cooperative Transmission in Cognitive Radio Networks

6.1 Introduction

In this chapter[1]. we propose a decode-and-forward transmission strategy that exploits the presence of spectrum holes both in time and in space. Two cooperative communication strategies based on decode-and-forward that exploit the presence of spectrum holes both in time and in space are consider: cognitive decode-and-forward with fixed decoding delay and cognitive decode-and-forward with variable decoding delay. Our results show that the proposed scheme, employing joint spatial-temporal sensing, significantly reduces the average symbol error probability compared to schemes based on pure temporal or pure spatial sensing. We also propose incremental relaying protocol and soft-bit detection scheme which further improves the spectral efficiency of the proposed schemes.

In other paper [69] and in Chapter 5, we studied cooperative communication in a cognitive radio network based on amplify-and-forward strategy. In this chapter, we consider decode-and-forward cooperative communications.

On a given frequency channel, a spectrum hole can be characterized as spatial or temporal. A *spatial* spectrum hole can be specified in terms of the maximum transmission power that a secondary user can employ without causing harmful interference to primary users that are receiving transmissions from another primary user that is transmitting on the given channel. Spatial spectrum sensing is investigated [17], wherein the maximum interference-free transmit power (MIFTP) of a given secondary user is estimated based on signal strengths received by a group of secondary nodes. To calculate the MIFTP for a secondary node, estimates of both the location and transmit power of the primary transmitter

[1]The preliminary contents of this chapter appeared in [80].

are estimated collaboratively by a group of secondary nodes. Using these estimates, each secondary node determines its approximate MIFTP, which bounds the size of its spatial spectrum hole.

A *temporal* spectrum hole is a period of time for which the primary transmitter is idle. During such idle periods, a secondary user may opportunistically transmit on the given channel without causing harmful interference. The problem of detecting when the primary is ON or OFF is called *temporal* spectrum sensing. Cooperative temporal sensing has been studied in [8, 23]. The decision on the ON/OFF status of the primary transmitter can be made either at individual secondary nodes or collaboratively by a group of secondary nodes. In [60], a temporal spectrum sensing strategy that exploits multiuser diversity among secondary nodes is proposed. joint spatial-temporal sensing was proposed in [49, 50] wherein a secondary node performs spatial sensing to determine its MIFTP when the primary transmitter is ON and uses localization information obtained in the process of spatial sensing to improve the performance of temporal sensing, which estimates the ON/OFF state of the primary transmitter.

In a previous chapter 5, we developed a cooperative communication strategy with amplify-and-forward relay that employ joint spatial-temporal sensing to improve the transmission capacity of secondary users in a cognitive radio network. In this chapter, we consider the case of decode-and-forward cooperative communications. In Fig. 5.1(a), the secondary transmitter (ST), labeled as node a, can communicate directly with the secondary receiver (SR), labeled as node b, due to the existence of a spatial spectrum hole with respect to the primary transmitter (PT). However, in the scenario depicted in Figs. 5.1(b), ST can communicate directly with SR only when PT is in the OFF state. In this scenario, when PT is ON, ST transmits to SR via a relay (R), labeled as node r. By enabling the use of both the direct and relay channels, joint spatial-temporal sensing can significantly improve the transmission performance of the secondary systems.

Cooperative relay communications or cooperative diversity has received a lot of attention

in recent years (cf. [42, 43, 46, 70]). Two well-known cooperative strategies are amplify-and-forward (AF) and decode-and-forward (DF). The non-regenerative AF strategy achieves diversity via maximal ratio combining [43] and requires storage of analog waveforms at relay nodes. The regenerative DF strategy is simple and more practical but cannot achieve full diversity unless sophisticated combining is employed at the destination to account for the unreliability of the link from the source to the relay and the link from the relay to the destination [43]. In [46], a smart DF strategy is proposed to achieve available diversity.

In this chapter, we propose a cooperative communication protocol for cognitive radio networks based on the DF strategy. Our protocol decodes the received signals after three time frames. No constraints are placed on the ON/OFF activity of the primary transmitter, i.e., the proportion of time spent in the ON state may be greater or less than that in the OFF state. We focus on the case of a single relay channel.

The remainder of the chapter is organized as follows. Section 6.2 describes the system model. Section 6.3.3 discusses the performance of the system. Section 6.7 presents simulation results. Finally, the chapter is concluded in Section 6.8.

6.2 System Model

We assume the basic system configuration shown in Fig. 5.1. For convenience, we label ST as a, SR as b, and R as r.

6.2.1 Transmission frames and PT behavior

We assume that time on the wireless channel is divided into frames consisting of N_s symbols each. We shall assume perfect symbol-level timing synchronization between the nodes of the secondary system. The case of imperfect synchronization has been studied in [70]. The PT alternates between the ON and OFF states on a per-frame basis according to the on-off Markov model of Fig. 5.2. The ON and OFF durations of the PT are modeled as

geometric random variables with parameters q and p, respectively (cf. [71]). The steady-state probability that PT is ON is given by $p_{\text{on}} = q/(p+q)$, while the probability that PT is OFF is $p_{\text{off}} = p/(p+q)$. In [69], we considered the scenario in which on average, PT in the ON state a greater proportion of time than in the OFF state, i.e., $q > p$. In this chapter, this restriction is removed.

6.2.2 Channel modeling

The received signal according to simple wireless channel model with flat (frequency non-selective) fading without shadowing is given by [72]

$$y = \sqrt{P(d,\epsilon)}hs + n, \tag{6.1}$$

where

$$P(d,\epsilon) \triangleq \delta^2 \left(\frac{d_0}{d}\right)^{\alpha} \epsilon$$

denotes the equivalent transmitted power after taking into account the effect of path loss. Here, δ^2 is the free space signal-power attenuation factor between the source and a reference distance d_0, d is the distance between the source and destination, α is the propagation exponent, $h \sim \mathcal{CN}(0,1)$ is a complex Gaussian random variable with variance σ_h^2, $n \sim \mathcal{CN}(0, N_0)$, and s is the transmitted signal.

When PT is ON, ST and R are limited in the amount of power they can use in order to avoid causing harmful interference to the primary users who receive the transmissions from the PT. The maximum power that can be used by a given secondary node while avoiding harmful interference to primary users is called the *maximum interference-free transmit power* (MIFTP) (cf. [17, 73]). A method for a secondary node to estimate its MIFTP is presented in [17] for the case of a single primary transmitter; the multiple transmitter case is addressed in [53]. Let ϵ_a and ϵ_r denote the MIFTPs of ST and R, respectively, when PT is ON. We

also define

$$P_{ar} = P(d_{ar}, \epsilon_a),\ P_{rb} = P(d_{rb}, \epsilon_r),$$

as the equivalent transmitted powers when PT is ON from ST to R and from R to SR, respectively. Here, d_{ar} and d_{rb} denote the distances between the node pairs (ST, R) and (R, SR), respectively. When PT is ON, the received signal at R and SR consist of the transmitted signal, the noise at the receiver and the co-channel interference from PT. We treat the co-channel interference as noise and the total noise at receiver is zero mean and variance of $N_0 + N_p$ where N_p is the variance of co-channel noise. The co-channel noise is assume to be very small compare to the receiver noise, thus, we can approximate the noise component at the receiver when PT is ON by $\mathcal{N}(0, N_0 + N_p)$. For the case when PT is OFF, we define

$$\tilde{P}_{ab} = P(d_{ab}, \epsilon_m),\ \tilde{P}_{ar} = P(d_{ar}, \epsilon_m),\ \tilde{P}_{rb} = P(d_{rb}, \epsilon_m),$$

as the equivalent transmitted powers from ST to SR, ST to R, and R to SR, respectively. Here, d_{ab} denotes the distance between ST and SR and ϵ_m denotes the maximum transmit power that secondary nodes can use when PT is OFF.

In a cognitive radio network where $\epsilon_a \ll \epsilon_m$, ST may not be able to communicate directly with ST when PT is ON because P_{ar} could be below the required threshold for SR to detect the received signal. In this case, ST can communicate with SR through the relay node R, since $d_{ar} < d_{ab}$.

6.3 Cognitive Decode-and-Forward with Fixed Decoding Delay (CDF-FD)

6.3.1 CDF-FD protocol

We follow the approach of [80] to develop a general decode-and-forward (DF) cooperative transmission protocol for cognitive radio networks. We assume that both ST and R employ

omnidirectional antennas. The secondary receiver (SR) decodes received signals once every three time frames. In general, SR can decodes a signal after any number of time frames. However, increasing the number of transmission time frames results in the low spectral efficiency of the system and higher decoding delay. Therefore, we first consider a fixed number of frames, i.e., three, for transmission and compare the performance of our scheme with various spectrum sensing strategies. In Section 6.4, we also show that by adaptively allocating the number of frames depending on the state of PT, the performance of the scheme can be improved both in terms of probalility of error and spectral efficiency.

Suppose the secondary transmitter (ST) desires to transmit N_s symbols to SR; i.e., it requires one full frame in which PT is OFF. We assume that a time division multiple access (TDMA) protocol is used to coordinate the transmissions of ST and R. During a given time frame, only ST or R is allowed to transmit to SR. Our proposed CAF-DF protocol works as follows:

- In the first two time frames, if PT is OFF, ST transmits to SR. Otherwise, ST transmits signal to R.
- In the third time frame, R transmits to SR.

In order to achieve this, the secondary nodes perform joint spatial-temporal sensing, as discussed in [49, 50]. In particular, all secondary users estimate their MIFTPs based on signal strength measurements, which they exchange with one another. They also decide whether the PT is ON or OFF, by transmitting their local decisions to a fusion center, which then makes the final decision. Maximal ratio combining (MRC) is used at both R and SR to combine the received signals.

The state of PT over three consecutive time frames can be characterized by a three-bit state sequence $c_1c_2c_3$ where $c_i = 1$ if PT is ON during the ith frame and $c_i = 0$, otherwise. Therefore, there are $2^3 = 8$ possible state sequences. During a frame in which PT is OFF, the ST communicates directly with SR using the maximum transmission power ϵ_m. Since an omnidirectional antenna is used at ST, the relay node R receives the signal transmitted

by ST. Let $\boldsymbol{c}$ denote a sequence of frame states and let $|\boldsymbol{c}|$ denote the length of the sequence.

For a given state sequence $\boldsymbol{c}$, let $w_{\boldsymbol{c}}$, $u_{\boldsymbol{c}}$ and $v_{\boldsymbol{c}}$ denote the signals received at SR for link (ST, SR), R for link (ST, R) and at SR for link (R, SR), respectively, at the end of the $|\boldsymbol{c}|$-th frame. For example, u_{10} denotes the received signal at R due to source ST after two time frames, where PT is ON in the first frame and OFF in the second. Let $y_{c_1c_2c_3}$ denote the final MRC-received signal (i.e., the signal obtained using MRC) at SR after three time frames. For example y_{000} is the MRC-received signal at SR after a sequence of three time frames in which PT is OFF during all three frames.

Let f_i, g_i and h_i denote the channel fading coefficients during time frame $i, i = 1, 2, 3$ from ST to SR, ST to R and R to SR, respectively. We assume that f_i, g_i and h_i are constant, independently and identically distributed from one frame to another. Further, the channel states f_i and h_i are available at SR, i.e., via training sequences, but they are not available at ST and R. Also, the g_i are available at R, but not at ST. Hence, maximum likelihood detection can be used at R and SR. Let s be the transmitted signal at ST and let s_d be the decoded signal at R. We model the noise component during time frame i by $n_i \sim \mathcal{CN}(0, N_0), i = 1, 2, 3$, when PT is OFF and $n_i \sim \mathcal{CN}(0, N_0 + N_p), i = 1, 2, 3$, when PT is ON.

Consider the state sequence 000. During the first two time frames, ST transmits the same signal to SR, i.e., a repetition code [74] is used. After the second frame, the received signal at SR from ST is

$$w_{00} = \sqrt{\tilde{P}_{ab}} \sum_{i=1}^{2} |f_i|^2 s + \sum_{i=1}^{2} f_i^* n_i,$$

where x^* denotes the complex conjugate of x. In traditional cooperative transmission scenarios, one advantage of decode-and-forward over amplify-and-forward is that it does not require the storage of an analog signal at the relay thus reducing receiver complexity. However, the MRC at the relay requires the storage of analog signal at the relay which may eliminate advantage of conventional decode-and-forward compared to amplify-and-forward.

For this reason, we propose a practical schems for decoding and combining the received signal at both the relay and SR based on log-likelihood detection in section 6.6. However, we will use the MRC approach because it is easier to analyze and the performance of MRC approach can be used as the upper bound on performance of our system. The numerical results presented in Section 6.7 show that the performance of soft detection approach is closed to MRC approach.

In the MRC approach, the received signal at R is

$$u_{00} = \sqrt{\tilde{P}_{ar}} \sum_{i=1}^{2} |g_i|^2 s + \sum_{i=1}^{2} g_i^* n_i.$$

In the third time frame, R decodes u_{00} to obtain s_d and then forwards s_d to SR. The received signal at SR from R is

$$v_{000} = \sqrt{\tilde{P}_{rb}} h_3 s_d + n_3.$$

The final received signal at SR after MRC is

$$y_{000} = w_{00} + h_3^* v_{000}. \tag{6.2}$$

For state sequence 001, the received signal at SR from ST after the first two time frames is

$$w_{00} = \sqrt{\tilde{P}_{ab}} \sum_{i=1}^{2} |f_i|^2 s + \sum_{i=1}^{2} f_i^* n_i.$$

By using a repetition code, the received signal at the relay R after MRC over the first two time frames is u_{00}. The relay decodes u_{00} and forwards s_d to SR during the third time frame when PT is ON. The received signal at SR from R after the third frame is

$$v_{001} = h_3 \sqrt{P_{rb}} s_d + n_3.$$

The final received signal at SR after MRC is

$$y_{001} = w_{00} + h_3^* v_{001}. \tag{6.3}$$

Consider state sequence 010. During the first time frame, ST transmits the signal

$$w_0 = \sqrt{\tilde{P}_{ab}} f_1 s + n_1.$$

to SR. In the second time frame, ST transmits this signal to R. The received signal at R after two time frames is

$$u_{01} = \left(\sqrt{\tilde{P}_{ar}} |g_1|^2 + \sqrt{P_{ar}} |g_2|^2 \right) s + g_1^* n_1 + g_2^* n_2.$$

The relay R then decodes and forwards the decoded signal s_d to SR, so that

$$v_{010} = \sqrt{\tilde{P}_{rb}} h_3 s_d + n_3.$$

The final received signal at SR is given by

$$y_{010} = f_1^* w_0 + h_3^* v_{010}. \tag{6.4}$$

For the remaining state sequences, the final signal received at SR can be derived similarly.

The results are given as follows:

$$y_{011} = f_1^* w_0 + h_3^* v_{011}, \qquad v_{011} = \sqrt{P_{rb}} h_3 s_d + n_3, \tag{6.5}$$

$$y_{100} = f_2^* w_{10} + h_3^* v_{100}, \qquad v_{100} = \sqrt{\tilde{P}_{rb}} h_3 s_d + n_3, \tag{6.6}$$

$$y_{101} = h_3^* v_{101} + f_2^* w_{10}, \qquad v_{101} = h_3 \sqrt{P_{rb}} s_d + n_3, \tag{6.7}$$

$$y_{110} = h_3^* v_{110}, \qquad v_{110} = h_3 \sqrt{\tilde{P}_{rb}} s_d + n_3, \tag{6.8}$$

$$y_{111} = h_3^* v_{111}, \qquad v_{111} = h_3 \sqrt{P_{rb}} s_d + n_3. \tag{6.9}$$

6.3.2 Pure spatial and pure temporal sensing models

The pure spatial sensing model is equivalent to the case when PT is ON during all three frame, i.e., the state sequence is 111. Therefore, the received signal at SR in the case of pure spatial sensing is given by

$$y^s = y_{111} = h_3^* v_{111}. \tag{6.10}$$

In pure temporal sensing, except for state sequence 000, the transmission strategy is simple repetition code over the time frames during which PT is OFF. The received signal at SR under pure temporal sensing for the eight possible state sequences can be derived as

follows:

$$y^t_{000} = y_{000} \tag{6.11}$$

$$y^t_{001} = \sqrt{\tilde{P}_{ab}} \sum_{i=1}^{2} |f_i|^2 s + \sum_{i=0}^{2} f_i^* n_i \tag{6.12}$$

$$y^t_{010} = (|f_1|^2 + |f_3|^2)\sqrt{\tilde{P}_{ab}} s + f_1^* n_1 + f_3^* n_3 \tag{6.13}$$

$$y^t_{011} = |f_1|^2 \sqrt{\tilde{P}_{ab}} s + f_1^* n_1 \tag{6.14}$$

$$y^t_{100} = (|f_2|^2 + |f_3|^2)\sqrt{\tilde{P}_{ab}} s + f_2^* n_2 + f_3^* n_3 \tag{6.15}$$

$$y^t_{101} = |f_2|^2 \sqrt{\tilde{P}_{ab}} s + f_2^* n_2 \tag{6.16}$$

$$y^t_{110} = |f_3|^2 \sqrt{\tilde{P}_{ab}} s + f_3^* n_3 \tag{6.17}$$

Note that there is no transmission for the state sequence 111, in which PT is ON during all three frames.

The spectral efficiencies for joint-spatial temporal sensing and spatial sensing are equal. The spectral efficiency of temporal sensing is smaller than that of joint spatial-temporal sensing because there is no transmission during state sequence 111. If the joint spatial-temporal sensing scheme has spectral efficiency of 1 then pure temporal sensing has a spectral efficiency of $1 - p_{\text{on}}^3$ where p_{on} is the steady-state probability that PT is ON during a given frame.

6.3.3 Performance analysis

We analyze the performance of decode-and-forward strategy in terms of symbol error probability (SEP). Let denote $\text{SEP}_{\boldsymbol{c}}$ denote the SEP under state e sequence $\boldsymbol{c} = c_1 c_2 c_3$ and let SEP denote the SEP averaged over all possible state sequences for joint spatial-temporal sensing. Under the system model discussed in Section 6.2, the average SEP can be obtained

as

$$\mathrm{SEP} = [p_{\mathrm{off}}^3 \mathrm{SEP}_{000} + p_{\mathrm{off}}^2 p_{\mathrm{on}} (\mathrm{SEP}_{001} + \mathrm{SEP}_{010} + \mathrm{SEP}_{100})$$

$$+ p_{\mathrm{off}} p_{\mathrm{on}}^2 (\mathrm{SEP}_{011} + \mathrm{SEP}_{101} + \mathrm{SEP}_{110}) + p_{\mathrm{on}}^3 \mathrm{SEP}_{111}]. \tag{6.18}$$

We shall assume that M-PSK modulation is used. Using the moment generating function approach in [78, 79], the SEP of M-PSK signals with MRC of L independent fading paths can be expressed as

$$\frac{1}{\pi} \int_0^{\frac{(M-1)\pi}{M}} \prod_{k=1}^{L} M_{\gamma_k} \left(-\frac{g_{\mathrm{PSK}}}{\sin^2 \phi} \right) \mathrm{d}\phi, \tag{6.19}$$

where $g_{\mathrm{PSK}} = \sin^2(\pi/M)$ and $M_{\gamma_l}(u) = (1 - u\bar{\gamma}_l)^{-1}$ is the moment generating function of Rayleigh fading with average SNR γ_l. Let $\mathbf{\Gamma} = (\gamma_1, \gamma_2, \ldots, \gamma_L)$ denote a vector of L average SNR values corresponding to L independent fading paths. Then the SEP can be expressed as

$$\psi(\boldsymbol{P}) = \frac{1}{\pi} \int_0^{\frac{(M-1)\pi}{M}} \prod_{k=1}^{L} \left(1 + \frac{g_{\mathrm{PSK}}}{\sin^2 \phi} \gamma_k \right)^{-1} \mathrm{d}\phi. \tag{6.20}$$

Let $\hat{S}_d$ denote the signal decoded at relay SR. Let $\tilde{\gamma}_{ab} = E\big[|f_i|^2 \frac{\tilde{P}_{ab}}{N_0}\big] = \frac{\tilde{P}_{ab}}{N_0}$ be the average SNR at SR when the transmitter is ST. The average SNR at SR when the transmitter is the relay R is $\gamma_{rb} = E\big[|h_i|^2 \frac{P_{rb}}{(N_0+N_p)}\big] = \frac{P_{rb}}{(N_0+N_p)}$ when PT is ON and $\tilde{\gamma}_{rb} = E\big[|h_i|^2 \frac{\tilde{P}_{rb}}{N_0}\big] = \frac{\tilde{P}_{rb}}{N_0}$ when PT is OFF. Let s_k denote the kth signal in the M-PSK signal constellation, $k = 1, \ldots, M$. For state sequence 000, the received signal is given by (6.2) and the SEP can be expressed as

$$\mathrm{SEP}_{000} = \Pr[\hat{S}_d = s_k] \cdot \mathrm{SEP}_{000|\hat{S}_d = s_k} + \Pr[\hat{S}_d \neq s_k] \cdot \mathrm{SEP}_{000|\hat{S}_d \neq s_k}, \tag{6.21}$$

where s_k is the transmitted signal $k = 1, 2, \ldots M$, and

$$\Pr[\hat{S}_d = s_k] = 1 - \psi(\tilde{\gamma}_{ar}, \tilde{\gamma}_{ar}), \;\; \Pr[\hat{S}_d \neq s_k] = \psi(\tilde{\gamma}_{ar}, \tilde{\gamma}_{ar}),$$

are the probabilities of successful and unsuccessful decoding at the relay, respectively. Here,

$$\mathrm{SEP}_{000|\hat{S}_d = s_k} = \psi(\tilde{\gamma}_{ab}, \tilde{\gamma}_{ab}, \tilde{\gamma}_{rb})$$

is the SEP under state sequence 000 given that $\hat{S}_d = s_k$, and $\mathrm{SEP}_{000|\hat{S}_d \neq s_k}$ is the SEP given that $\hat{S}_d \neq s_k$. The SEP for state sequence 000 can then be written as

$$\begin{aligned} \mathrm{SEP}_{000} = {} & [1 - \psi(\tilde{\gamma}_{ar}, \tilde{\gamma}_{ar})]\psi(\tilde{\gamma}_{ab}, \tilde{\gamma}_{ab}, \tilde{\gamma}_{rb}) \\ & + \psi(\tilde{\gamma}_{ar}, \tilde{\gamma}_{ar}) \cdot \mathrm{SEP}_{000|\hat{S}_d \neq s_k}. \end{aligned} \tag{6.22}$$

Since $\tilde{\gamma}_{ar} \gg \tilde{\gamma}_{ab}$, we have $\psi(\tilde{\gamma}_{ar}, \tilde{\gamma}_{ar}) \to 0$ as $\tilde{\gamma}_{ab} \to \infty$. Therefore, for sufficiently large $\tilde{\gamma}_{ab}$, the right hand side of (6.22) is dominated by the first term. Thus, in this case we have

$$\mathrm{SEP}_{000} \approx [1 - \psi(\tilde{\gamma}_{ar}, \tilde{\gamma}_{ar})]\psi(\tilde{\gamma}_{ab}, \tilde{\gamma}_{ab}, \tilde{\gamma}_{rb}).$$

The validity of this approximation is confirmed in Section 6.7, wherein the simulation results match well with the results from the analytical approximation.

Using similar approach as for the sequence 000, the following expressions for SEP corresponding to the sequences 001 to 101 can be obtained as follows:

$$\mathrm{SEP}_{001} \approx [1 - \psi(\tilde{\gamma}_{ar}, \tilde{\gamma}_{ar})]\psi(\tilde{\gamma}_{ab}, \tilde{\gamma}_{ab}, \gamma_{rb}), \tag{6.23}$$

$$\mathrm{SEP}_{010} \approx [(1 - \psi(\tilde{\gamma}_{ar}, \gamma_{ar})]\psi(\tilde{\gamma}_{ab}, \tilde{\gamma}_{rb}), \tag{6.24}$$

$$\mathrm{SEP}_{011} \approx [1 - \psi(\tilde{\gamma}_{ar}, \gamma_{ar})]\psi(\tilde{\gamma}_{ab}, \gamma_{rb}), \tag{6.25}$$

$$\mathrm{SEP}_{100} \approx [(1 - \psi(\gamma_{ar}, \tilde{\gamma}_{ar})]\psi(\tilde{\gamma}_{ab}, \tilde{\gamma}_{rb}), \tag{6.26}$$

$$\mathrm{SEP}_{101} \approx [1 - \psi(\gamma_{ar}, \tilde{\gamma}_{ar})]\psi(\tilde{\gamma}_{ab}, \gamma_{rb}). \tag{6.27}$$

Let $\hat{S}$ denote the decoded signal at SR. For state sequence 110, we have

$$\mathrm{SEP}_{110} = \Pr[\hat{S} = s_k] \cdot \mathrm{SEP}_{110|\hat{S}_d = s_k} + \Pr[\hat{S}_d \neq s_k] \Pr[\hat{S} \neq s_k].$$

Given that $S_d \neq s_k$, we have $\Pr[\hat{S} \neq s_k] = \Pr[\hat{S} = s_d]$ for BPSK signals. For M-PSK signals with $M \geq 4$,

$$\Pr[\hat{S} \neq s_k] = \Pr[\hat{S} = s_d] + \sum_{i \neq d, i \neq k} \Pr[\hat{S} = s_i]. \tag{6.28}$$

The second term on the right hand side of (6.28) is the probability that ST erroneously decodes the signal given that the transmitted signal from R is s_d. In practice, the probability is on the order of $10^{-\kappa}$, where $\kappa \geq 3$ is a constant. The probability of correct detection at SR given that s_d is transmitted from the relay, is $\Pr[\hat{S} = s_d]$ and is on the order of $1 - 10^{-\kappa}$ where $\kappa \geq 3$. Thus, $\Pr[\hat{S} \neq s_k] \approx \Pr[\hat{S} = s_d]$. Hence, we find that

$$\mathrm{SEP}_{110} = [1 - \psi(\gamma_{ar}, \gamma_{ar})]\psi(\tilde{\gamma}_{rb}) + \psi(\gamma_{ar}, \gamma_{ar})[1 - \psi(\tilde{\gamma}_{rb})], \tag{6.29}$$

$$\mathrm{SEP}_{111} = [1 - \psi(\gamma_{ar}, \gamma_{ar})]\psi(\gamma_{rb}) + \psi(\gamma_{ar}, \gamma_{ar})[1 - \psi(\gamma_{rb})] \tag{6.30}$$

.

6.3.4 Pure spatial and pure sensing

Pure spatial sensing is equivalent to the scenario given by state sequence 111. Hence, the SEP under pure spatial sensing is $\mathrm{SEP}^s = \mathrm{SEP}_{111}$. The SEP under pure temporal sensing is

$$\mathrm{SEP}^t = \frac{1}{1-p_{\mathrm{on}}^3}[p_{\mathrm{off}}^3\mathrm{SEP}_{000} + 3\mathrm{p}_{\mathrm{off}}^2\mathrm{p}_{\mathrm{on}}\mathrm{SEP}_{100} + 3\mathrm{p}_{\mathrm{off}}\mathrm{p}_{\mathrm{on}}^2\mathrm{SEP}_{101}]$$

where $\mathrm{SEP}_{000}^t = \mathrm{SEP}_{000}$, $\mathrm{SEP}_{001}^t = \mathrm{SEP}_{010}^t = \mathrm{SEP}_{100}^t = \psi(\tilde{\gamma}_{ab}, \tilde{\gamma}_{ab})$ and $\mathrm{SEP}_{101}^t = \mathrm{SEP}_{110}^t = \mathrm{SEP}_{011}^t = \psi(\tilde{\gamma}_{ab})$.

6.4 Cognitive Decode-and-Forward with Variable Decoding Delay -(CDF-VD)

In this section, we propose a modified joint spatial-temporal sensing cooperative transmission scheme for cognitive radio networks. Our modified scheme guarantees that the final received signals after maximal ratio combining at secondary receiver always have a diversity order of 2.

6.4.1 CDF-VD Protocol

We propose a cognitive decode-and-forward with variable decoding delay (CDF-VD) cooperative communication protocol in which the MRC received signals at SR always have diversity order of 2. If PT is OFF in the first time frame, the SR will decode the received signals at the end of the second time frame. For state sequence 00, the received signal at SR after MRC is

$$y_{00} = \sqrt{\tilde{P}_{ab}}\sum_{i=1}^{2}|f_i|^2 s + \sum_{i=1}^{2} f_i^* n_i, \tag{6.31}$$

For state sequence 01, the received signal at SR at the end of the first time frame $w_0 = \sqrt{\tilde{P}_{ab}} f_1 s + n_1$ and the received signal at the relay R is $u_0 = \sqrt{\tilde{P}_{ar}} g_1 s + n_1$. In the second time frame, when PT is ON, R decodes the signal u_0 and forwards the decoded signal s_d to SR. The received signal at SR from R is $v_{01} = h_2 \sqrt{P_{rb}} s_d + n_2$. Finally, the received signal at SR with MRC is

$$y_{01} = h_2^* v_{01} + f_1^* w_0 \tag{6.32}$$

If PT is ON during the first time frame and OFF during the second time frame, we have two possible state sequence 100 and 101. The transmission strategy and the received signals at SR for these two *frame sequences* are similar to those presented by CDF-FD protocol (see (6.6) and (6.7)). When PT is ON during the first and second time frames, the possible state sequences for CDF-FD protocol is 110 and 111. If SR decodes the received signal after 3 time frames, the received signals have a diversity order of 1 (see (6.8)) and (6.30). To make the protocol more efficient, SR decodes the received signal after 4 frames. We then have the following possible state sequences 1100, 1101, 1110 and 1111. During the first and second time frames when PT is ON, ST forward the signals to R using a repetition code. The relay R then combines the signals using MRC and decodes and forwards the received signals to SR in the third and fourth time frames. SR combines the received signal during the third and fourth time frames. Hence, the final received signal at SR with MRC has a diversity order of 2.

For state sequence 1100, the received signal at R is $u_{11} = \sqrt{P_{ar}} \sum_{i=1}^{2} |g_i|^2 s + \sum_{i=1}^{2} g_i^* n_i$. The relay R decodes and forwards signal s_d to SR. After combining the two signals, the received signals at SR is

$$y_{1100} = (|h_3|^2 + |h_4|^2) \sqrt{\tilde{P}_{rb}} s_d + h_3^* n_3 + h_4^* n_4. \tag{6.33}$$

Similarly, the received signals for 1101, 1110 and 1111 can be expressed, respectively, as

$$y_{1101} = (|h_3|^2\sqrt{\tilde{P}_{rb}} + |h_4|^2\sqrt{P_{rb}})s_d + h_3^* n_3 + h_4^* n_4, \tag{6.34}$$

$$y_{1110} = (|h_3|^2\sqrt{P_{rb}} + |h_4|^2\sqrt{\tilde{P}_{rb}})s_d + h_3^* n_3 + h_4^* n_4, \tag{6.35}$$

$$y_{1111} = (|h_3|^2 + |h_4|^2)\sqrt{P_{rb}}s_d + h_3^* n_3 + h_4^* n_4. \tag{6.36}$$

6.4.2 Performance Analysis

The CDF-VD protocol has following state sequences: 00, 01, 100, 101, 1100, 1101, 1110 and 1111. The SEP lower bound for state sequences 100 and 101 can be obtained from (6.26) and (6.27). We also have,

$$\mathrm{SEP}_{00} = \psi(\tilde{\gamma}_{ab}, \tilde{\gamma}_{ab}) \text{ and } \mathrm{SEP}_{01} \approx [1 - \psi(\tilde{\gamma}_{ar})]\psi(\tilde{\gamma}_{ab}, \gamma_{ab}).$$

$$\begin{aligned} \mathrm{SEP}_{1100} &= \psi(\tilde{\gamma}_{rb}, \tilde{\gamma}_{rb}) \quad , \mathrm{SEP}_{1101} = \psi(\tilde{\gamma}_{\mathrm{rb}}, \gamma_{\mathrm{rb}}) \\ \mathrm{SEP}_{1110} &= \mathrm{SEP}_{1101} \quad , \mathrm{SEP}_{1111} = \psi(\gamma_{\mathrm{rb}}, \gamma_{\mathrm{rb}}) \end{aligned} \tag{6.37}$$

The average SEP lower bound for diversity-efficient protocol $\mathrm{SEP_d}$ is given vy

$$\begin{aligned} \mathrm{SEP_d} = {} & \mathrm{p_{off}^2 SEP_{00}} + \mathrm{p_{off} p_{on} SEP_{01}} + \mathrm{p_{off}^2 p_{on} SEP_{100}} \\ & + \mathrm{p_{off} p_{on}^2 SEP_{101}} + \mathrm{p_{off}^2 p_{on}^2 SEP_{1100}} + \mathrm{p_{off} p_{on}^3 SEP_{1101}} \\ & + \mathrm{p_{off} p_{on}^3 SEP_{1110}} + \mathrm{p_{on}^4 SEP_{1111}} \end{aligned} \tag{6.38}$$

6.4.3 Spectral efficiency

We normalize the spectral efficiencies of spatial sensing and joint spatial-temporal sensing cognitive cooperative transmission to 1 and denote them as $\mathrm{SE_s}$ and $\mathrm{SE_j}$, respectively, i.e., $\mathrm{SE_j} = \mathrm{SE_s} = 1$. In both the spatial sensing and joint spatial-temporal sensing schemes, one frame of the signal (N_s symbols) is decoded after 3 time frames. In the temporal sensing scheme, there is no transmission for the state sequence 111. Hence, the spectral efficiency of temporal sensing is $\mathrm{SE_t} = 1 - \mathrm{p_{on}}^3$. In the CDF-VD protocol, for state sequence 00, one signal frame is decoded after two time frames. Thus, the spectral efficiency of state sequence 00 is 3/2 compared to joint spatial-temporal sensing. Similarly, the spectral efficiency of state sequence 01, 100, 101, 1100, 1101, 1110 and 1111 are 3/2, 3/3, 3/3, 3/4, 3/4, 3/4 and 3/4, respectively. The spectral efficiency of CDF-VD protocol is then given by

$$\mathrm{SE_d} = 1.5(\mathrm{p_{off}^2} + \mathrm{p_{off}p_{on}}) + \mathrm{p_{on}p_{off}^2} + \mathrm{p_{on}^2p_{off}} + 0.75(\mathrm{p_{on}^2p_{off}}^2 + 2\mathrm{p_{on}^3p_{off}} + \mathrm{p_{on}^4})$$

6.5 Incremental Relaying

Both the CDF-FD and CDF-VD protocols make inefficient use of spectral efficiency because the relay and ST repeat their transmissions all the time. The incremental relaying protocol, proposed in [43] can be applied to our cognitive radio scenarios. The incremental protocol exploits limited feedback, i.e., a single bit feedback, from the secondary transmitter to indicate the success or failure of the transmission. The incremental protocol can be viewed as a hybrid automatic-repeat-request (ARQ) wherein the secondary transmitter or the relay retransmits if the secondary receiver provides negative feedback. Every time the ST receives a signal from ST or R, it decodes the received signal and sends a feedback signal to both ST and R indicate the success/failure of the transmission. If the transmission is successful, ST continues to transmit the next frame. Otherwise, ST or R continues to transmit the signal according to the operation of protocol. We show by simulation in Section 6.7 that incremental relaying significantly improves the spectral efficiency of the system.

6.6 Soft detection

In this section, we propose a more practical decoding approach for relay and secondary receiver. In Section 6.3 and 6.4, the received signals at the relay R and SR are combined using the MRC technique and then decoded. This approach requires the ability to store the analog signal at both R and SR. The advantage of decode-and-forward compare to amplify-and-forward cooperative strategy is that the decode-and-forward does not require the storage of analog signal at the relay. However, the decoding approach proposed in Sections 6.3 and 6.4 still requires the storage of an analog signal. In this section, we propose a soft detection decoding approach which requires only the storage of soft bit information of the received signal. The soft bit information can be quantized and stored in digital form. The soft detection approach is similar to that proposed in [81] and [82]. We follow [81] to compute the log-likelihood of the transmitted bits for simple wireless channel in (6.1), assuming M-PSK modulation. Notice that the received signal y corresponds to M bits. Thus, we need to compute the log-likelihood of M bit using y. We denote the vector of M bit by

$$\mathbf{b} = (b_1, \ldots, b_M).$$

The log-likelihood of kth element of b, b_k is given by

$$\Lambda(b_k) = \log \frac{\Pr[\mathrm{b_k} = 1|\mathrm{y}]}{\Pr[\mathrm{b_k} = 0|\mathrm{y}]} = \log \frac{\Pr[\mathrm{b_k} = 1, \mathrm{y}]}{\Pr[\mathrm{b_k} = 0, \mathrm{y}]}$$

which can be written as

$$\Lambda(b_k) = \log \frac{\sum_{s:s=f(b),b_k=1} \Pr[\mathrm{b_k} = 1, \mathrm{y}]}{\sum_{s:s=f(b),b_k=0} \Pr[\mathrm{b_k} = 0, \mathrm{y}]}$$

By knowing $\mathbf{b}$ we can also obtain knowledge of s; thus,

$$\Lambda(b_k) = \log \frac{\sum_{s:s=f(b),b_k=1} \Pr[\mathrm{y}, \mathrm{s}]}{\sum_{s:s=f(b),b_k=0} \Pr[\mathrm{y}, \mathrm{s}]}$$

where $f(\cdot)$ is the mapping from $\mathbf{b}$ to the transmitted signal s. Because all the constellations points of s are equally likely, we have

$$\Lambda(b_k) = \log \frac{\sum_{s:s=f(b),b_k=1} \Pr[\mathrm{y}|\mathrm{s}]}{\sum_{s:s=f(b),b_k=0} \Pr[\mathrm{y}|\mathrm{s}]}.$$

By substituting in the noise statistics, we obtain

$$\Lambda(b_k) = \log \frac{\sum_{s:s=f(b),b_k=1} \exp\left(-\frac{|y-\sqrt{P}hs|^2}{N_0} \right)}{\sum_{s:s=f(b),b_k=0} \exp\left(-\frac{|y-\sqrt{P}hs|^2}{N_0} \right)}.$$

Combining the log-likelihoods over K time frames is equivalent to summing the log-likelihoods of the individual frames. For example, for state sequence 001, the log-likelihood of the received bit after first two time frames is obtained by taking the sum of the log-likelihood of the received signal of the first and second time frame. In the third time frame, the relay decodes the log-likelihood and convert the bits to M-PSK symbols and forwards them to SR. The log-likelihood of the received signal at SR is the sum of the log-likelihood values of the received signals from ST and from the relay. In this chapter, we assume an uncoded system. However, for coded systems, the log-likelihood values of bits can be directly fed in to the input of a channel decoder using a convolutional code or a turbo code. The performance of the soft detection scheme is compared with MRC detection scheme is evaluated in Section6.7.

6.7 Numerical Results

In this section, we investigate the performance of the proposed decode-and-forward cooperative communication scheme in terms of SEP. The simulation is implemented using MATLAB. We assume that the channel fading coefficients f_i, g_i, $h_i \sim \mathcal{CN}(0,1)$ $(i = 1, 2, 3)$ andthe frame length $N_s = 100$ symbols. The co-channel noise is assumed to be very small, i.e., $N_p = 0$. We assume $\tilde{P}_{ab} = P_{ar} = P_{rb}$ and $\tilde{P}_{ar} = \tilde{P}_{rb} = \tilde{P}_{ab}$+10 (dB) and SNR = $\tilde{\mathrm{P}}_{\mathrm{ab}}/\mathrm{N}_0$.

In Fig. 6.1, we compare the performance of pure temporal sensing and spatial sensing with that of joint spatial temporal-sensing and diversity-efficient protocol when $p_{\text{off}} = p_{\text{on}} = 0.5$ and BPSK modulation is used. We observe that the simulation and analytical results match well with each other. From Fig. 6.1, we see that the performance of the proposed DF cooperative transmission strategy with joint spatial-temporal sensing is about 10 dB and 6 dB better than that of pure spatial sensing and temporal sensing, respectively. Also joint spatial-temporal sensing has better spectral efficiency than pure temporal sensing by a factor of $1/(1 - p_{on}^3) = 1.142$. At BER $= 10^{-4}$, the performance of CDF-VD is about 10 dB better than that of CDF-FD. In Fig 6.2, we compare the performance of all schemes when $p_{\text{off}} = 2p_{on} = 0.66667$, i.e., the PT is OFF a greater portion of time than PT is ON. The analytical and simulation results agree closely with each other. At the BER of interest, the SNR of CDF-FD is 17 dB and 10 dB better than the spatial sensing and temporal sensing, respectively. At BER $= 10^{-4}$, the performance of CDF-VD is about 5 dB better than CDF-FD. When PT is OFF a greater portion of time than PT is ON, the performance of joint spatial-temporal sensing increases as p_{off} increases. This is due to the fact that the portion of time ST can transmit with maximum power increases. However, the performance of CDF-VD is almost unchanged as p_{off} increases. In Fig 6.3, we compare the performance of all scheme with $p_{\text{on}} = 2p_{\text{off}} = 0.66667$, i.e., the PT is ON a greater portion of time than PT is OFF. Both analytical and simulation results are well matched. At the BER of interest, the CDF-FD is 17 dB and 10 dB better than the spatial sensing and temporal sensing, respectively. At BER $= 10^{-4}$, the performance of CDF-VD is about

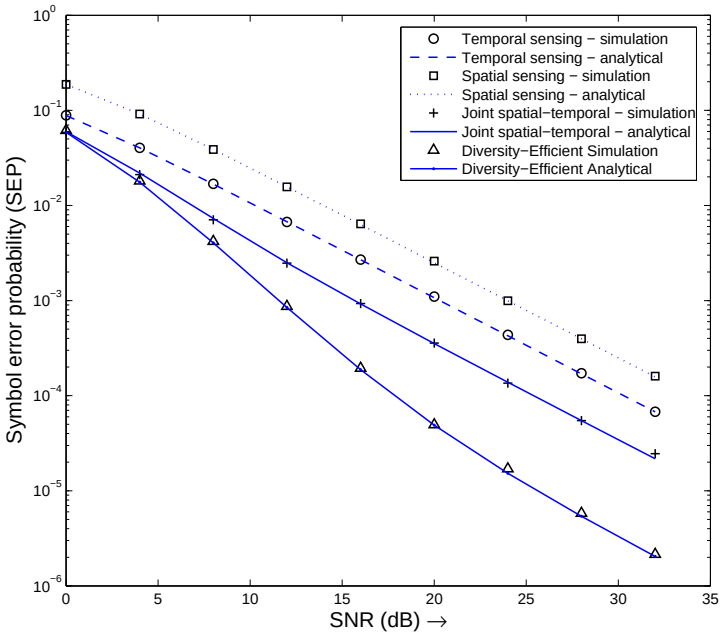

Figure 6.1: Performance of cooperative communication with BPSK modulation $p_{\text{off}} = p_{\text{on}} = 0.5$

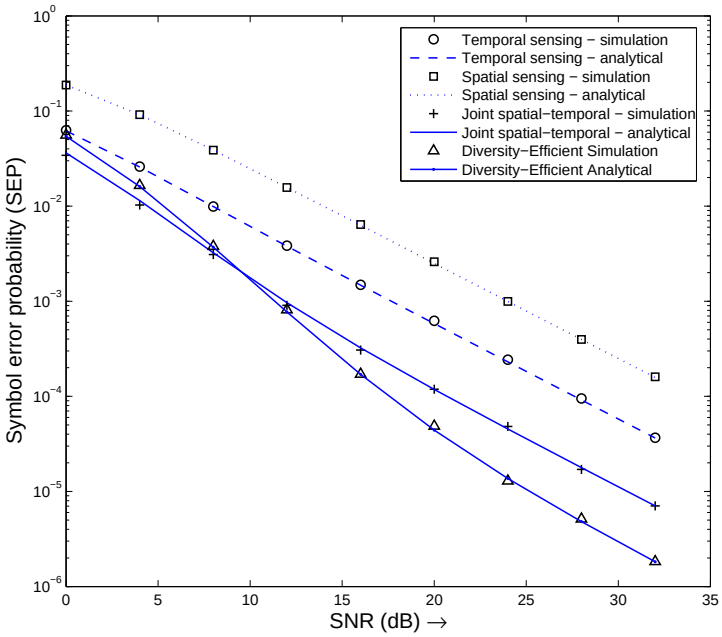

Figure 6.2: Performance of cooperative communication with BPSK modulation $p_{\text{off}} = 2p_{\text{on}} = 0.66667$

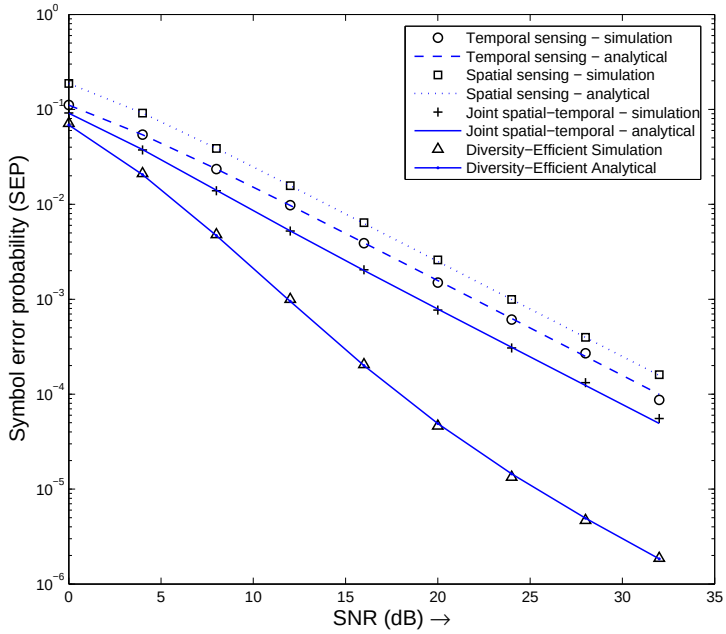

Figure 6.3: Performance of cooperative communication with BPSK modulation $2p_{\text{off}} = p_{\text{on}} = 0.66667$

5 dB better than CDF-FD. Fig. 6.4 shows the performance of the different schemes with QPSK modulation and $p_{\text{off}} = p_{\text{on}} = 0.5$. The simulation and analytical results show close agreement. Note that the performance of our CDF-FD is about 10 dB and 6 dB better than that of pure spatial sensing and temporal sensing, respectively when SEP $= 10^{-3}$. The performance of CDF-VD protocol is about 12 dB better than the performance of CDF-FD at SEP $= 10^{-4}$. In Fig. 6.5, we compare the performance of spatial sensing, temporal sensing, CDF-FD and CDF-VD with cognitive amplify-and-forward with fixed decoding delay (CAF-FD) and variable decoding delay (CAF-VD) discussed in Chapter 5, for different values of $p_{\text{off}} = p/(p+q)$ and SNR $= 16$ dB. CDF-FD outperforms both spatial sensing and temporal sensing for all values of p_{off}. The CDF-VD outperforms CDF-FD for most of value of p_{off}. Note that when $p_{\text{off}} = 1$, the joint spatial-temporal scheme is equivalent to pure temporal sensing, whereas when $p_{\text{off}} = 0$, joint spatial-temporal is equivalent to pure spatial sensing. The CAF-VD outperforms the performance of CDF-VD. Fig. 6.6 compares the spectral efficiencies of the different strategies with and without incremental

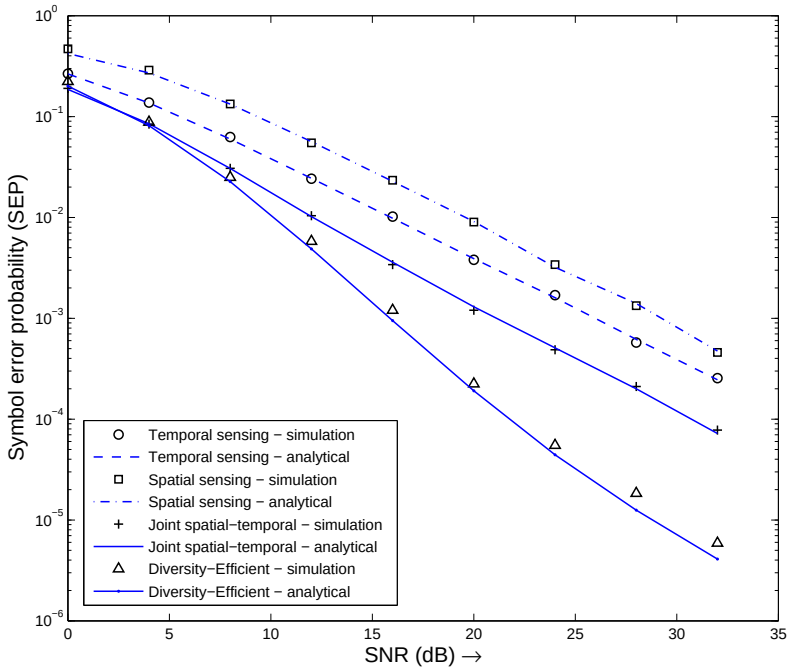

Figure 6.4: Performance of cooperative communication with QPSK modulation.

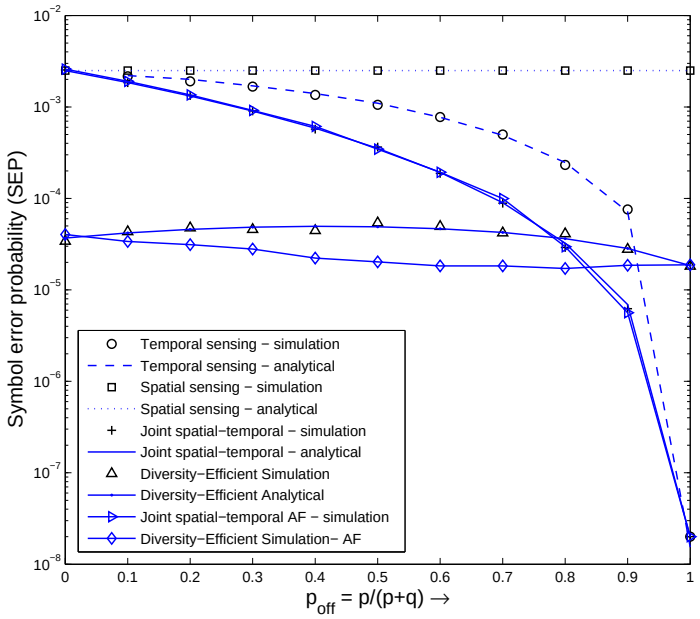

Figure 6.5: Performance of cooperative communication with BPSK modulation vs. $p_{\text{off}} = p/(p+q)$.

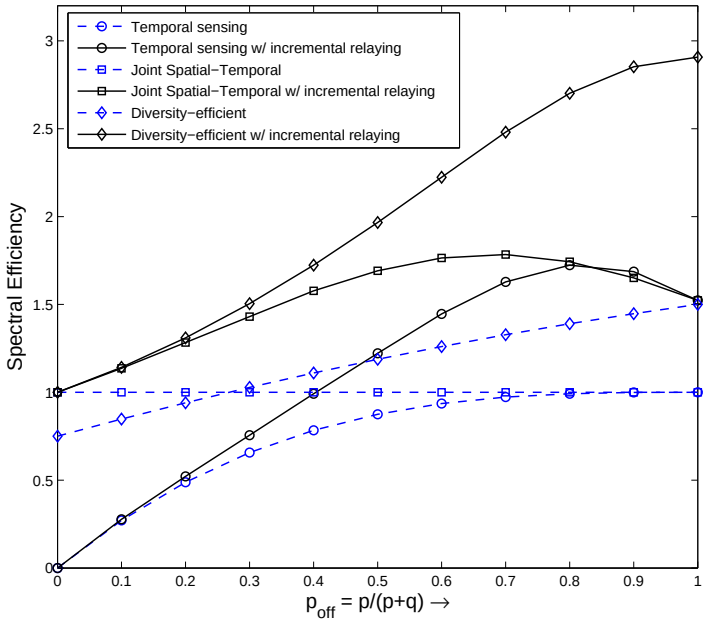

Figure 6.6: Spectral efficiency of all schemes.

relaying. The spectral efficiencies of spatial sensing and CDF-FD are the same and are normalized as 1. As we can see, the spectral efficiency of temporal sensing is smaller than that of CDF-FD. When $p_{\text{off}} = 0$, there is no transmission for temporal sensing, implying that the spectral efficiency is zero in this case. For all scheme, the spectral efficiency with incremental relaying is much higher than that without incremental relaying. In Fig. 6.7 and Fig. 6.8, we compare the performance of the log-likelihood detection scheme with the schemes discussed in Section 6.3 and section 6.4 for BPSK and QPSK modulation. For both BPSK and QPSK modulation, the performance of log-likelihood scheme is close to the performance of schemes of Sections 6.3 and 6.4.

6.8 Conclusion

We proposed a cooperative communication protocol with decode-and-forward relays for opportunistic spectrum access in cognitive radio networks. Our protocols combine joint spatial-temporal spectrum sensing and relaying to increase the transmission capacity of

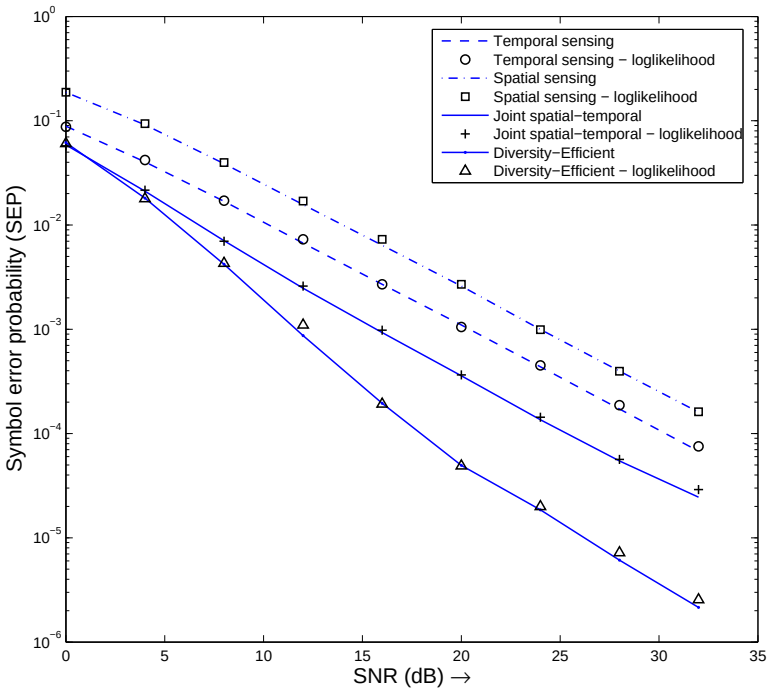

Figure 6.7: Performance of log-likelihoood detection with BPSK.

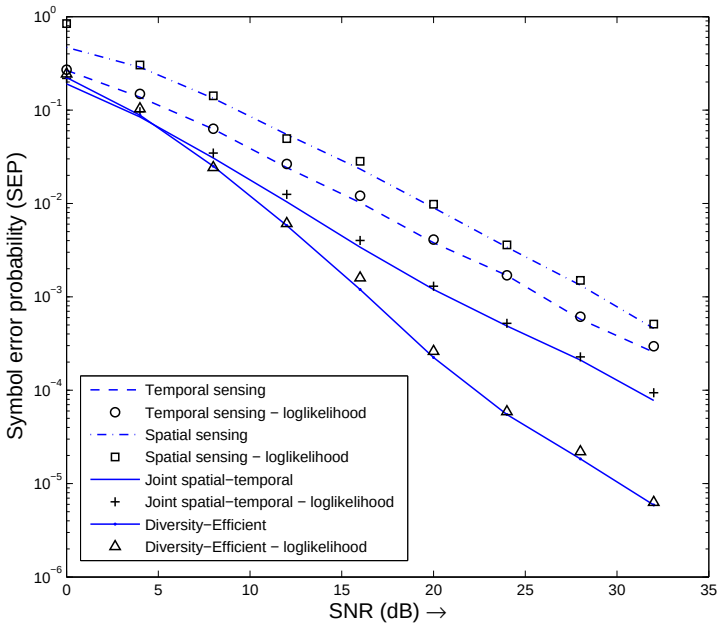

Figure 6.8: Performance of log-likelihoood detection with QPSK.

cognitive radio networks. Both simulation and analytical results confirm that the proposed scheme outperforms schemes based on pure spatial sensing or pure temporal sensing alone.

Chapter 7: Exploiting Multichannel Diversity in Cognitive Radio Networks

7.1 Introduction

In this chapter[1], we consider a multichannel cognitive radio network scenario in which a secondary transmitter can switch to different channels for opportunistic communications. Multichannel diversity can be achieved by dynamically switching to different channels during transmission. Our numerical results show that even a simple randomized channel switching scheme can significantly reduce the average symbol error probability. We also propose a scheduling algorithm based on maximizing the signal-to-noise ratio to further improve the performance of cognitive transmission. Finally, we study the performance of our multichannel switching schemes combined with *capacity achieving* turbo codes. Our numerical results show that combination of randomized multichannel switching with turbo codes significantly improves the performance of the system.

On a given frequency channel, a spectrum hole can be characterized as spatial or temporal. A *spatial* spectrum hole can be specified in terms of the maximum transmission power that a secondary user can employ without causing harmful interference to primary users that are receiving transmissions from another primary user that is transmitting on the given channel. Spatial spectrum sensing is investigated [17], wherein the maximum interference-free transmit power (MIFTP) of a given secondary user is estimated based on signal strengths received by a group of secondary nodes. To calculate the MIFTP for a secondary node, estimates of both the location and transmit power of the primary transmitter are estimated collaboratively by a group of secondary nodes. Using these estimates, each

[1]The preliminary contents of this chapter appeared in [83, 84].

secondary node determines its approximate MIFTP, which bounds the size of its spatial spectrum hole.

A *temporal* spectrum hole is a period of time for which the primary transmitter is idle. During such idle periods, a secondary user may opportunistically transmit on the given channel without causing harmful interference. The problem of detecting when the primary is ON or OFF is called *temporal* spectrum sensing. Cooperative temporal sensing has been studied in [8, 23]. The decision on the ON/OFF status of the primary transmitter can be made either at individual secondary nodes or collaboratively by a group of secondary nodes. In [60], a temporal spectrum sensing strategy that exploits multiuser diversity among secondary nodes is proposed.

In earlier work [49, 50], we proposed a joint spatial-temporal sensing for cognitive radio networks. In this scheme, a secondary node performs spatial sensing to determine its MIFTP when the primary transmitter is ON and uses localization information obtained in the process of spatial sensing to improve the performance of temporal sensing, which estimates the ON/OFF state of the primary transmitter. Joint spatial-temporal sensing has higher achievable capacity compared to pure spatial or temporal sensing [50]. In [69], a combined joint spatial-temporal sensing and amplify-and-forward cooperative relaying scheme is proposed to improve the performance of cognitive transmission. A decode-and-forward cooperative communication scheme is investigated in [80].

In this chapter, we consider a multichannel cognitive radio network in which N primary transmitters (PTs) operate on N different channels with frequencies f_i, $i = 1, \ldots, N$. Multichannel cognitive radio networks have been studied in [35–38]. In [36, 37], a dynamic programming approach is proposed to search for an optimal sensing order among the channels. In [35], a *channel-aware switching* algorithm is developed to decide *where* and *when* to switch among the candidate channels. Sequential temporal sensing algorithms are developed for OFDM-based hierarchical cognitive radio systems in [38]. In all of the aforementioned works, only pure temporal spectrum sensing is considered.

In this chapter, we investigate channel switching in multichannel cognitive radio networks employing joint spatial-temporal sensing with repetition codes [74] and also turbo codes [85]. In our scheme, secondary users can switch to a new channel even when the primary user on that channel is ON and continue to transmit using MIFTP. We show that even for a simple *randomized channel switching* scheme, our scheme outperforms the conventional scheme in which secondary users stay on the same channel during transmission. We propose a *maximized signal-to-noise ratio* scheduling scheme that can further improve the performance of secondary user transmissions. This scheme requires the knowledge of *channel state information* (CSI) and the ON/OFF states of each PT before scheduling transmission. The CSI can be estimted at secondary reciever and feedback to the centralized scheduler. We assume that perfect estimated CSI at both secondary receiver and the scheduler, i.e, the CSI feed back channel is error free.

We also study the performance of our multichannel switching scheme in combination with *capacity achieving* turbo codes instead of repetition codes. Turbo codes are a class of high performance forward error correction (FEC) codes developed in 1993 [85], which were the first practical codes to closely approach the channel capacity. Turbo codes are used extensively in 3G [86] and 4G mobile standards, e.g., in High Speed Packet Access (HSPA), Long Term Evolution (LTE) and IEEE 802.16 (WIMAX) [87,88]. We first consider a system model for *randomized channel switching* wherein the secondary transmitter is switched to only one channel during frame transmission. We then consider scenarios in which secondary transmitter can switch to multiple channels during signal transmission. We show that the performance of repetition codes does not improve as the secondary transmitter switches to multiple channels, but that of turbo codes does improve.

The remainder of the chapter is organized as follows. Section 7.2 describes the system model. Section 7.3 discusses the randomized channel switching algorithm and its performance. The maximizing SNR scheduling algorithm is proposed in Section 7.4. Section 7.5 presents the combined turbo codes with multichannel switching algorithms. Section 7.6 presents numerical results. Finally, the chapter is concluded in Section 7.7.

7.2 System Model

7.2.1 Transmission frames and PT behavior

We assume that the licensed wireless spectrum consists of N non-overlapping channels with frequencies f_i, $i = 1, 2, \ldots, N$. There is one PT on each channel. Secondary users are equipped with a single half-duplex transceiver capable of switching to different channels. Time on the wireless channel is divided into frames consisting of N_s symbol transmission times. Each PT alternates between the ON and OFF states on a per-frame basis according to the on-off Markov model of Fig. 5.2. The ON/OFF states of PTs are independent from one PT to another. The ON and OFF durations of PT i are modeled by geometric random variables with parameters q_i and p_i, respectively (cf. [71]). The steady-state probability that PT i is ON is given by $p_i^{\text{on}} = q_i/(p_i + q_i)$, while the probability that PT is OFF is $p_i^{\text{off}} = p_i/(p_i + q_i)$.

7.2.2 Channel modeling

When a PT is ON, a secondary transmitter (ST) is limited in the amount of power it can use in order to avoid causing harmful interference to the primary users who receive the transmissions from the PT. The maximum power that can be used by a given secondary node while avoiding harmful interference to primary users is called the *maximum interference-free transmit power* (MIFTP) (cf. [17, 73]). A method for a secondary node to estimate its MIFTP is presented in [17] for the case of a single primary transmitter; the multiple transmitter case is addressed in [53].

In [49, 50], a joint spatial-temporal sensing scheme is proposed for one PT with a single channel at frequency f. This scheme can easily be extended to the multichannel scenario. In particular, at the beginning of each transmission frame, a set of secondary nodes collaboratively estimates the ON/OFF state of PT i by switching to channel f_i using temporal sensing algorithms proposed in [49, 50]. Spatial spectrum holes on channel i in terms of MIFTP can be estimated by a group of secondary users switching to frequency f_i. We

assume that the MIFTP of a secondary user on channel f_i remains unchanged until the location of PT i changes.

Both spatial sensing and temporal sensing over N cognitive channels can be performed simultaneously by using N sets of temporal or spatial sensing nodes or sequentially by one set of temporal or spatial sensing nodes which sequentially switches among the set of N channels. In practice, the time scale over which the PT changes its location is much larger than the time scale of its ON/OFF durations. Under this assumption, the extra overhead of joint spatial-temporal sensing compared to pure temporal sensing is not significant.

For a given PT i with frequency f_i, the wireless channel is modeled by Rayleigh fading with time correlation [89]. We assume that the channel remains constant for a duration of $N_s/2$ symbols. For the first half of the transmission frame, the received signal of a simple wireless channel model with flat (frequency non-selective) fading without shadowing is given by [72]

$$y_1 = \sqrt{P(d,\epsilon)} h_i s_1 + n_1, \tag{7.1}$$

where

$$P(d,\epsilon) \triangleq \delta^2 \left(\frac{d_0}{d}\right)^{\alpha} \epsilon$$

denotes the equivalent transmitted power after taking into account the effect of path loss. Here, δ^2 is the free space signal power attenuation factor between the source and a reference distance d_0, d is the distance between the source and destination, α is the propagation exponent, $h_i \sim \mathcal{CN}(0,1)$ is a complex Gaussian random variable with variance 1, $n_1 \sim \mathcal{CN}(0, N_0)$, and s_1 is the transmitted signal.

For the second half of the frame, we have

$$y_2 = \sqrt{P(d,\epsilon)} g_i s_2 + n_2, \tag{7.2}$$

where

$$g_i = \rho_i h_i + \sqrt{1-\rho_i^2}\alpha_i, \tag{7.3}$$

where $\alpha_i \sim \mathcal{CN}(0,1)$ and ρ_i is the channel autocorrelation at delay time τ [89]

$$\rho_i = J_0(2\pi D_i \tau)$$

with D_i is the Doppler shift of the channel i and τ is the time to transmit $N_s/2$ symbols

Let ϵ_i and $\tilde{\epsilon_i}$ denote the MIFTP of a given ST when PT i is ON and the maximum transmission power that can be used when PT i is OFF, respectively. We also define

$$P_i = P(d, \epsilon_i),\ \tilde{P}_i = P(d, \tilde{\epsilon_i}),$$

as the equivalent transmitted powers when PT i is ON from ST to a given secondary receiver (SR) at a distance d from ST when PT i is ON and OFF, respectively. To combat the low SNR at the secondary receiver (SR) due to limited transmit power at ST, a repetition code [74] is used at ST to transmit signals to SR. We note that the repetition code is close to optimal in the low SNR regime [74]. By using a repetition code, ST transmits the same signal $s_1 = s_2 = s$ during both halves of the transmission frame. We also assume that the channel fading coefficients h_i and g_i can be estimated at SR, i.e., via training sequences. We further assume that maximal ratio combining (MRC) is used to combine the received signal at SR. Hence, the final received signal at SR is

$$y = \sqrt{P}(|h_i|^2 + |g_i|^2)s + h_i^* n_1 + g_i^* n_2, \tag{7.4}$$

where $P = P_i$ when PT i is ON and $P = \tilde{P}_i$ when PT i is OFF.

7.3 Exploiting multichannel diversity

Consider a simple scenario in which we have two communicating pairs (ST 1, SR 1) and (ST 2, SR 2) over two cognitive radio channels with frequencies f_1 and f_2, respectively. When there is no channel switching, i.e., ST i uses the same channel f_i to communicate with SR i, the received signal at SR (cf. (7.4)) cannot achieve a diversity order of two because h_i and g_i are correlated. To exploit multichannel diversity, during the first half of the frame, ST 1 uses channel f_1 to communicate with SR 1 and switches to channel f_2 during the second half of the frame. Thus, the received signal at SR 1 is

$$y = (\sqrt{\mu_1}|h_1|^2 + \sqrt{\mu_2}|g_2|^2)s + h_1^* n_1 + g_2^* n_2, \tag{7.5}$$

where $\mu_1 = P_1$ or $\mu_1 = \tilde{P}_1$ if PT 1 is ON or OFF, respectively and $\mu_2 = P_2$ or $\mu_2 = \tilde{P}_2$ if PT 2 is ON or OFF, respectively. Since h_1 and g_2 are independent, the received signal at SR 1 has a diversity order of two. Similarly, the received signal at SR 2 also has a diversity order of two.

We expect that the average symbol error probability (SEP) will decrease compared to the case when there is no channel switching. In the general scenario, we may have N channels with frequencies f_i and N pairs (ST i, SR i), $i = 1, 2, \ldots, N$. In this case, pair (ST i, SR i) can switch to channel $j \neq i$ during the second half of the transmission frame as long as there is no transmission on channel j. We assume that there is a centralized scheduler or a medium access control protocol to oversee the process of channel switching for the secondary users.

7.3.1 Performance Analysis

Randomized channel switching one channel

Next, we analyze the performance in terms of the average symbol error probability (SEP) of our scheme. Let p_i^{on} and p_i^{off}, respectively, denote the ON and OFF probabilities of PT i,

$i = 1, 2$. We shall assume that M-PSK modulation is used. Using the moment generating function (MGF) approach in [78,79], the SEP of M-PSK signals with MRC of L independent fading paths can be expressed as

$$\frac{1}{\pi}\int_0^{\frac{(M-1)\pi}{M}} \prod_{k=1}^{L} M_{\gamma_k}\left(-\frac{g_{\text{PSK}}}{\sin^2\phi}\right) \mathrm{d}\phi, \tag{7.6}$$

where $g_{\text{PSK}} = \sin^2(\pi/M)$ and $M_{\gamma_l}(u) = (1 - u\bar{\gamma_l})^{-1}$ is the moment generating function of Rayleigh fading with average SNR γ_l.

Let $\mathbf{\Gamma} = (\gamma_1, \gamma_2, \ldots, \gamma_L)$ denote a vector of L average signal-to-noise ratio values corresponding to L independent fading paths. Then the SEP can be expressed as

$$\psi(\mathbf{\Gamma}) = \frac{1}{\pi}\int_0^{\frac{(M-1)\pi}{M}} \prod_{k=1}^{L} \left(1 + \frac{g_{\text{PSK}}}{\sin^2\phi}\gamma_k\right)^{-1} \mathrm{d}\phi. \tag{7.7}$$

The received signal in (7.5) is obtained via maximal ratio combining of two independent Rayleigh fading channel. Using the MGF approach, the SEP values for different states of PT 1 and PT 2 are given by

$$\begin{aligned} \text{SEP}_{\text{on,on}} &= \psi(\gamma_1, \gamma_2), \quad \text{SEP}_{\text{on,off}} = \psi(\gamma_1, \tilde{\gamma_2}), \\ \text{SEP}_{\text{off,on}} &= \psi(\tilde{\gamma_1}, \gamma_2), \quad \text{SEP}_{\text{off,off}} = \psi(\tilde{\gamma_1}, \tilde{\gamma_2}), \end{aligned} \tag{7.8}$$

respectively. The average SEP over all possible states of PT 1 and PT 2 is given by

$$\begin{aligned} \overline{\text{SEP}}_{\text{rand}} &= p_1^{\text{on}} p_2^{\text{on}} \text{SEP}_{\text{on,on}} + \text{p}_1^{\text{on}} \text{p}_2^{\text{off}} \text{SEP}_{\text{on,off}} \\ &\quad + p_1^{\text{off}} p_2^{\text{on}} \text{SEP}_{\text{off,on}} + \text{p}_1^{\text{off}} \text{p}_2^{\text{off}} \text{SEP}_{\text{off,off}}. \end{aligned} \tag{7.9}$$

In the case of pure spatial sensing, PT 1 and PT 2 always transmit with their MIFTP values, so the average SEP in this case is simply $\text{SEP}_{\text{on,on}}$.

No channel switching

When there is no channel switching, the received signal at a secondary receiver is given by (7.4). Since $h_i \sim \mathcal{CN}(0,1)$, we can write $h_i = a_i + jb_i$, where $a_i, b_i \sim \mathcal{N}(0, 0.5)$. In (7.3), let $\alpha_i = c_i + jd_i$ where $c_i, d_i \sim \mathcal{N}(0, 0.5)$. The term $|h_i|^2 + |g_i|^2$ in (7.4) can be rewritten as

$$|h_i|^2 + |g_i|^2 = (1+\rho^2)(a_i^2 + b_i^2) + (1-\rho^2)(c_i^2 + d_i^2)$$

$$+ 2\rho\sqrt{1-\rho^2}(a_i c_i + b_i d_i).$$

We have $E[(a_i c_i + b_i d_i)] = 0$ where $E[\cdot]$ denotes the expectation operator. Hence, we can approximate

$$|h_i|^2 + |g_i|^2 \approx (1+\rho^2-\delta)(a_i^2+b_i^2) + (1-\rho^2)(c_i^2+d_i^2), \tag{7.10}$$

where the constant δ accounts for the fact that when the term $a_i c_i + b_i d_i$ is negative, the received SNR is effectively reduced, resulting in erroneous symbol detection. An approximate value for δ can be determined by computer simulation. We obtain

$$\delta = \begin{cases} \rho^2(1-\rho), & \text{if } \rho < 0.7, \\ \rho(1-\rho), & \text{if } \rho \geq 0.7. \end{cases} \tag{7.11}$$

Combining (7.10) and (7.4), we have

$$y_a \approx \sqrt{P}\big[(1+\rho^2-\delta)|h_i|^2 + (1-\rho^2)|\alpha_i|^2\big]s + z, \tag{7.12}$$

where $z = h_i^* n_1 + g_i^* n_2$. The received signal y_a in (7.12) can be approximated by the maximal ratio combination of two independent channels with Rayleigh fading coefficients h_i and α_i and average SNRs $\gamma_1 = P(1+\rho^2-\delta)/N_0$ and $\gamma_2 = P(1-\rho^2)/N_0$. Finally, the

average SEP at the secondary receiver in the absence channel switching is

$$\mathrm{SEP}_{\mathrm{conv}} = \psi(\gamma_1, \gamma_2). \tag{7.13}$$

Our analysis is confirmed by simulation results presented in Section 7.6.

7.4 Maximized SNR scheduling algorithm

In this section, we propose a scheduling algorithm for exploiting multichannel diversity in cognitive radio networks. Our scheduling algorithm maximizes the signal-to-noise ratio of the received signal at SR. We assume that N cognitive channels with frequencies f_i, $i = 1, 2, \ldots, N$, allow the simultaneously transmission of up to N pairs of (ST, SR). Let $K \leq N$ be the number of concurrent secondary transmissions. We also assume that the scheduler knows the ON/OFF state of PT i. The scheduler maintains a state vector $\boldsymbol{p}$ whose ith component $p(i) = 1$ when PT i is OFF and $p(i) = 0$ when PT i is ON.

Through spatial sensing, scheduler can obtain an estimate of the distance between ST i and SR i and therefore an estimate of the equivalent transmitted powers P_i and $\tilde{P}_i$. The scheduler is assumed to have knowledge of the channel state information (CSI) matrix H at the beginning of each transmission frame. The CSI matrix G is also available during the second half of the transmission frame. These CSI matrices can be estimated at the SR via training and then forwarded to scheduler. The elements of the channel matrix $\boldsymbol{H}$ are denoted by $H(i, j) = h_{ij}$, where $1 \leq i \leq N$ and $1 \leq j \leq K$ and h_{ij} is the channel gain between ST j and SR j on channel i for the first half of the transmission frame. The (i, j) element of the channel matrix $\boldsymbol{G}$, $G(i, j) = g_{ij}$, is the channel gain between ST j and SR j on channel i for the second half of the transmission frame. We have

$$g_{ij} = \rho_{ij} h_{ij} + \sqrt{1 - \rho_{ij}^2}\alpha_{ij},$$

where ρ_{ij} is the channel autocorrelation between ST j and SR j on channel i at time τ and

$\alpha_{ij} \sim \mathcal{CN}(0,1)$.

The scheduler also maintains an idle/reserved channel status matrix $\boldsymbol{S}$ of dimension $N \times 2$, where $S(i,1) = 0$ if the first half of transmission frame of channel i is idle; otherwise $S(i,1) = 1$, i.e., the first half of transmission frame of channel i is reserved for transmission. We also have $S(i,2) = 0$ if the second half of transmission frame of channel i is idle, otherwise $S(i,2) = 1$, i.e., second half of transmission frame of channel i is reserved for transmission.

Algorithm 2 Maximized SNR channel scheduling algorithm

Input: ON/OFF state vector $\mathbf{p}$, CSI matrices $\mathbf{H}$ and $\mathbf{G}$, idle/reserved matrix $\mathbf{S}$
for $j = 1$ to K **do**
  $t \leftarrow 0$
  while $t < K$ **do**
    $k \leftarrow j + t \mod K$
    $\mathbf{S} \leftarrow \mathbf{0}$
    if (First half of transmission frame) **then**
      $S_1(k) \leftarrow \arg\max_{i,S(i,1)=0}\{(\gamma_i + p(i)(\tilde{\gamma}_i - \gamma_i))|h_{ij}|^2\}$
      $S(S_1(k),1) \leftarrow 1$
    end if
    ST i transmits on channel $S_1(i)$ for $i = 1,2,\ldots,K$ during the first half of the transmission frame
    if (Second half of transmission frame) **then**
      $S_2(k) \leftarrow \arg\max_{i,S(i,2)=0}\{(\gamma_i + p(i)(\tilde{\gamma}_i - \gamma_i))|h_{ij}|^2\}$
      $S(S_2(k),2) \leftarrow 1$
    end if
    $t \leftarrow t + 1$
  end while
  ST i transmits in channel $S_2(i)$ for $i = 1,2,\ldots,K$ during the second half of the transmission frame
end for

At the beginning of transmission frame, Algorithm 2 starts with user 1. It finds the channel k in the list of N available channels such that the received SNR γ_k is maximized where $\gamma_k = P_k|h_{k1}|^2/N_0$ if PT is ON and $\gamma_k = \tilde{P}_k|h_{k1}|^2/N_0$ if PT is OFF. After channel k is reserved for user 1, it is removed from the list of available channels. The algorithm the proceeds to user 2 and repeats with the list of $N-1$ remaining channels. The algorithm continues until all the users have been scheduled.

Thus, the number of idle channels for user K is $N-K+1$ because $K-1$ channels have been reserved for the $K-1$ previous users. Because of the multichannel fading diversity,

the larger the number of idle channels, a larger value of γ_k can be obtained. Clearly, in this algorithm, the first user has the greatest advantage. Therefore, to ensure fairness among users, in the next transmission frame, Algorithm 2 starts with user 2 and ends with user 1. After completing the scheduling task, i.e., the vector $\mathbf{S_1} = (S_1(k),\ k = 1, \ldots, K)$ is obtained, which indicates that ST k uses channel $S_1(k)$ to transmit to SR k, $k = 1, \ldots, K$ in the first half of the transimission frame. The same algorithm is used to obtain $\mathbf{S_2} = (S_2(k),\ k = 1, \ldots, K)$, the scheduling vector for the second half of the transmission frame. The performance of the proposed maximized SNR scheme is expected to outperform that of the simple randomized channel switching scheme discussed in Section 7.3. This is confirmed by our numerical results presented in Section 7.6.

7.5 Channel switching combined with turbo codes

In this section, we study the performance of a coded multichannel cognitive radio system. In particular, we combine *capacity achieving* turbo codes with our proposed multichannel switching algorithms. Turbo codes, proposed in [85], can achieve a performance close to the Shannon limit if the code length is sufficiently long.

7.5.1 System modeling with turbo codes

In Section 7.2, we proposed a system model for exploiting multichannel diversity in which the repetition code is used. Although, repetition codes are close to optimal in the low SNR regime [74], they have been shown to be bandwidth inefficient in moderate and high SNR regimes. If we use turbo codes, repetition codes are not needed. We follow the system model described in [81]. At the transmitter side, the data is divided in to the block of N_b bits and encoded by a binary turbo code. The turbo code consists of two systematic recursive convolutional codes concatenated in parallel via a pseudorandom interleaver [85]. The output turbo-encoded bits are then interleaved by an interleaver and mapped to a particular signal constellation by the modulator. The additional interleaver is used to

remove the correlation between the consecutive bits being transmitted. The size of the interleaver is chosen based on the delay requirement of the application. Since the coded modulation is obtained by concatenating a binary encoder to a modulator through a bit interleaver, it has the form of bit-interleaved coded modulation [90].

At the receiver, when there is no channel switching, the received signal is

$$y_1 = \mu_i h_i s + n_1$$

for the first half of the transmission frame and

$$y_2 = \mu_i g_i s + n_2,$$

for the second half, where s is the transmitted signal, h_i and g_i are the channel gains during the first and second half of the time frame of channel i (7.3) and $\mu_i = P_i$ or $\mu_i = \tilde{P}_i$ if PT i is ON or OFF, respectively. Using a similar approach, the received signals with randomized channel switching for the first and second halves of the transmission frame are given by

$$y_1 = \mu_i h_i s + n_1 \text{ and } y_2 = \mu_j g_j s + n_2,$$

respectively, where h_i and g_j are, respectively, the channel gains during the first half of the transmission frame of channel i and the second half of the transmission frame of channel j. Here, $\mu_j = P_j$ or $\mu_j = \tilde{P}_j$ if PT j is ON or OFF, respectively. Since h_i and g_j are independent, we can achieve diversity using an interleaver for decoding the turbo code. The decoded bit is mostly erroneous only if both h_i and g_j are in deep fade. The probability of both h_i and g_j being in deep fade is much smaller than that of h_i or g_i being in deep fade individually.

The received signal is fed to a log-likelihood computation [81], which computes the log-likelihoods of the transmitted bits, and uses them as if they were the likelihoods of the observations of BPSK transmission over an additive white Gaussian noise (AWGN) channel.

The log-likelihood bits are then de-interleaved and fed into the turbo decoder which decodes the received bits. The log-likelihood computation algorithm is presented in [81] for general multi-antenna systems. Here we consider a simple single antenna system and assume M-PSK modulation. Since the received signal y_1 corresponds to M bits, we need to compute the log-likelihood of M bit using y_1. We use the same approach for the received signal y_2. We denote the M received bits by a vector

$$\mathbf{b} = (b_1, \ldots, b_M).$$

The log-likelihood of the kth element of b, b_k, is given by

$$\Lambda(b_k) = \log \frac{\Pr[\mathrm{b_k} = 1|\mathrm{y}]}{\Pr[\mathrm{b_k} = 0|\mathrm{y}]} = \log \frac{\Pr[\mathrm{b_k} = 1, \mathrm{y}]}{\Pr[\mathrm{b_k} = 0, \mathrm{y}]},$$

which can be written as

$$\Lambda(b_k) = \log \frac{\sum_{s:s=f(b),b_k=1} \Pr[\mathrm{b_k} = 1, \mathrm{y}]}{\sum_{s:s=f(b),b_k=0} \Pr[\mathrm{b_k} = 0, \mathrm{y}]}.$$

Since knowledge of $\mathbf{b}$ provides knowledge of s, we have

$$\Lambda(b_k) = \log \frac{\sum_{s:s=f(b),b_k=1} \Pr[\mathrm{y}, \mathrm{s}]}{\sum_{s:s=f(b),b_k=1} \Pr[\mathrm{y}, \mathrm{s}]},$$

where $f(\cdot)$ is the mapping from $\mathbf{b}$ to the transmitted signal s. Because all the constellations points s are equally likely, we have

$$\Lambda(b_k) = \log \frac{\sum_{s:s=f(b),b_k=1} \Pr[\mathrm{y}|\mathrm{s}]}{\sum_{s:s=f(b),b_k=1} \Pr[\mathrm{y}|\mathrm{s}]}$$

Substituting in the noise statistics, we obtain

$$\Lambda(b_k) = \log \frac{\sum_{s:s=f(b),b_k=1} \exp\left(-\frac{|y-\sqrt{\mu_i}hs|^2}{N_0}\right)}{\sum_{s:s=f(b),b_k=1} \exp\left(-\frac{|y-\sqrt{\mu_i}hs|^2}{N_0}\right)}.$$

The soft-output bits of the log-likelihood computation are fed into an iterative turbo decoder. The iterative process requires the decoding algorithms to make use of a priori information as well as deliver reliability information for each decoded information bit in addition to the hard decision. The symbol-by-symbol *maximum a posteriori* (MAP) algorithm [91], is an optimal decoding algorithm for minimizing the bit error rate of convolutional codes. It can be applied straightforwardly for turbo decoding [92–94]. However, the MAP algorithm requires a large number of computations as well as large memory size, which complicates its hardware implementation.

The Soft Output Viterbi Algorithm (SOVA) [95] based on the soft-input soft-output (SISO) Viterbi algorithm, can make use of a priori information after suitable modification [94, 96]. The SOVA algorithm can be implemented for turbo decoding with moderate complexity and hence is preferable in practice. However, the coding gain of SOVA is generally about 0.7 dB less than that of MAP for turbo decoding [97]. In Section 7.6, we use SOVA as our decoding algorithm.

7.5.2 Randomized switching to multiple channels

In the channel switching algorithm described in the previous section, the secondary transmitter switches to only one channel during the transmission frame. The received signal always has a diversity order of 2. In general, the secondary transmitter can jump to more than one channel during a frame transmission time. Since turbo codes can exploit time diversity of the channels, jumping to more than one channel may increase the decoding diversity and hence improve the performance of the scheme. For example, the secondary

transmitter could switch to 2 channels during the transmission frame. During the transmission of the first $N_s/3$ symbols, it stays with channel i and switches to channel j during the second $N_s/3$ symbols. Finally, in the last $N_s/3$ symbol, the secondary transmitter switches to channel k. The secondary receiver decodes the received signal with three different fading values hence decoding diversity is increased.

In the case of repetition codes, when switching to 2 channels, the transmitted signal is repeated 3 times, which reduces the spectral efficiency. For a fair comparision, if the primary transmitter switches to one channel during transmission with QPSK modulation, 8-PSK modulation is used for switching to two channels during the frame transmission. The performance analysis for randomized switching to multiple channels follows the same approach as in Section 7.3.1. In Section 7.6, we will show that the performance of randomized switching with turbo codes is improved when the secondary transmitter switches to more than one channel but the performance of randomized switching with repetition codes is not improved under multichannel switching.

7.6 Numerical Results

7.6.1 Repetition code

In this section, we evaluate the performance in terms of SEP for the proposed switching schemes. For all simulations, we use BPSK modulation and a transmission frame length $N_s = 640$ symbols. All channels have the same P_i and $\tilde{P}_i$. The average SNR $\gamma_i = P_i/N_0$ and $\tilde{\gamma}_i = \tilde{P}_i/N_0$. We assume that $\tilde{\gamma}_i = \gamma_i + 10$ dB and in all figures SNR $= \gamma_{\mathrm{i}}$. Except for Fig. 7.3, the ON/OFF probabilities of a PT are assumed to be the same across all channels, i.e., $p_i^{\mathrm{on}} = p_i^{\mathrm{off}} = 0.5$.

In Fig. 7.1, we compare the performance of our randomized channel switching scheme vs. a conventional scheme with no channel switching. We assume all channels have the same correlation $\rho = 0.8$. As seen in Fig. 7.1, the randomized channel switching scheme effectively reduces the average SEP. For spatial sensing, the randomized channel switching

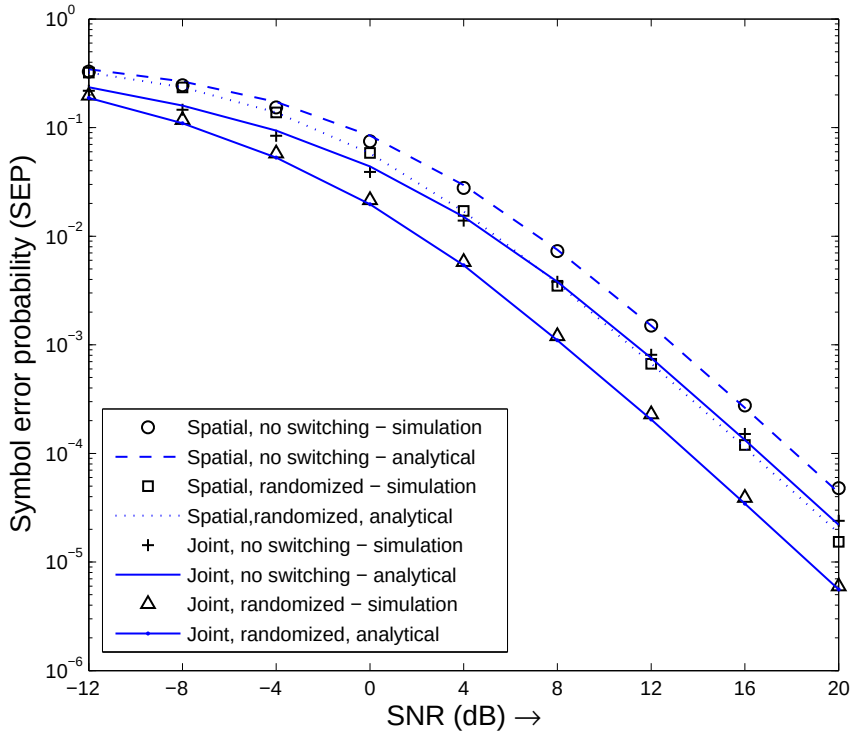

Figure 7.1: Performance of randomized channel switching.

scheme is about 3 dB better in the SEP range of interest, i.e., SEP $\leq 10^{-3}$, than the conventional scheme. For joint spatial-temporal sensing, the random switching scheme is about 4 dB better than the conventional scheme. For joint spatial-temporal sensing, randomized channel switching exploits both fading diversity and diversity of the ON/OFF state of the PT. Clearly, joint spatial-temporal sensing always outperforms spatial sensing for a given switching scheme. In Fig. 7.1, the simulation and analytical results derived in Section 7.3.1 are seen to be closely matched. In Fig. 7.2, we compare the SEP of the conventional scheme with randomized channel switching over different values of the channel correlation $\rho_1 = \rho_2 = \rho$. We use $\gamma_i = 12$ dB and $\tilde{\gamma}_i = 22$ dB with $i = 1, 2$. As in Fig. 7.2, the performance of randomized channel switching is not affected by the channel correlation because the ST switches to a new channel with independent channel fading. The SEP of the conventional scheme increases as ρ increases. At $\rho = 0$, i.e., there is no correlation, under pure spatial sensing, the SEP of conventional scheme equals that of the randomized

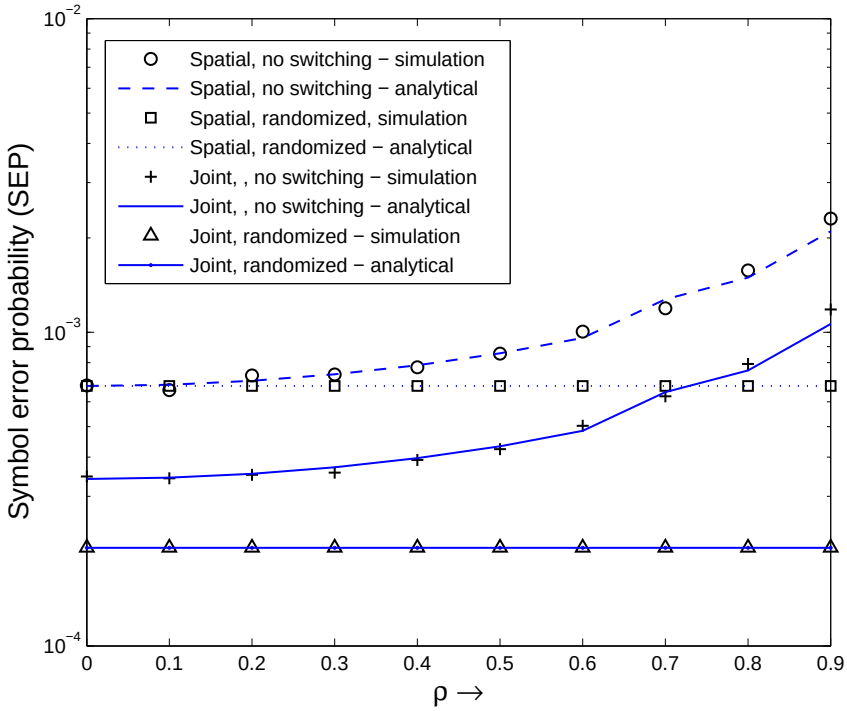

Figure 7.2: Performance of different switching schemes vs. ρ.

channel switching scheme. However, at $\rho = 0$, the randomized channel switching scheme still outperforms the conventional scheme when joint spatial-temporal sensing is used. The reason is that even when $\rho = 0$, random switching can exploit multichannel diversity in terms of the ON/OFF diversity of the PT. In particular, low received SNR normally occurs when both PTs are ON for joint spatial-temporal sensing, i.e., with probability $p_1^{\text{on}} p_2^{\text{on}}$, and when PT 1 or PT 2 is ON, i.e., with probabilities p_1^{on} or p_2^{on}, respectively. We investigate scenarios in which two channels have different p^{off} probabilities in Fig. 7.3: $p_1^{\text{off}} = 0.8$ and $p_1^{\text{off}} = 0.4$, respectively. Clearly, if user 1 always uses channel 1 and user 2 always uses channel 2, the performance experienced by user 1 will always be better than that of user 2. As p^{off} increases, the probability that ST can transmit with maximum power increases, and thus the performance improves. This may create fairness issues in multichannel cognitive radio networks. However, by employing randomized switching, both users will have the same performance. Also, in the SEP range of interest, i.e., SEP $\leq 10^{-3}$, the performance

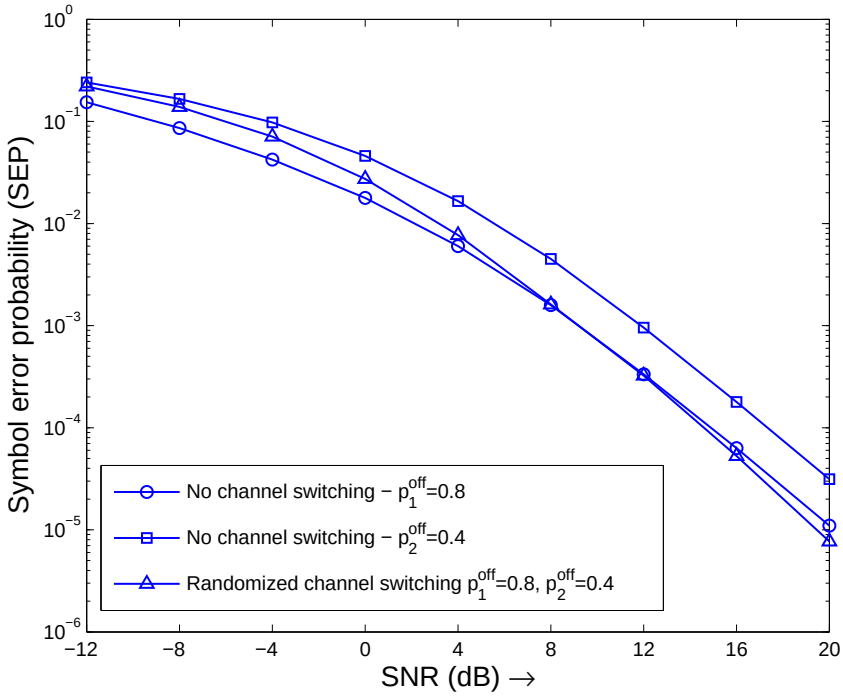

Figure 7.3: Randomized channel switching and user's fairness.

of randomized channel switching is equal or even better compared to the performance of user 1 when there is no channel switching. Randomized channel switching not only improves performance but also guarantees fairness among the secondary users. In Fig. 7.4, we compare the performance of the randomized channel switching scheme in conjunction with the maximized SNR scheduling scheme of Algorithm 2. In maximized SNR scheduling, a total of $N = 4$ channels is used. When SEP $=10^{-5}$, our maximized SNR scheduling scheme with $K = 4$ concurrent (ST,SR) transmissions performs about 10 dB better than randomized channel switching. As the number of concurrent transmissions, K, decreases, the average SEP decreases. When $K = 1$, the maximized SNR scheduling scheme is about 13 dB better than randomized channel switching and about 3 dB better than maximized SNR scheduling with $K = 4$. In Fig. 7.5, we investigate the performance of maximized SNR scheduling algorithm as the number of channels N increases. We assume $K = 1$ and all channels have $\rho = 0.8$. We also assume that $\gamma_i = 4$ dB and $\tilde{\gamma}_i = 14$ dB. The simulation

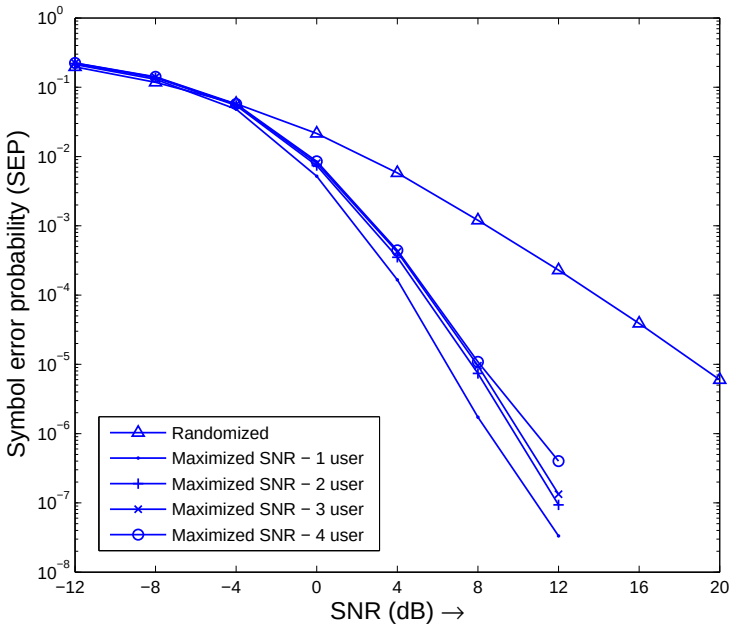

Figure 7.4: Performance of maximized SNR scheduling.

results show that the SEP of our proposed scheduling scheme decreases significantly as the total number of users N increases. When more channels are available, the maximized SNR of all channels increases and hence, the performance of the maximized SNR scheduling algorithm improves.

7.6.2 Turbo codes

In this section, we present the performance of our multichannel switching scheme with turbo code. We assume that BPSK modulation is used. The component codes of the turbo code are two recursive systematic convolutional codes with generator matrices $G_1 = [1 \;\; 1 \;\; 1]$ and $G_2 = [1 \;\; 0 \;\; 1]$. The turbo code employs a random interleaver and has a rate of $R = 1/2$ obtained by periodically puncturing the parity bits. The interleaver that scrambles the turbo coded bit consists of one pseudorandom interleaver with length equal to the frame length $N_s = 1920$. The SOVA decoding algorithm with 5 iterations is used. All channels have the same P_i and $\tilde{P}_i$. The average SNR $\gamma_i = P_i/N_0$ and $\tilde{\gamma}_i = \tilde{P}_i/N_0$. We assume that

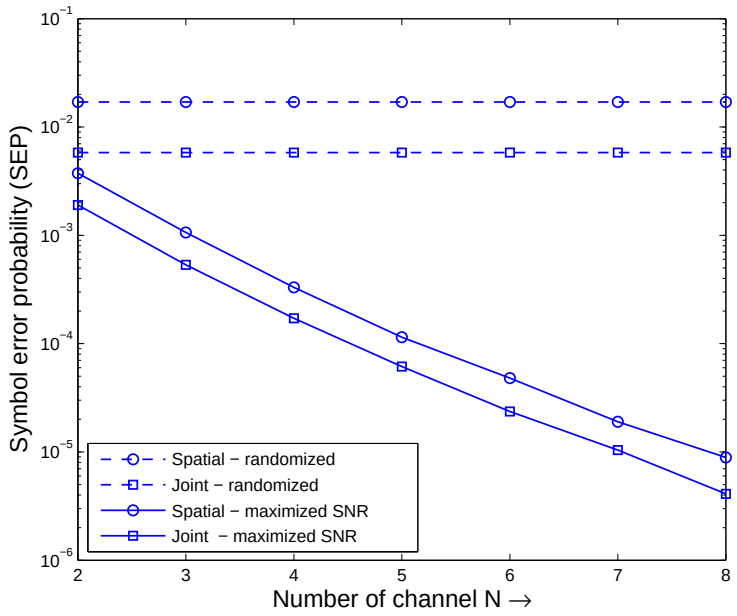

Figure 7.5: Performance of maximized SNR scheduling vs. number of channels N.

$\tilde{\gamma}_i = \gamma_i + 10$ dB and in all figures SNR $= \gamma_{\mathrm{i}}$. The ON/OFF probabilities of a PT are assumed to be the same across all channels, i.e., $p_i^{\mathrm{on}} = p_i^{\mathrm{off}} = 0.5$. The channel correlation is also the same for all channels: $\rho_i = 0.8$. In Fig. 7.6(a), we compare the frame error rate (FER) of the randomized channel switching scheme with no channel switching for both spatial and temporal sensing. At FER values of interest, the randomized channel switching scheme is about 8 dB better than no channel switching scheme. The joint spatial-temporal sensing scheme is about 4 dB better than spatial sensing. In Fig. 7.6(b), we compare the bit error rate (BER) of randomized channel switching scheme with no channel switching for both spatial and temporal sensing. Similar to FER performance, the randomized channel switching scheme is about 8 dB better than no channel switching. In terms of BER, the joint spatial-temporal sensing scheme is about 4 dB better than spatial sensing. In Fig. 7.7(a) and Fig. 7.7(b), we compare the FER and BER of maximized SNR channel switching scheme with the randomized channel switching scheme and no channel switching. Here, the total number of channels $N = 4$ and the number of concurent user transmission is $K = 4$. As we can see, the performance of maximized SNR scheduling is significantly

better than that of randomized channel switching. At an FER of 10^{-2} and a BER of 10^{-3}, maximized SNR scheduling is about 11 dB better than randomized switching. In Fig. 7.8(a) and Fig. 7.8(b), we compare the performance of randomized switching on two channels to channel switching schemes on more than two channels. We use the QPSK, 8-PSK and 16-PSK modulation schemes on 1, 2 and 3 channels with joint spatial-temporal sensing and QPSK with no channel switching. The spectral efficiencies of the three channel switching schemes and no channel switching are equal. As we can see from the numerical results, the performance of randomized switching with repetition codes does not increase when the secondary transmitter switches to multiple channels. However, in Fig. 7.9(a) and Fig. 7.9(b), with spatial sensing, the performance of randomized switching on multiple channels with turbo codes improves as the number of switched channels increases. At an FER of 10^{-3} and a BER of 10^{-4}, randomized switching on two channels performs about 8 dB better than randomized switching on one channel. Asymptotically, for a frame transmssion of N_s symbols, if we have N_s available channels, the secondary transmitter can switch to $N_s - 1$ channels during the frame transmission time. The performance of this "asymptotic channel switching scheme" is shown in Fig. 7.10(a) and Fig. 7.10(b). At an FER of 10^{-2} and a BER of 10^{-3}, the asymptotic channel switching is about 8 dB better than the multichannel switching scheme on 3 channels. Fig. 7.11, we compare the performance in term of BER of repetition code with turbo code for spatial sensing. In the single channel case, the simple repetition code outpeforms turbo codes with no channel switching and randomized channel switching. However, as the number of switching channels is increased, the performance of turbo codes becomes better than that of the repetition code. For example, at a BER of 10^{-5} with three channels, the performance of turbo codes is about 5 dB better than of the repetition code.

7.7 Conclusion

We considered a multichannel cognitive radio network with joint spatial-temporal spectrum sensing. In a multichannel cognitive radio network, fading diversity exists among different channels at a given time. We showed that by using a simple randomized switching among different channels during transmission, the performance of cognitive transmission significantly increases. We proposed a maximized signal-to-noise ratio (SNR) algorithm that further improves the performance of the cognitive radio tranmission link when the channel fading coefficients and the ON/OFF states of all primary transmitters are available. We also studied the performance of our switching schemes combined with turbo codes. We showed that our combined scheme with turbo codes outperformed a conventional scheme with no channel switching. In addition, the performance gain achieved using turbo codes with randomized switching increases as the number of channels increases.

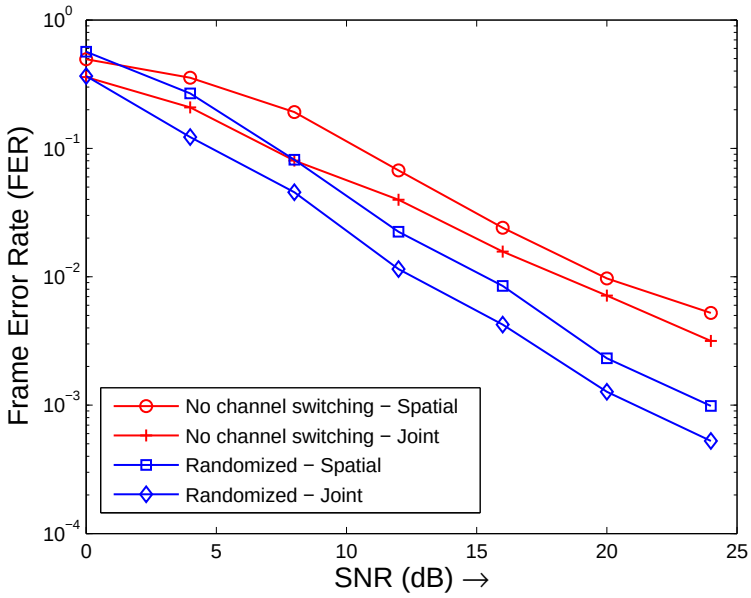

(a) Frame Error Rate (FER).

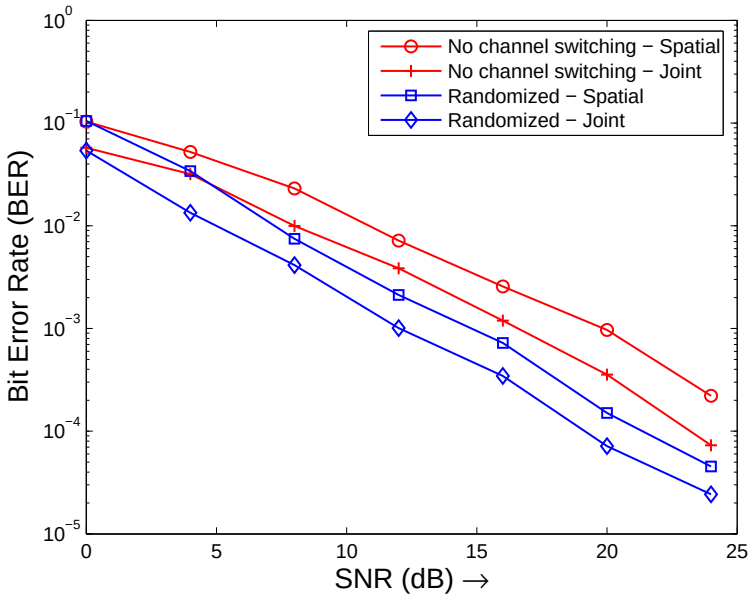

(b) Bit Error Rate (BER).

Figure 7.6: Performance of randomized channel switching with turbo codes.

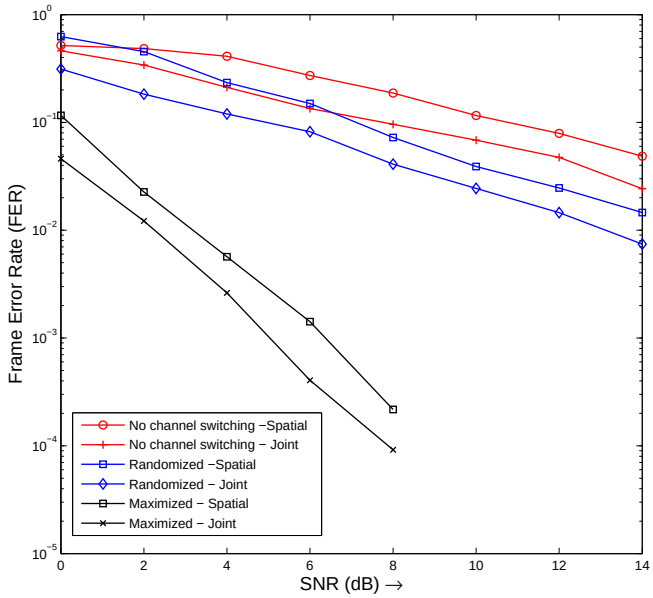

(a) Frame Error Rate (FER).

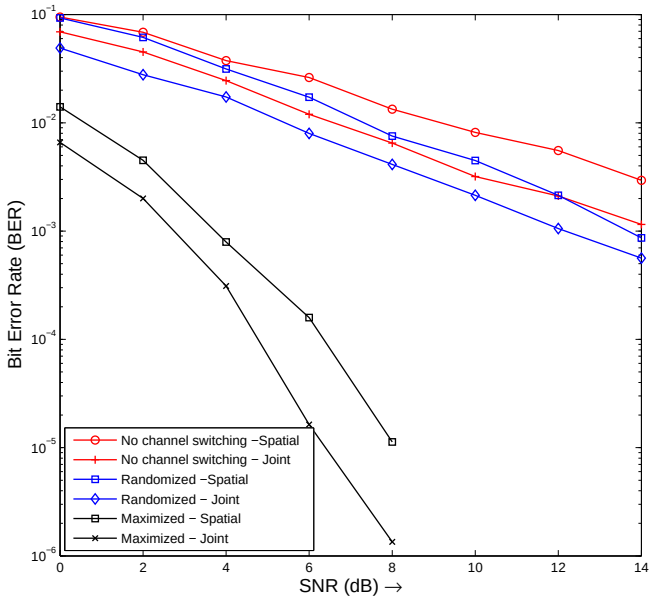

(b) Bit Error Rate (BER).

Figure 7.7: Performance of maximized SNR scheduling channel switching with turbo codes.

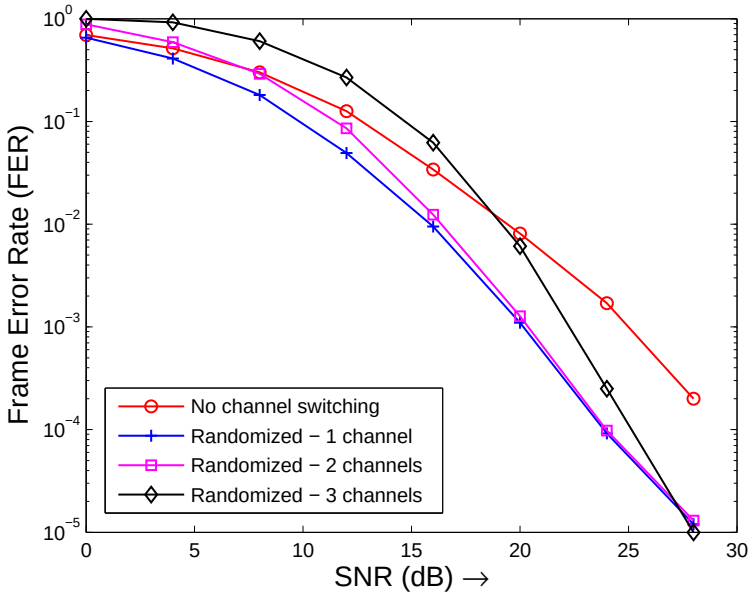

(a) Frame Error Rate (FER).

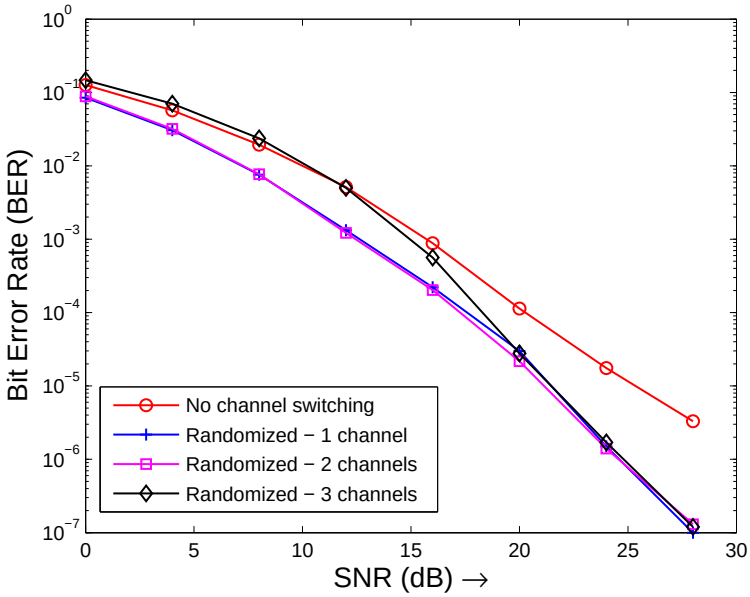

over

(b) Bit Error Rate (BER).

Figure 7.8: Performance of randomized channel switching with repetition codes and multiple channels.

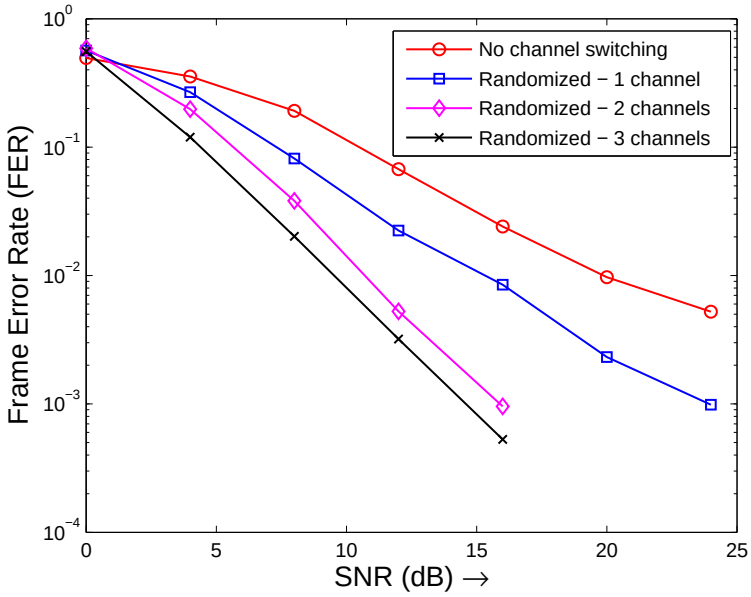

(a) Frame Error Rate (FER).

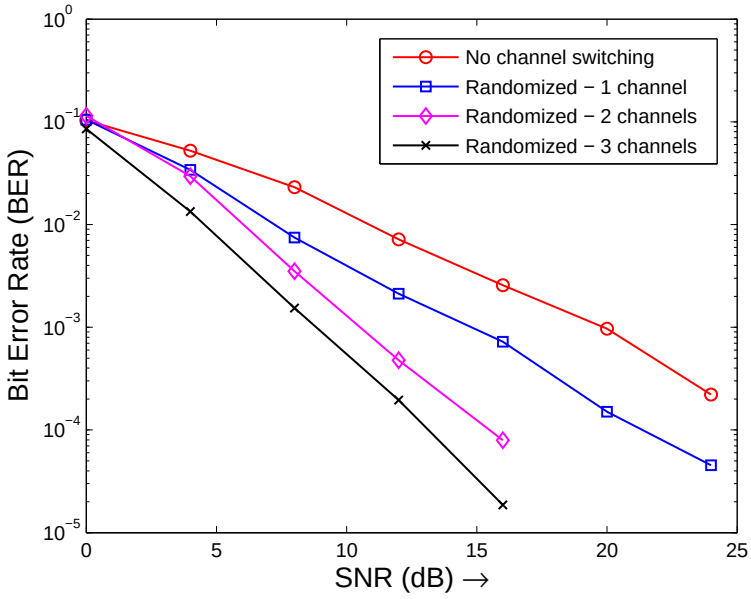

(b) Bit Error Rate (BER).

Figure 7.9: Performance of randomized channel switching with turbo codes and multiple channels.

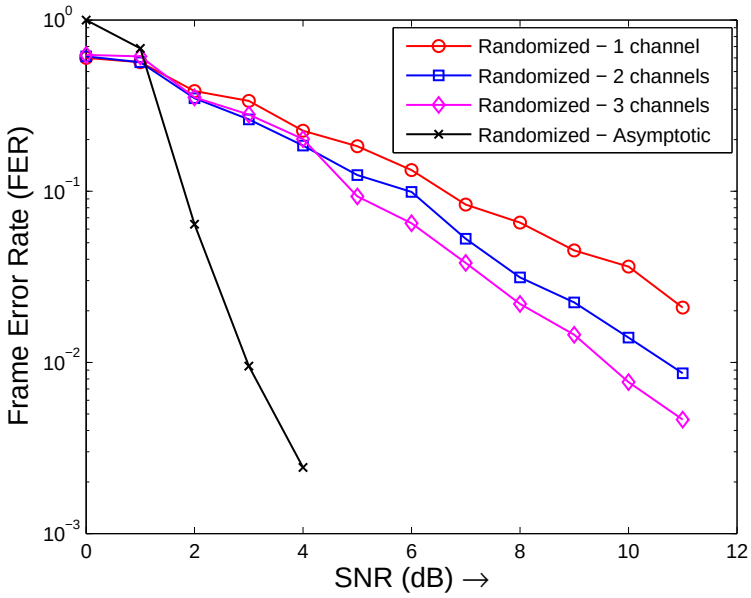

(a) Frame Error Rate (FER).

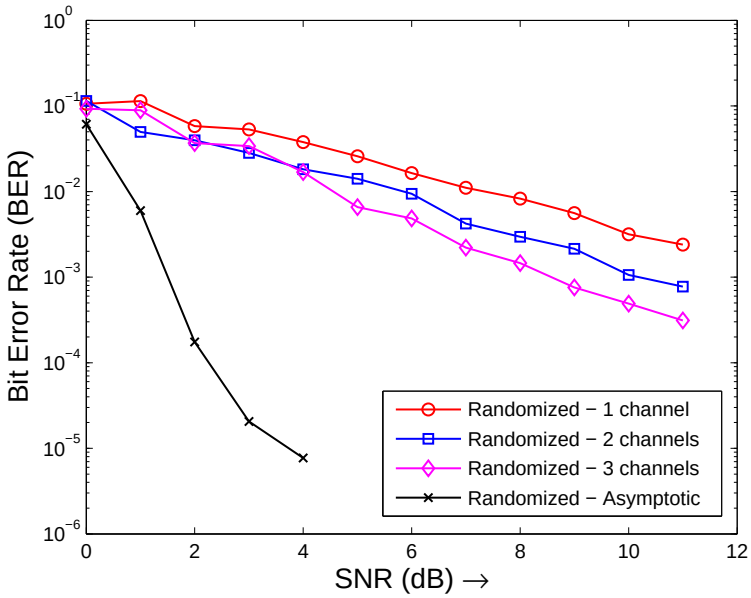

(b) Bit Error Rate (BER).

Figure 7.10: Asymptotic performance of randomized channel switching with turbo codes.

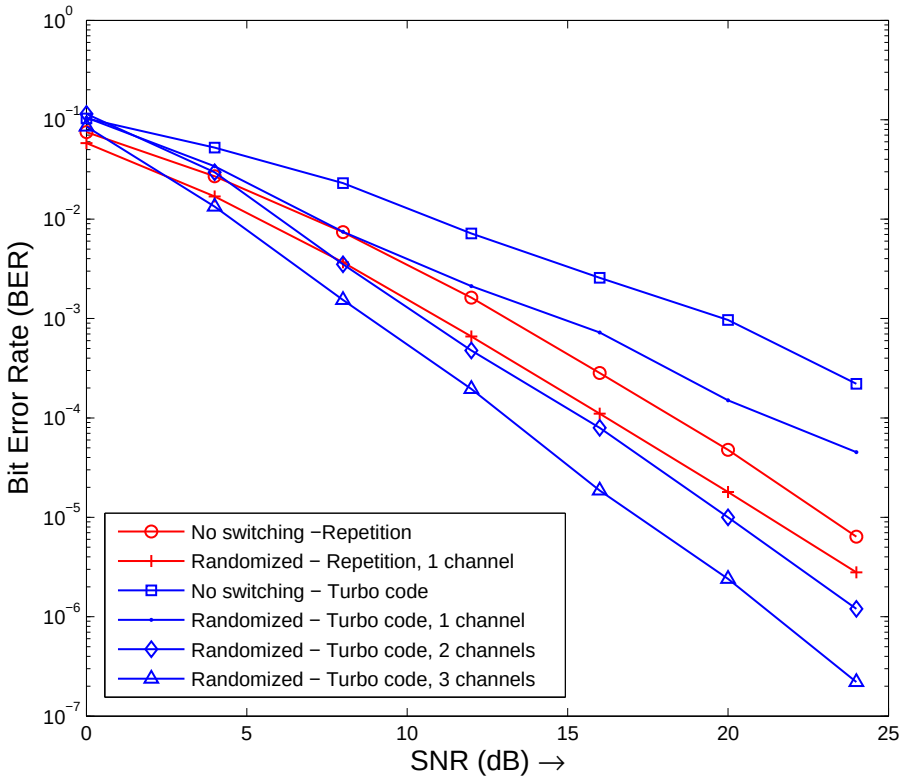

Figure 7.11: Compare the performance of repetition and turbo code.

Chapter 8: Conclusions

8.1 Summary

In this dissertation, we investigated a joint spatial-temporal spectrum sensing strategy, spectrum sensing with multiuser diversity, cooperative relaying schemes that exploits the spatial-temporal spectrum holes and multichannel switching algorithms.

In Chapter 2.6, we developed a model for joint spatial-temporal spectrum sensing in cognitive radio networks. Our approach combines the spatial information of primary transmitters obtained through spatial sensing to improve the performance of temporal sensing. Depending on the amount of correlation between nodes, we propose two strategies for temporal sensing node selection. When the correlation is high, we choose nodes that are closest to the primary transmitter. When the correlation is small and all the temporal sensing nodes have similar average SNR, we choose nodes that minimize correlation. Our numerical results show that by incorporating spatial information into temporal sensing, the performance of temporal sensing can be significantly improved. We also quantify the performance benefit of the joint spatial-temporal scheme over pure temporal or spatial sensing in term of achievable capacity. The achievable capacity of joint spatial-temporal sensing is significantly higher compared to that of temporal or spatial sensing only. We also analyzed a multi-level quantization feedback scheme that can improve temporal sensing performance. We showed that by using multi-feedback quantization, the performance of temporal sensing can be improved when the correlation between nodes is small.

In Chapter 4, we proposed a distributed approach to spectrum sensing that exploits multiuser diversity among secondary users to improve sensing capability in cognitive radio networks. Our approach is based on a cooperative sensing framework which has advantages in low SNR and shadowed environments. Independent, identically distributed fading

is used to model the fading between secondary nodes. We investigated the performance of soft combination, 1-out-N rule and counting rule, and compared with traditional spectrum sensing without multiuser diversity. We also proposed a medium access control protocol based on carrier sensing multiple access (CSMA) protocol to coordinate transmissions between secondary nodes and the fusion center. Our numerical result show that our scheme significantly outperforms the traditional scheme that does not exploit multiuser diversity. We also show that when the number of secondary user is large enough, a hard decision 1-out-N rule outperforms the soft combination scheme.

In Chapter 5, we proposed two cooperative transmission strategies, CAF-FD and CAF-VD which exploit spatial and temporal spectrum holes in a cognitive radio network. We analyze the average symbol error rate of all strategies. We using moment generating functions to analyze the symbol error probability. Our analytical and simulation results show that our cooperative communication strategies, which exploit both spatial and temporal spectrum holes, significantly reduce the average symbol error probability compared to that of pure spatial and temporal sensing. Of the two cooperative schemes, CAF-VD results in a lower symbol error probability because the diversity order of the received signal at secondary receiver has the order of two. We also propose an incremental relaying protocol which further improves the spectral efficiencies of our schemes.

In Chapter 6, we proposed two cooperative communication protocols with decode-and-forward relays: cognitive decode-and-forward with fixed decoding delay (CDF-FD) and with variable decoding delay (CDF-VD) for opportunistic spectrum access in cognitive radio networks. The CDF-VD has better performance than CDF-FD because the diversity order of the received signal at secondary receiver has the order of two. Both simulation and analytical results confirm that the proposed scheme outperform schemes based on pure spatial sensing or pure temporal sensing alone. We proposed an incremental relaying protocol for CDF-FD and CDF-VD to further increase their spectral efficiencies. The simulation results show that by employing one bit feedback from the secondary receiver to indicate

the success/failure of transmission, our incremental relaying protocol can dramatically improve the spectral efficiency of our schemes. Finally, a practical decoding scheme based on computation of a log-likelihood was proposed.

In Chapter 7, we studied a multichannel cognitive radio network with joint spatial-temporal spectrum sensing. In a multichannel cognitive radio network, fading diversity exists among different channels at a given time. We showed that simple randomized switching among different channels during transmission significantly improve the performance of cognitive transmission. We also proposed a maximized signal-to-noise algorithm to further improve the performance of the cognitive radio transmission link. We analyzed the performance of our schemes in terms of average symbol error probability. We also studied the performance of our schemes in combination with turbo codes. We showed that our combined scheme with turbo codes has outperformed a scheme with no channel switching scheme. In addition, turbo codes improve the performance of the randomized scheme when secondary switching to multiple channels during the frame transmission. In randomized switching, the performance of repetition codes is better than turbo codes when switching to only one channel. However, turbo codes outperforms repetition codes when switching to multiple channels.

8.2 Directions of future research

The joint spatial-temporal sensing scheme developed inChapter 2.6 can be extended to a scenario that has multiple cochannel primary transmitters. In order to work effectively with multiple primary transmitters, the strategy needs to track the ON/OFF status of all primary transmitters. Depending on which primary transmitter is ON or OFF, we can obtained a different MIFTP for each secondary user. For our proposed spectrum sensing scheme exploiting multiuser diversity, it would be worthwhile to investigate a fading model of secondary nodes in which the assumption are independent but not identically distributed fading is removed, i.e., they have different average SNRs. It would also be of interest to investigate the case when a secondary node is equipped multiple antenna but the fading

between antennas are correlated. Further work could examine a practical implementation of our multiuser diversity scheme in a more realistic setting, i.e., the IEEE 802.22 standard.

In Chapters 5 and 6, we considered coherent detection at the secondary receiver. In order to perform coherent detection, channel state information must be obtained. However, in fast fading channel, channel state information may be too difficult to estimate. Future research along those lines could investigate a differential modulation scheme for fast fading channel wherein no channel state information is needed at the secondary receiver.

In Chapter 7, we analyzed the performance of our schemes using average symbol error probability. In the ongoing work, we are investigating the achievable capacity of our proposed multichannel schemes and the effect imperfect channel state information feedback to the performance of maximized SNR scheduling. Imperfect channel state information can significantly degrade the decoding performance of coherent detection scheme which requires estimation of channel state information. However, our maximized SNR scheduling may be robust against the imperfect channel estimation.

Appendix A:

[Proof of proposition 1] We have,

$$\gamma_b \leq \frac{\gamma_{ar}\gamma_{rb}}{\gamma_{ar}+\gamma_{rb}} \leq \frac{\sqrt{\gamma_{ar}\gamma_{rb}}}{2} = \frac{\sqrt{P_{ar}P_{rb}}}{2N_0}\sqrt{\tilde{g}\tilde{h}} \tag{.1}$$

Taking expectations on both sides, we have

$$E[\gamma_b] \leq \frac{\sqrt{P_{ar}P_{rb}}}{2N_0}E[\sqrt{\tilde{g}\tilde{h}}]. \tag{.2}$$

Note that $g_i, h_j \sim \mathcal{CN}(0,1)$ then $2\tilde{g}$ and $2\tilde{h}$ are independent χ^2-distributed random variables with $2K_u$ and $2K_v$ degrees of freedom, respectively. Applying Jensen's inequality,

$$E\left[\sqrt{\tilde{g}\tilde{h}}\right] \leq \sqrt{E[\tilde{g}\tilde{h}]} = \frac{1}{2}\sqrt{E[2\tilde{g}]E[2\tilde{h}]} = \sqrt{K_uK_v}. \tag{.3}$$

From (.2) and (.3), we have

$$E[\gamma_b] \leq \frac{\sqrt{P_{ar}P_{rb}}}{2N_0}\sqrt{K_uK_v}. \tag{.4}$$

Assuming M-PSK modulation, the average SEP can be expressed as follows [78]:

$$\text{SEP} = \frac{1}{\pi}\int_0^{\frac{(M-1)\pi}{M}} M_{\gamma_b}(-\omega)\,\mathrm{d}\theta, \tag{.5}$$

where $M_{\gamma_b}(u) \triangleq E[e^{u\gamma_b}]$ is the moment generating functions γ_b and $\omega \triangleq \frac{k}{\sin^2\theta} \geq 0$. Applying Jensen's inequality and (.4), we have

$$M_{\gamma_b}(-\omega) = E[e^{-\omega\gamma_b}] \geq e^{-\omega E[\gamma_b]} \geq e^{-\beta\sqrt{K_uK_v}}, \tag{.6}$$

where $\beta \triangleq \omega\sqrt{P_{ar}P_{rb}}/(2N_0 + 2N_p) \geq 0$. The lower bound for the SEP is then obtained by substituting the right hand side of (.6) into (.5).

If K is even, i.e., $K = 2m$ where m is an integer, $2\sqrt{K_u K_v} \leq K_u + K_v = 2m$, with equality holding when $K_u = K_v = m$. In this case, (.6) implies that the choice of $K_u = K_v$ maximizes the performance of our proposed scheme. If K is odd, i.e., $K = 2m + 1$, let $K_u = K_v + n$, where $n \geq 1$ is an integer. We have $2K_v = 2m + 1 - n$,

$$4K_u K_v = 4m^2 + 4m + 1 - n^2 \leq 4m^2 + 4m. \tag{.7}$$

The equality in (.7) holds for $n = 1$ or $n = -1$ or equivalent $K_u = K_v + 1$ or $K_v = K_u + 1$ will minimizes $M_{\gamma_b}(-\omega)$ and hence the SEP. In the cooperative relaying scenario wherein SR combines the received signals from both relay and direct channel, information-theoretic results in [98] suggest the choice $K_u > K_v$, in order to maximize the SNR at the first hop or $K_u = K_v + 1$. This analysis is confirmed by simulation in [69].

Bibliography

Bibliography

[1] "FCC Frequency Allocation Chart," National Telecommunications and Information Administration (NTIA). [Online]. Available: wwww.ntia.dov.gov/osmhome/allochrt.pdf

[2] FCC, "Spectrum Policy Task Force Report," Nov. 2002.

[3] M. A. McHenry, "NSF Spectrum occupancy measurements project summary," Shared Spectrum Company, Tech. Rep., Aug. 2005.

[4] "Corvus: A cognitive radio approach for usage of virtual unlicensed spectrum," White Paper, Univ. California Berkeley, Jul 2004.

[5] I. J. Mitola, "Software radios: Survey critical evaluation and future directions," *IEEE Aerospace and Electronics Systems Magazine*, vol. 8, pp. 25–31, Apr. 1993.

[6] C. Cordeiro, K. Challapali, and D. Birru, "IEEE 802.22: an introduction to the first wireless standard based on cognitive radios," *Academic Publisher J. of Communications*, vol. 1, no. 1, pp. 38–47, Apr. 2006.

[7] B. L. Mark and A. O. Nasif, "Estimation of maximum interference-free power level for opportunistic spectrum access," *IEEE Transactions on Wireless Communications*, vol. 8, no. 5, pp. 2505–2513, May 2009.

[8] J. Unnikrishnan and V. Veeravalli, "Cooperative sensing for primary detection in cognitive radio," *IEEE Journal Sel. Topics Signal Process.*, vol. 2, no. 1, pp. 18–27, Feb 2008.

[9] J. Mitola, "Cognitive radio: Making software radios more personal," *IEEE Personal Communications Magazine*, vol. 6, pp. 13–18, 1999.

[10] A. Goldsmith, S. A. Jafar, I. Maric, and S. Srinivasa, "Breaking spectrum gridlock with cognitive radios: An information theoretic perspective," *Proceeding of IEEE*, vol. 97, no. 5, pp. 894–914, May 2009.

[11] Q. Zhao and B. M. Sadler, "A survey of dynamic spectrum access," *IEEE Signal Processing Magazine*, vol. 24, no. 3, pp. 79–89, May 2007.

[12] I. Maric, A. Goldsmith, G. Kramer, and S. Shamai, "On the capacity of interference channels with a partially cogntive transmitter," in *2007 IEEE International Symposium on Information Theory*, Nice, France, Jun 2007.

[13] N. Devroye, P. Mitran, and V. Tarokh, "Achievable rates in cognitive radio channels," *IEEE Transactions on Information Theory*, vol. 52, no. 5, pp. 1813–1827, May 2006.

[14] ——, "Limits on communications in a cognitive radio channel," *IEEE Communications Magazine*, vol. 44, no. 6, pp. 44–49, June 2006.

[15] A. Jovicic and P. Viswanath, "Cognitive radio: An information-theoretic perspective," in *IEEE Int. Symp. on Information Theory*, Jul. 2006, pp. 2413 – 2417.

[16] S. Haykin, D. J. Thomson, and J. H. Reed, "Spectrum sensing for cognitive radio," *Proceeding of IEEE*, vol. 97, no. 5, pp. 849–873, May 2009.

[17] B. L. Mark and A. O. Nasif, "Estimation of maximum interference-free transmit power level for opportunistic spectrum access," *IEEE Transactions on Wireless Communications*, vol. 8, no. 5, pp. 2505–2513, 2009.

[18] ——, "Estimation of interference-free transmit power for opportunistic spectrum access," in *Proc. IEEE Wireless Comm. and Networking Conf. (WCNC'08)*, Las Vegas, NV, Apr 2008.

[19] S. Geirhofer, L. Tong, and B. M. Sadler, "Dynamic spectrum access in the time domain: Modeling and exploiting white space," *IEEE Communications Magazine*, vol. 45, pp. 66–72, May 2007.

[20] ——, "A measurement-based model for dynamic spectrum access in WLAN channels," in *Proc. IEEE MILCOM*, Washington DC, Oct. 2006, pp. 1–7.

[21] Q. Zhao, S. Geirhofer, L. Tong, and B. M. Sadler, "Optimal dynamic spectrum access via periodic channel sensing," in *Proc. IEEE Wireless Communications and Networking Confernece (WCNC'07)*, Hong Kong, Mar. 2007, pp. 33–37.

[22] Y. Chen, Q. Zhao, and A. Swami, "Joint Design and Separation Principle for Opportunistic Spectrum Access in the Presence of Sensing Errors," *IEEE Trans. on Information Theory*, vol. 54, no. 5, pp. 2053–2071, May 2008.

[23] S. Mishra, A. Sahai, and R. W. Brodersen, "Cooperative sensing among cognitive radios," in *Proc. IEEE Int. Conf. Communications*, vol. 4, Istanbul, Jun 2006, pp. 1658–1663.

[24] E. Visotsky, S. Kuffner, and R. Peterson, "On collaborative detection of TV transmissions in support of dynamic spectrum sharing," in *Proc. 1st IEEE Int. Symp. New Frontier in Dynamic Spectrum Access Networks DySPAN*, Nov 2005, pp. 338–345.

[25] A. Sahai and N. Hoven and S. M. Mishra, "Fundamental tradeoffs in robust spectrum sensing for opportunistic frequency reuse," [Online], Mar. 2006, Available at: http://www.eecs.berkeley.edu/~sahai/Papers/CognitiveTechReport06.pdf.

[26] A. N. Mody *et al.*, "Machine learning based cognitive communications in white as well as the gray space," in *Proc. IEEE MILCOM*, FL, U.S.A., Oct. 2007, pp. 1–7.

[27] D. Cabric and S. M. Mishra and R. W. Brodersen, "Implementation issues in spectrum sensing for cognitive radios," in *Proc. Thirty-Eighth Asilomar Conf. on Signals, Systems and Computers*, Nov. 2004, pp. 772–776.

[28] S. Haykin, D. J. Thomson, and J. H. Reed, "Spectrum sensing for cognitive radio," *Proceedings of the IEEE*, vol. 97, no. 5, pp. 849–877, 2009.

[29] J. G. Proakis, *Digital Communications*, 4th ed. NewYork, NY: McGrall-Hill, 2000.

[30] A. Sahai, N. Hoven, and R. Tandra, "Some fundamental limits on cognitive radio," in *Proc. of Allerton Conference*, Monticello, IL, Oct. 2004.

[31] S.-J. Kim and G. B. Giannakis, "Rate-optimal and reduced-complexity sequential sensing algorithms for cognitive OFDM radios," in *Proc. Conference on Information and systems (CISS)*, Baltimore, MD, March 2009.

[32] L. Lai, Y. Fan, , and H. V. Poor, "Quickest detection in cognitive radio: A sequential change detection framework," in *Proc. IEEE Global Telecommunications Conference (GLOBECOM)*, New Orleans, LA, Nov. 2008, pp. 1–5.

[33] A. Ghasemi and E. Sousa, "Collaborative spectrum sensing for opportunistic access in fading environments," in *Proc. IEEE Int. Symp. on New Frontiers in Dynamic Spectrum Access Networks (DySPAN)*, Nov. 2005, pp. 131–136.

[34] G. Ganesan and Y. Li, "Cooperative spectrum sensing in cognitive radio networks," in *Proc. IEEE Int. Symp. on New Frontiers in Dynamic Spectrum Access Networks (DySPAN)*, Nov. 2005, pp. 137–143.

[35] A. W. Min and K. G. Shin, "Exploiting multi-channel diversity in spectrum-agile networks," in *Proc. IEEE Infocom 2008*, Apr. 2008, pp. 1921 – 1929.

[36] H. Jiang, L. Lai, R. Fan, and H. V. Poor, "Cognitive radio: How to maximally utilize spectrum opportunities in sequential sensing," in *Proc. IEEE Globecom 2008*, Nov 2008, pp. 4851–4855.

[37] ——, "Optimal selection of channel sensing order in cognitive radio," *IEEE Transactions on Wireless Communications*, vol. 8, no. 1, pp. 297–307, 2009.

[38] S.-J. Kim and G. B. Giannakis, "Rate-optimal and reduced-complexity sequential sensing algorithms for cognitive OFDM radios," *EURASIP Journal on Advances in Signal Processing, Special Issue on Dynamic Spectrum Access for Wireless Networking*, September 2009.

[39] D. Wilkins, G. Denker, M.-O. Stehr, D. Elenius, R. Senanayake, and C. Talcott, "Policy-Based Cognitive Radios," *IEEE Wireless Communications Magazine*, vol. 14, pp. 41–46, Aug. 2007.

[40] R. Knopp and P. Humblet, "Information capacity and power control in single-cell multiuser communications," in *Proc. IEEE Int. Conf. Comm. (ICC'95)*, Seattle, WA, Jun. 1995, pp. 331–335.

[41] X. Qin and R. A. Berry, "Distributed approaches for exploiting multiuser diversity in wireless networks," *IEEE Transactions on Information Theory*, vol. 52, no. 2, pp. 392–413, Feb. 2006.

[42] J. N. Laneman and G. W. Wornell, "Distributed space-time-coded protocols for exploiting cooperative diversity in wireless networks," *IEEE Transactions on Information Theory*, vol. 49, no. 10, pp. 2415–2425, Oct. 2003.

[43] J. N. Laneman, D. N. C. Tse, and G. W. Wornell, "Cooperative diversity in wireless networks: Efficient protocol and outage behavior," *IEEE Transactions on Information Theory*, vol. 50, no. 12, pp. 3062–3080, Dec. 2004.

[44] A. Sendonaris, E. Erkip, and B. Aazhang, "User cooperation diversity - Part I: System description," *IEEE Transactions on Communications*, vol. 51, no. 11, pp. 1927–1938, Nov. 2003.

[45] A. Ribeiro, X. Cai, and G. B. Giannakis, "Symbol error probabilities for general cooperative links," *IEEE Transactions on Wireless Communications*, vol. 4, no. 3, pp. 1246–1273, May 2005.

[46] T. Wang, G. B. Giannakis, and R. Wang, "Smart regenerative relays for link-adaptive cooperative communications," *IEEE Transactions on Communications*, vol. 56, no. 11, pp. 1950–1960, Nov. 2008.

[47] M. Janani, A. Hedayat, T. Hunter, and A. Nosratinia, "Coded cooperation in wireless communications: space time transmission and iterative decoding," *IEEE Transactions on Signal Processing*, vol. 52, no. 2, pp. 362–371, Feb. 2004.

[48] Z. Han, X. Zhang, and H. V. Poor, "High performance cooperative transmission protocols based on multiuser detection and network coding," *IEEE Transactions on Wireless Communications*, vol. 8, no. 5, pp. 2352–2361, May 2009.

[49] T. Do and B. L. Mark, "Joint spatial-temporal spectrum sensing for cognitive radio networks," in *Proc. 43rd Conf. on Information Systems and Sciences (CISS)*, Baltimore, MD, Mar. 2009.

[50] ——, "Joint spatial-temporal spectrum sensing for cognitive radio networks," *IEEE Transactions on Vehicular Technology*, vol. 59, no. 7, pp. 3480–3490, September 2010.

[51] B. Picinbono and P. Duvaut, "Optimal linear-quadratic systems for detection and estimation," *IEEE Transactions on Information Theory*, vol. 34, no. 2, pp. 304–311, 1988.

[52] C. Perez-Vega and J. M. Zamanillo, "Path-loss model for broadcasting applications and outdoor communication systems in the VHF and UHF bands," *IEEE Trans. on Broadcasting*, vol. 48, no. 2, pp. 91–96, Jun. 2002.

[53] B. L. Mark and A. O. Nasif, "Opportunistic spectrum sharing with multiple cochannel primary transmitters," *IEEE Transactions on Wireless Communications*, vol. 8, no. 11, pp. 5702–5710, Nov. 2009.

[54] H. V. Poor, *An Introduction to Signal Detection and Estimation*, 2nd ed. NewYork, NY: Springer-Verlag, 1994.

[55] Z. Motamedi and M. R. Soleymani, "For better or worse: The impact of shadow fading on the capacity of large MIMO networks," in *IEEE Global Telecommunication Conference (Globecom 2007)*, Nov 2007, pp. 3200 – 3204.

[56] D. Zhang, Z. Tian, and G. Wei, "Spatial capacity of narrowband vs. ultra-wideband cognitve radio systems," *IEEE Transactions on Wireless Communications*, vol. 7, no. 11, pp. 4670–4680, 2008.

[57] Y.-C. Liang, Y. Zeng, E. C. Y. Peh, and A. T. Hoang, "Sensing-throughput tradeoff for cognitive radio networks," *IEEE Trans. on Wireless Commun.*, vol. 7, no. 4, pp. 1326–1337, April 2008.

[58] A. M. Aziz, "A simple and efficient suboptimal multilevel quantization approach in geographically distributed sensor system," *Elsevier North-Holland Signal Process.*, vol. 88, no. 7, pp. 1698–1714, Jan. 2008.

[59] M. Gudmundson, "Correlation model for shadow fading in mobile radio systems," *IEEE Electronics Letters*, vol. 27, no. 23, pp. 2145–2146, Nov 1991.

[60] T. Do and B. L. Mark, "Expoiting multiuser diversity for spectrum sensing in cognitive radio networks," in *Proc. IEEE Radio and Wireless Symposium*, New Orleans, Jan 2010.

[61] J. Ma and Y. Li, "Soft combination and detection for cooperative spectrum sensing in cognitive radio networks," in *Proc. IEEE Global Telecommun. Conf. (Globecom'07)*, Nov 2007, pp. 3139–3143.

[62] P. Viswanath, D. N. C. Tse, and R. Laroia, "Opportunistic beamforming using dumb antennas," *IEEE Transactions on Information Theory*, vol. 48, no. 6, pp. 1277–1294, 2002.

[63] Q. Zhao and L. Tong, "Opportunistic carrier sensing for energy-effcicient information retrieval in sensor networks," *EURASIP Journal on Wireless Communications and Networking*, no. 2, pp. 231–241, 2005.

[64] C.-S. Hwang, K. Seong, and J. M. Cioffi, "Opportunistic p-persistent CSMA in wireless networks," in *IEEE Int. Conf. on Commun. (ICC)*, 2006, pp. 183–188.

[65] C.-S. Hwang and J. M. Cioffi, "Using opportunistic CSMA/CA to achieve multi-user diversity in wireless LAN," in *IEEE Globecom*, 2007, pp. 4952–4956.

[66] F. F. Digham, M. S. Alouini, and M. K. Simon, "On the energy detection of unknown signals over fading channels," in *Proc. IEEE Int. Conf. on Comm. (ICC'03)*, May 2003, pp. 3575–3579.

[67] A. Ghasemi and E. S. Sousa, "Collaborative spectrum sensing for opportunitic access in fading enviroments," in *Proc. IEEE DySPAN'05*, Nov 2005, pp. 131–136.

[68] *IEEE Standard for Wireless LAN Medium Access Control (MAC) and Physical Layer (PHY) Specifications*, IEEE Std., Nov. 1997.

[69] T. Do and B. L. Mark, "Combining cooperative relaying with spectrum sensing in cognitive radio networks," in *Proc. IEEE Radio and Wireless Symposium*, New Orleans, Jan 2010.

[70] S. Wei, D. Goeckel, and M. Valenti, "Asynchronous cooperative diversity," *IEEE Transactions on Wireless Communications*, vol. 6, no. 6, pp. 1547–1557, 2006.

[71] A. Motamedi and A. Bahai, "MAC protocol design for spectrum-agile wireless networks: Stochastic control approach," in *Proc. IEEE DySPAN'07*, April 2007, pp. 448–451.

[72] J. Boyer, D. D. Falconer, and H. Yanikomeroglu, "Multihop diversity in wireless relaying channels," *IEEE Transactions on Communications*, vol. 52, no. 10, pp. 1820–1830, Oct. 2004.

[73] A. E. Leu, M. McHenry, , and B. L. Mark, "Modeling and analysis of interference in listen-before-talk spectrum access schemes," *Int. J. Network Mgmt*, vol. 16, pp. 131–141, 2006.

[74] D. Tse and P. Viswanath, *Fundamentals of Wireless Communication.* Cambridge University Press, 2005.

[75] P. A. Anghel and M. Kaveh, "Exact symbol error probaility of a cooperative network in a rayleigh-fading environment," *IEEE Transactions on Wireless Communications*, vol. 3, no. 5, pp. 1416–1421, Sep. 2004.

[76] G. Farhadi and N. C. Beaulieu, "On the outage and error probability of amplify-and-forward multihop diversity transmission systems," in *Proc. International Conference on Communications (ICC) 2008*, Beijing, China, May 2008.

[77] M. O. Hasna and M. S. Alouini, "Harmonic mean and end-to-end performance of transmission systems with relays," *IEEE Transactions on Wireless Communications*, vol. 4, no. 3, pp. 1246–1273, May 2005.

[78] M. K. Simon and M.-S. Alouini, *Digital Communication over Fading Channels*, 2nd ed. Wiley Interscience, 2004.

[79] M.-S. Alouini, "A unified approach for calculating error rates of linearly modulated signals over generalized fading channels," *IEEE Transactions on Communications*, vol. 47, no. 9, pp. 1324–1334, 1999.

[80] T. Do and B. L. Mark, "Cooperative communication in cognitive radio networks with regenerative relays," in *Proc. Conference on Information and systems (CISS)*, Princeton, NJ, Mar. 2010.

[81] A. Stefanov and T. M. Duman, "Turbo-coded modulation for systems with transmit and receive antenna diversity over block fading channels: System model, decoding approaches and practical considerations," *IEEE Journal on Selected Areas in Communications*, vol. 19, pp. 958–968, May 2001.

[82] S. L. Goff, A. Glavieux, and C. Berrou, "Turbo codes and high spectral efficiency modulation," in *Proc. of IEEE Conf. Communications*, May 1994, pp. 645–649.

[83] T. Do and B. L. Mark, "Exploiting multichannel diversity in cognitive radio networks," in *Proc. IEEE International Conference on Computer Communication Networks (ICCCN) 2010*, Zurich, Switzerland, August 2010.

[84] ——, "Exploiting multichannel diversity in cognitive radio networks (submitted)," *EURASIP J. on Wireless Communications and Networking (Special Issue on "Multiple Access Communications in Future-Generation Wireless Networks")*, 2010.

[85] C. Berrou, A. Glavieux, and P. Thitimajshima, "Near shannon limit error-correcting coding and decoding: Turbo codes," in *Proc. IEEE International Conference on Communications (ICC)*, Genava, Switzerland, May 1993, pp. 1064–1070.

[86] L. N. Lee, A. R. H. Jr., F. W. Sun, , and M. Eroz, "Application and standardization of turbo codes in third-generation high-speed wireless data services," *IEEE Transactions on Vehicular Technology*, vol. 49, pp. 2198–2207, November 2000.

[87] S.-J. Lee, M. Goel, Y. Zhu, J.-F. Ren, and Y. Sun, "Forward error correction decoding for WiMAX and 3GPP LTE modems," in *In Proc. 42nd Asilomar Conference on Signals, Systems and Computers*, October 2008, p. 11431147.

[88] Y. Sun, Y. Zhu, M. Goel, and J. R. Cavallaro, "Configurable and scalable high throughput turbo decoder architecture for multiple 4G wireless standards," in *in Proc. International Conference on Application-Specific Systems, Architectures and Processors ASAP 2008*, July 2008, p. 209214.

[89] W. C. Jakes, *Microwave Mobile Communications.* New York, NY: John Wiley and Sons, 1975.

[90] G. Caire, G. Taricco, and E. Biglieri, "Bit-interleaved coded modulation," *IEEE Transactions on Information Theory*, vol. 44, pp. 927–946, May 1998.

[91] L. R. Bahl, J. Cocke, F. Jelinek, and J. Raviv, "Optimal decoding of linear codes for minimizing symbol error rate," *IEEE Transactions on Information Theory*, vol. 20, pp. 248–287, March 1974.

[92] P. Robertson, "Illuminating the structure of code and decoder of parallel concatenated recursive systematic (turbo) codes," in *IEEE Globecom*, Dec. 1994, pp. 1298–1303.

[93] C. Berrou and A. Glavieux, "Near optimum error-correcting coding and decoding: Turbo codes," *IEEE Transactions on Communications*, vol. 44, no. 10, pp. 1261–1271, October 1996.

[94] J. Hagenauer, "Iterative decoding of binary block and convolutional codes," *IEEE Transactions on Information Theory*, vol. 42, pp. 429–445, March 1996.

[95] J. Hagenauer and P. Hoeher, "A Viterbi algorithm with soft-decision outputs and its applications," in *IEEE Globecom*, Nov 1989, pp. 1680–1686.

[96] J. Hagenauer, "Source-controlled channel decoding," *IEEE Transactions on Communications*, vol. 43, no. 9, pp. 2449–2457, September 1995.

[97] P. Robertson, E. Villebrun, and P. Hoeher, "A comparison of optimal and sub-optimal MAP decoding algorithms operating in the log domain," in *IEEE ICC*, June 1995, pp. 1009–1013.

[98] G. Kramer, M. Gastpar, and P. Gupta, "Capacity theorems for wireless relay channels," in *41st Allerton Conf. on Commun. Control and Comp.*, Oct 2003.

Curriculum Vitae

Tuan T. Do graduated from Vietnam National University gifted high school and received a Bachelor of Engineering in Telecommunication Engineering from University of Communications and Transports, Hanoi, Vietnam in 1996 and 2001, respectively. As an undergraduate student, he won third prize in National Math Olympic Competition and Second Prize in University of Communication and Transport Computer Programming Competition. From 2001 to 2003, he worked as a software developer for Vietnam Data Communication Company. He received a Master of Science in Telecommunications and Computers from The George Washington University, Washington, DC in 2005. He has worked for Information System and Imaging Science Center at Georgetown University, Washington, DC from January 2008 to September 2010. Currently, he is working for Global Wireless Solutions Inc., Dulles, Virginia.